Master's thesis

NTNU
Norwegian University of Science and Technology
Faculty of Natural Sciences
Department of Chemical Engineering

Adelén Torset

Large Scale Production of Blue Hydrogen

Master's thesis in Chemical Engineering
Supervisor: Magne Hillestad
June 2023

NTNU
Norwegian University of
Science and Technology

Adelén Torset

Large Scale Production of Blue Hydrogen

Master's thesis in Chemical Engineering
Supervisor: Magne Hillestad
June 2023

Norwegian University of Science and Technology
Faculty of Natural Sciences
Department of Chemical Engineering

NTNU
Norwegian University of
Science and Technology

Abstract

The global energy demand is increasing, with a projected demand of 180 Mt hydrogen in 2030. The current production method of hydrogen, mainly steam reforming of natural gas, is responsible for more than 900 Mt of the annual CO_2 emissions. Therefore, to achieve a net-zero emission by 2050, low-carbon hydrogen production can be a part of the solution.

This thesis focused on hydrogen production from natural gas with carbon capture by the physical absorption process, the Selexol process. Two process designs of a hydrogen production plant were compared. The first process design consisted of a gas heated reformer (GHR) coupled with an autothermal reformer (ATR), while the second process design consisted of an autothermal reformer. Both process designs were simulated with Aspen HYSYS V12.

Based on the simulations, it was found that a production capacity of 500 tonnes/day of hydrogen required 61.89 tonnes/h and 68.5 tonnes/h of natural gas in the first and second process design, respectively. In addition, it was found that the oxygen consumption in the first and second design was 1,779 kmol/h and 2,497 kmol/h, respectively. Both processes were self-sufficient with heat. The natural gas efficiency was 85.5% and 77.3% in the first and second process design, respectively.

The total investment was 530.59 and 456.95 MUSD in the first and second process design, respectively. The net present value of the first and second process design was estimated to be 675.47 MUSD and 430.44 MUSD, respectively. Finally, the levelised cost of hydrogen (LCOH) was found to be 1.729 and 1.896 USD/kgH_2 in the first and second process design, respectively.

Sammendrag

Den globale etterspørselen etter energi øker, med en forventet etterspørsel på 180 Mt hydrogen i 2030. Den nåværende hydrogenproduksjonsmetoden er hovedsakelig dampreformering av naturgass, som er ansvarlig for 900 Mt av de årlige CO_2-utslippene. Derfor kan lav-karbonproduksjon av hydrogen være en del av løsningen for å oppnå netto nullutslipp innen 2050.

Denne avhandlingen fokuserte på hydrogenproduksjon fra naturgass med karbonfangst ved bruk av den fysiske absorpsjonsprosessen, Selexol-prosessen. To prosessdesign for hydrogenproduksjon ble sammenlignet. Det første prosessdesignet besto av en gassoppvarmet reformer (GHR) koblet med en autotermisk reformer (ATR), og det andre prosessdesignet besto av en autotermisk reformer. Begge prosessdesignene ble simulert med Aspen HYSYS V12.

Basert på simuleringene ble det funnet at en produksjonskapasitet på 500 tonn/dag hydrogen krever henholdsvis 61,89 tonn/time og 68,5 tonn/time naturgass i det første og andre prosessdesignet. I tillegg ble det funnet at oksygenforbruket i det første og andre designet var henholdsvis 1779 kmol/time og 2497 kmol/time. Begge prosessene var selvforsynte med varme. Naturgasseffektiviteten var 85.5% i det første prosessdesignet og 77,3% i det andre prosessdesignet.

Den totale investeringen var henholdsvis 530,59 og 456,95 MUSD i det første og andre prosessdesignet. Netto nåverdien for det første og andre prosessdesignet ble estimert til henholdsvis 675,47 og 430,44 MUSD. Til slutt ble den utjevnede kostnaden for hydrogen (LCOH) funnet til å være 1,729 og 1,896 USD/kgH_2 i det første og andre prosessdesignet.

Preface

This Master's thesis was written in the spring of 2023 at the Norwegian University of Science and Technology (NTNU) as a part of the five-year Master's program in Chemical Engineering and Biotechnology. The work performed in this thesis is a continuation of the specialisation project carried out in the fall of 2022. The final report is the result of TKP4900 - Chemical Process Technology Master's Thesis, in the Environmental Engineering and Reactor Technology research area.

First, I would like to express my greatest gratitude to my supervisor Professor Magne Hillestad for the guidance and valuable advice during my specialisation and master project. Finally, I would like to thank my parents, my sister and Emil for your love, support and encouragement.

"I declare that this is an independent work according to the exam regulations of the Norwegian University of Science and Technology (NTNU)."

Adelén Torset
Trondheim, 12th June 2023

Contents

List of Figures

List of Tables

Acronyms

ASU	Air Separation Unit.
ATR	Autothermal Reformer.
CAPEX	Capital Expenditures.
CCS	Carbon Capture and Storage.
CCUS	Carbon Capture Utilisation and Storage.
CEPCI	Chemical Engineering Plant Cost Index.
CLC	Chemical Looping Combustion.
DEA	Diethanolamine.
DEPG	Dimethyl Ethers of Polyethylene Glycol.
GHR	Gas Heated Reformer.
HI	Heat Integration.
HT	High-Temperature.
IEA	International Energy Agency.
IRR	Internal Rate of Return.
ISBL	Inside Battary Limits.
IT	Intermediate-Temperature.
L/G	Liquid-to-Gas.
LCOH	Levelised Cost of Hydrogen.
LHV	Lower Heating Value.
LT	Low-Temperature.
Mt	Million Tonnes.
NPV	Net Present Value.

O/C	Oxygen-to-Carbon.
OPEX	Operating Expenditures.
OSBL	Outside Battery Limits.
PC-SAFT	Perturbed-Chain Statistical Associating Fluid Theory.
PFD	Process Flow Diagram.
PSA	Pressure Swing Adsorption.
S/C	Steam-to-Carbon.
SE-SMR	Sorption-Enhanced Steam Methane Reforming.
SE-WGS	Sorption-Enhanced Water-Gas Shift.
SMR	Steam Methane Reformer.
SMR-MR	Steam Methane Reforming Membrane Reactor.
TSA	Temperature Swing Adsorption.
WGS	Water-Gas Shift.
WGS-MR	Water-Gas Shift Membrane Reactor.

List of Symbols

ΔH_i	Heat required in interval i
ΔT_i	Interval temperature difference
ΔT_{lm}	Logarithmic mean temperature
ΔT_{min}	Minimum temperature difference between hot and cold stream
$\dot{m}$	Mass flow
$\dot{Q}$	Heat flow
η	Carnot efficiency
μ	Viscosity
ρ	Density
τ	Residence time
A	Annual operating costs
a	Cost constant
$A_{c,l}$	Liquid cross-section area
A_c	Cross section area
ANF	Annuity factor
B	Book value
b	Cost constant
C	ISBL cost
C_e	Purchased equipment cost
C_{FC}	Fixed capital investment
CF	Cash flow

CP Heat capacity

D Depreciation

D Diameter

$D\&E$ Design and engineering cost

E Joint efficiency

f_c Cost factor civil engineering

F_d Fixed depreciation factor

f_{el} Cost factor electrical

f_{er} Cost factor equipment erection

f_i Cost factor instrumentation and process control

f_l Cost factor lagging, insulation and paint

f_m Cost factor material

f_p Cost factor piping

f_s Cost factor structures and buildings

h Height

H_{OG} Height of gas transfer unit

h_v Height above liquid

h_v Height of liquid

I Cost index

K_4 Percentage flooding correlation factor

L_v Length of vessel

M Amount hydrogen produced

n Economic lifetime

n Scaling factor

N_{OG} Number of gas transfer units

$N_{operators}$ Number of operators

OS Offsite cost

P Pressure

p	Discount rate
Q	Duty
Q_{Cmin}	Minimum cold utility
Q_{Hmin}	Minimum hot utility
q_l	Volumetric flow of liquid
q_v	Volumetric flow of vapor
S	Maximum allowable stress
S	Sizing parameter
T^*	Shifted temperature
T_{act}	Actual temperature
t_w	Wall thickness
U	Overall heat transfer coefficient
u_s	Settling velocity
u_v	Vapour velocity
V	Volume
V_l	Liquid holdup volume
V_w^*	Gas mass flow per unit of cross section area
V_w^*	Gas mass flow per unit of cross-section area
X	Contingency charges
T	Temperature
W	Work

Chapter 1

Introduction

Climate change is enabled by increased concentrations of greenhouse gases, including carbon dioxide (CO_2), methane (CH_4) and nitrous oxides (NO_x), in the atmosphere. This is causing the global average temperature to rise. Therefore, reductions in these emissions are necessary to mitigate global warming. As a part of the Paris Agreement, numerous governments have adopted a regulatory framework, including emission trading and carbon taxation, intending to reduce global CO_2 emissions. The goal of the Paris Agreement is to limit the global temperature increase to 1.5°C [1]. In order to achieve this long-term temperature goal, the CO_2 emissions need to be net zero by 2050 [2].

Currently, the majority of hydrogen is produced from fossil fuels, resulting in an emission of approximately 900 million tonnes (Mt) CO_2 per year [3]. Therefore, it is necessary to reduce the carbon footprint of hydrogen production. Hydrogen is a key raw material in energy-intensive industrial processes, such as ammonia and methanol production, metal treatment and petroleum refining. According to the International Energy Agency (IEA), the global hydrogen demand reached 94 Mt in 2021, with the distribution as illustrated in Figure 1.1 [3].

The world's hydrogen demand is expected to reach 180 Mt by 2030, emphasising the need to decarbonise hydrogen production. In the net zero scenario by 2050, low-emission hydrogen produced from water electrolysis and fossil sources with carbon capture, utilisation and storage (CCUS) are needed to supply the world's increasing energy demand [3].

Hydrogen can be categorised into four main types based on production method: grey, brown, blue and green. Traditionally, hydrogen is produced through steam methane reforming (SMR) of natural gas or light hydrocarbons, which is a high-carbon method known as grey hydrogen. Another high-carbon production method is brown hydrogen, which is produced by coal gasification. Blue hydrogen is produced by steam reforming of natural gas with integrated carbon capture and storage (CCS) technology to reduce CO_2 emissions. This makes blue hydrogen a low-carbon process. Finally, hydrogen produced by water electrolysis fuelled by renewable energy, which leaves no carbon footprint, is called green hydrogen [4].

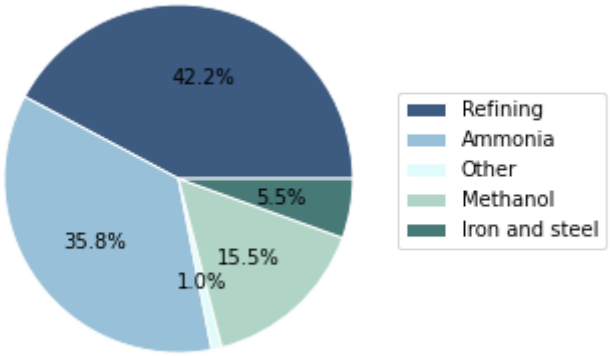

Figure 1.1: The distribution of the global hydrogen demand in 2021 [3].

The world is transitioning from a traditional fossil fuel-based economy to a low-carbon, sustainable economy, and hydrogen production has become an essential part of this transition. Blue hydrogen is a potential fuel in the transition to a low-carbon economy. Therefore, efficient and cost-effective production of blue hydrogen is of critical importance.

1.1 Objective

The main objective of this thesis is to compare two process configurations of blue hydrogen production, with a minimum overall capture rate of 95% of the produced CO_2, to evaluate their profitability and energy efficiency. This will be accomplished by modelling and simulating the processes with Aspen HYSYS, estimating the size of the main equipment, and carrying out cost and profitability analyses.

1.2 Outline of Thesis

Chapter 2 gives a detailed description of the different parts of the hydrogen production process. This chapter describes several technologies for carbon capture as well as an introduction to advanced hydrogen production technologies. This chapter provides the necessary information about the reactions and operating conditions. Chapter 3 provides the methodology applied in this thesis. Initially, information about how the HYSYS simulations were performed and the input parameters used are given. Further in the chapter, the method applied to the cost estimation and profitability analyses is described. Chapter 4 address the results obtained from the simulations and the profitability analyses. Chapter 5 gives a conclusion of the work performed in this thesis and gives recommendations and ideas for further work.

Chapter 2

Background

In this chapter, a detailed description of hydrogen production is given. Figure 2.1 gives a simplified block diagram of hydrogen production. As illustrated, the process design consists of three main parts; synthesis gas production, carbon capture and hydrogen purification. In the following sections, a description of the technologies used in each process step will be given.

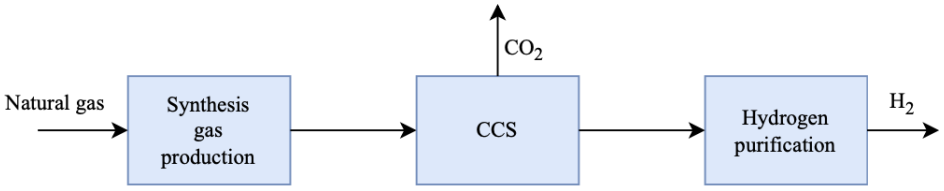

Figure 2.1: A simplified block diagram of the main parts of the hydrogen production: synthesis gas production, carbon capture and storage, and hydrogen purification.

2.1 Hydrogen

Hydrogen is the most abundant element in the universe and has great potential as a sustainable energy carrier. On Earth, the majority of the hydrogen occurs in water, fossil fuels, and biomass [5, 6]. Globally, less than 1% of the hydrogen exists in the form, H_2, the stable and preferred form of hydrogen from an energy perspective. Since hydrogen is not easily accessible for energy applications, it is usually referred to as an energy carrier rather than an energy source [4].

Hydrogen is the lightest molecule with the highest energy content, based on heating value, compared to other fuels. In contrast to fossil fuels, like petroleum and natural gas, hydrogen is an energy carrier with only water as the exhaust product, which is environmentally beneficial [7]. Since most hydrogen is bounded in molecules, it must be processed before utilisation.

One important aspect is the CO_2 emissions from the hydrogen industry. As mentioned, the hydrogen industry is responsible for approximately 900 Mt of the annual global CO_2 emissions [3]. Although hydrogen is a carbon-emission-free energy carrier, the total emissions depend on the production method. Hydrogen can be generated from both renewable sources and fossil sources. The different types of hydrogen are divided into colours based on production technology and source used. Grey and brown hydrogen is the conventional hydrogen produced through steam reforming of natural gas and coal gasification, respectively. These processes are considered high-carbon processes due to a high CO_2 emission. Blue hydrogen is produced mainly from natural gas with carbon capture and storage (CCS). Green hydrogen is produced through electrolysis of water using renewable power. Both blue and green hydrogen are considered low-carbon hydrogen.

Another obstacle to hydrogen production is storage due to its extremely low density [7]. Hydrogen can be stored as pressurised gas, cryogenic liquid, or physically or chemically bonded to a suitable solid-state material [7].

2.2 Synthesis Gas Production

The synthesis gas (syngas) production is based on converting natural gas, mainly methane, into a mixture of hydrogen, carbon monoxide and carbon dioxide. The main steps in syngas production are sulphur removal, pre-reforming, reforming and water-gas shift, as illustrated in Figure 2.2. The shifted syngas contains mainly hydrogen and carbon dioxide. Further in this section, the different steps of the synthesis gas production are described in detail.

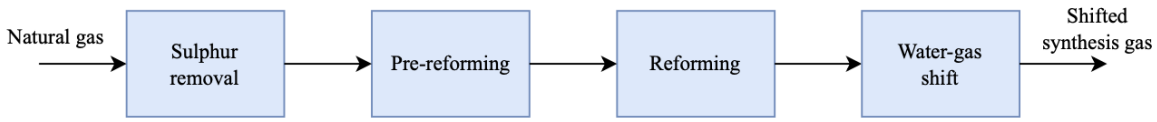

Figure 2.2: A simplified block diagram of the main parts of the synthesis gas production.

2.2.1 Sulphur Removal

The first step in synthesis gas production is sulphur removal. The natural gas contains a small amount of hydrogen sulphide, which is a poison to the nickel-based catalysts in the reformers. Therefore, a sulphur removal unit is necessary to obtain an optimal production. Various processes can be used to remove the sulphur, like scrubbing with a solvent, adsorption on activated carbon, and reaction with an oxide [8]. In this thesis, the synthesis gas is assumed to be sulphur free, and the sulphur removal unit is therefore not included in the process.

2.2.2 Pre-reformer

The natural gas consists of a small amount of heavy hydrocarbons, which are more reactive and have a higher coke-formation propensity than methane. Heavy hydrocarbons can easily form carbon (coke) at higher temperatures through the following reaction,

$$C_nH_{2n} \rightarrow C + H_2 \tag{2.1}$$

Coke deposition on the active sites of the reforming catalysts leads to deactivation. Therefore, the heavy hydrocarbons are converted into methane in the pre-reformer. The pre-reformer is normally an adiabatic catalytic fixed bed reactor operating at temperatures of 350-550°C with a nickel-based catalyst [8–10]. Implementing a pre-reformer gives economic and operational benefits for the synthesis gas production, like increased production capacity, increased catalyst lifetime and reduced coke formation. The use of a pre-reformer allows for a higher feed temperature in the reformers as a result of the reduced risk of coke formation, which has a great impact on the reformer duty [9, 10].

In the pre-reformer, steam reforming of the heavy hydrocarbons to methane and synthesis gas occurs. A generalised equation for the endothermic conversion of hydrocarbons to carbon monoxide and hydrogen (syngas) is given in the following equation,

$$C_nH_m + nH_2O \rightleftharpoons nCO + \left(n + \frac{m}{2}\right)H_2. \tag{2.2}$$

A generalised equation for the endothermic conversion of hydrocarbons to methane is given in the following equation [8],

$$C_nH_{2n+2} + \frac{1}{2}(n-1)\,H_2O \rightarrow \frac{1}{4}(3n+1)\,CH_4 + \frac{1}{4}(n-1)\,CO_2. \tag{2.3}$$

In addition, the exothermic water-gas shift reaction (2.4) occurs in the pre-reformer.

$$CO + H_2O \rightleftharpoons CO_2 + H_2 \tag{2.4}$$

2.2.3 Autothermal Reformer

The autothermal reformer (ATR) has a compact design consisting of a refractory-lined pressure vessel with a burner, combustion chamber and a nickel-based catalyst bed, as illustrated in Figure 2.3 [8, 11]. The process gas enters the top of the ATR. It is initially mixed with oxygen from an air separation unit (ASU) and additional steam, resulting in a combination of partial oxidation and steam reforming of methane.

Firstly, in the combustion chamber, methane is partially combusted to raise the process gas temperature, according to the reaction (2.5), (2.6) and (2.7). The exothermic oxidation reactions are used to generate the heat needed in the endothermic steam reforming reaction.

$$CH_4 + \frac{1}{2}O_2 \longrightarrow CO + 2\,H_2 \tag{2.5}$$

$$CH_4 + 2\,O_2 \rightleftharpoons CO_2 + 2\,H_2O \tag{2.6}$$

$$CH_4 + \frac{3}{2}O_2 \rightleftharpoons CO + 2\,H_2O \tag{2.7}$$

Then, in the catalyst bed, the remaining methane in the process gas is catalytically reformed through steam reforming (2.8) and water-gas shift (2.4).

$$CH_4 + H_2O \rightleftharpoons CO + 3\,H_2 \tag{2.8}$$

The steam-to-carbon (S/C) ratio is essential in the reformers to prevent coke formation [8]. In the ATR, a S/C ratio of 0.6 is commercialised by Topsoe [11]. Typically, the ATR operates in the range of 20-100 bar and at temperatures up to 1,500°C [8].

2.2.4 Steam Methane Reformer

The currently most widely used technology for steam reforming of natural gas is the fired steam methane reformer (SMR). The SMR consists of 40-400 nickel-based catalyst-filled tubes placed inside a combustion chamber. The reactor tubes are around 10-12 meters long, with a diameter of approximately 10-12 cm. The natural gas is converted to synthesis gas through steam reforming (2.8) and the water-gas shift reaction (2.4), which takes place over the catalyst bed inside the reformer tubes. The heat needed for the overall endothermic reforming is supplied by fuel combustion in the furnace, resulting in a flue gas with a low concentration of CO_2 at atmospheric pressure. Normally, the furnace consists of a radiant section, where the burners are placed, and a convection section to recover the waste heat of the flue gas leaving the radiant section. The burners in the SMR can be located in different places; on the top, bottom or furnace wall, referred to as top-fired, bottom-fired and side-fired, respectively. An illustration of a steam methane reformer is given in Figure 2.4. The reformer is top-fired in this illustration, ensuring a uniform temperature profile along the reformer tubes [12]. Typically, the inlet temperature of the natural gas entering the SMR is 450-650°C, and the synthesis gas exiting is around 800-950°C.

Figure 2.3: Illustration of an autothermal reformer by Topsoe [11]. The reformer consists of a refractory-lined pressure vessel, a combustion chamber and a catalyst bed.

2.2.5 Gas Heated Reformer

The gas heated reformer (GHR) is a compact alternative to the steam methane reformer. A GHR is a heat exchanger reformer consisting of a shell side and nickel-based catalyst-filled tubes. The natural gas enters the top of the reformer and flows downwards through the tubes. The natural gas is converted to syngas through equation (2.8) and (2.4), and produce a mixture of hydrogen, carbon oxides, methane and steam. The heating medium in the GHR can be hot synthesis gas exiting the ATR or flue gas from the combustion of natural gas. The hot gas enters the shell side of the GHR and flows counter-current upwards the reformer, which supplies sufficient heat for the endothermic steam reforming reaction (2.8) [10]. Figure 2.5 shows an illustration of a GHR.

The material in the GHR is exposed to the synthesis gas exceeding the ATR, which has both a high temperature and a high partial pressure of CO, which causes a considerable risk of metal dusting [10]. Metal dusting is an essential problem in synthesis gas production, which is a corrosive degradation of metals and alloys into fine, dust-like particles, which leads to the loss of the metal particles. Metal dusting occurs in carbonaceous gases at intermediate to high temperatures (400-800°C). The corrosion is initiated by undesired carbon formation on the inner surface of the process equipment, which is formed through the CO reduction reaction (2.9) and Boudouard reaction (2.10) [10, 13, 14]. Metal dusting is serious damage to the reformer and shortens the lifetime of the reformer tubes. When the synthesis gas from the ATR is cooled on the shell side of the GHR, metal dusting is of great concern. Therefore, the GHR needs to

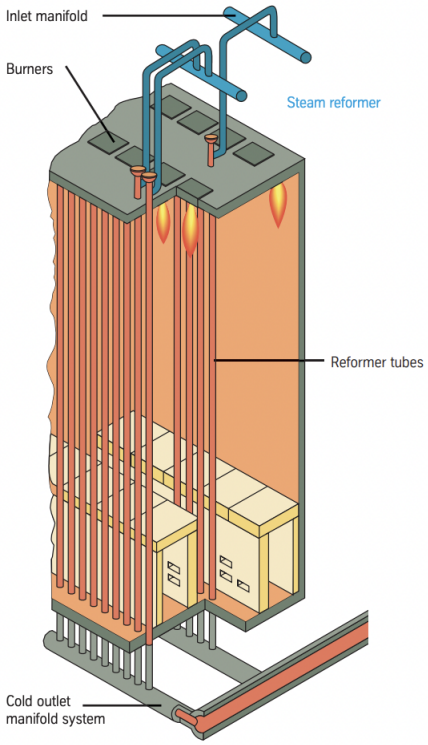

Figure 2.4: Illustration of a steam methane reformer (SMR) by Thyssenkrupp [12]. The reformer consists of catalyst-filled tubed, which are placed inside a furnace.

operate at a high steam-to-carbon ratio to reduce the risk of metal dusting [10].

$$CO + H_2 \leftrightarrow C + H_2O \tag{2.9}$$

$$2\,CO \leftrightarrow C + CO_2 \tag{2.10}$$

2.2.6 Water-Gas Shift Reactor

In hydrogen production, after the reforming part of the process, the H_2/CO ratio is increased. The produced CO is typically reacted with steam to produce H_2 and CO_2 through the water-gas shift reaction (2.4). This is an important reaction in hydrogen production since CO is shifted to CO_2, which is captured later in the process and maximises the hydrogen yield. The water-gas shift reaction is equilibrium limited and moderately exothermic. The equilibrium constant decreases with the temperature, and high conversions are favoured by low temperatures [6, 8, 16]. In the water-gas shift reaction, a high steam-to-carbon ratio is favoured as it improves the

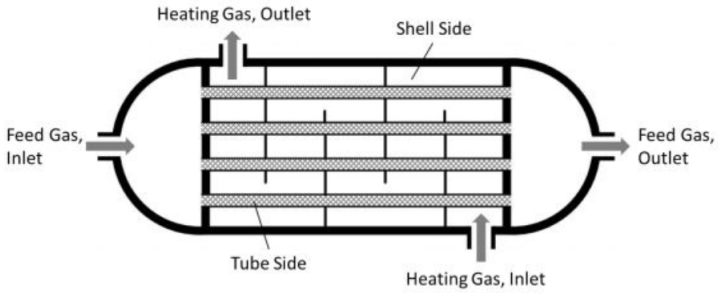

Figure 2.5: Illustration of a gas heated reformer (GHR) from [15]. The hot process gas enters the shell side, while the feed enters the tube side of the reformer.

CO conversion [6, 16]. In industry, three different versions of shift reactors are used in hydrogen production; high-temperature, intermediate-temperature and low-temperature [8, 17].

High-Temperature Shift

The high-temperature (HT) shift reactor operates typically in the range of 300-450°C, with a CO conversion down to approximately 2.5% CO on a dry basis [17, 18]. The catalyst used in the HT shift reactor is typically a copper-promoted iron-chromium catalyst [17].

Intermediate-Temperature Shift

The intermediate-temperature (IT) shift reactor typically operates at about 220-300°C. The conversion of CO in this reactor can reach down to 0.5% CO on a dry basis. The IT shift conversion of CO can be performed in an adiabatic reactor with integrated steam production for cooling of the process gas [18]. Figure 2.6 gives an illustration of an IT shift reactor with integrated catalyst cooling. The catalyst used in this shift reactor is typically a copper-zinc-alumina catalyst [17].

Low-Temperature Shift

The low-temperature (LT) shift reactor is normally installed downstream of a high-temperature shift reactor. The LT shift reactor can further reduce the amount of CO in the synthesis gas to approximately 0.2% on a dry basis. The LT shift reactor typically operates between 180-250°C and utilises a copper-zinc catalyst [8, 17, 18].

Figure 2.6: Isothermal shift reactor for CO conversion with a fixed bed for the exothermic catalytic reactions, and an integrated helically coiled tube heat exchanger for cooling of the catalyst. The heat from the exothermic reactions is used for steam production. Illustration by Linde [18].

2.3 Advanced Technologies for Hydrogen Production

In advanced hydrogen production, the synthesis gas production and gas separation are combined to get a more compact and efficient process [16]. Further in this section, a description of sorption-enhanced hydrogen production, membrane reactors and chemical looping will be given.

2.3.1 Sorption-Enhanced Hydrogen Production

Sorption-enhanced hydrogen production utilises an adsorbent to selectively remove one or more components formed in the equilibrium reactions, shifting the equilibrium and obtaining a higher production yield at milder conditions [16]. The sorption-enhanced hydrogen production technology combines the hydrogen-producing reactions and the adsorption technology presented in section 2.4.1. Further, two technologies that can be used in hydrogen production, sorption-enhanced water-gas shift and sorption-enhanced steam methane reformer, are described in more detail.

Sorption-Enhanced Water-Gas Shift

In sorption-enhanced water-gas shift (SE-WGS), the water-gas shift reaction (2.4) is carried out while CO_2 is continuously removed by a solid sorbent. The adsorption of CO_2 shifts the reaction towards increased hydrogen production. The reaction step is followed by an increase in temperature or a decrease in pressure and purging with steam, which regenerate the sorbent, and the desorbed CO_2 is separated. This process can be both a continuous process or a semi-continuous process. The principle of SE-WGS is illustrated in Figure 2.7.

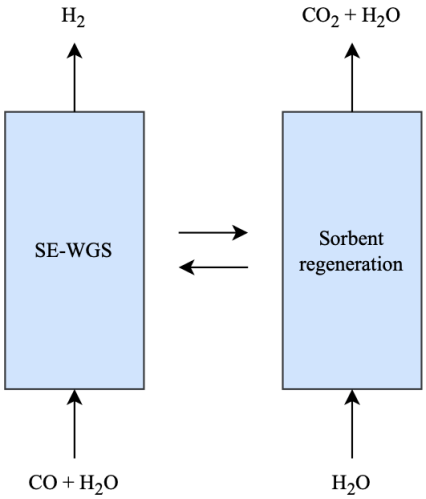

Figure 2.7: Illustration of the principle of SE-WGS. Reproduced from [16].

Sorption-Enhanced Steam Methane Reformer

In sorption-enhanced steam methane reformer (SE-SMR), the steam reforming reaction (2.8) and water-gas shift reaction (2.4) occur simultaneously with separation of CO_2 over a reforming catalyst mixed with a CO_2 sorbent. The principle of the SE-SMR is similar to the SE-WGS, but the reactions occur at higher temperatures [16].

2.3.2 Membrane Reactors

A membrane reactor is a reactor where the reaction and separation of one or more products occur simultaneously. The separation is performed by a selective membrane placed inside the reactor module, constituting an integrated reaction and separation system. The principle of a membrane reactor is to achieve the same performance as the traditional reformers but to operate at milder conditions [19]. In hydrogen production, the reformers and the water-gas shift reactor can be replaced with membrane reactors.

Steam Methane Reforming Membrane Reactor

In a steam methane reforming membrane reactor (SMR-MR), the steam reforming part, the water-gas shift part and the hydrogen purification part are combined. Conventionally, these parts of hydrogen production are carried out at different operating conditions to obtain optimal production. As illustrated in Figure 2.8, the hydrogen is continuously separated, shifting the equilibrium reactions and enhancing methane conversion due to Le Chatelier's principle. This shift effect enhances the reaction conversions for both the steam reforming reaction (2.8) and the water-gas shift reaction (2.4), and the hydrogen production. Hence, both reactions can occur simultaneously in a single unit. As mentioned, the steam reforming reaction is strongly endothermic, and the water-gas shift reaction is mildly exothermic. Therefore, heat must be supplied to the system [16, 19]. To increase the mass transfer through the membrane, a sweep gas can be used on the permeate side of the membrane. Sweeping by steam is effective in the production of high-purity hydrogen since it can be easily removed by condensation [16].

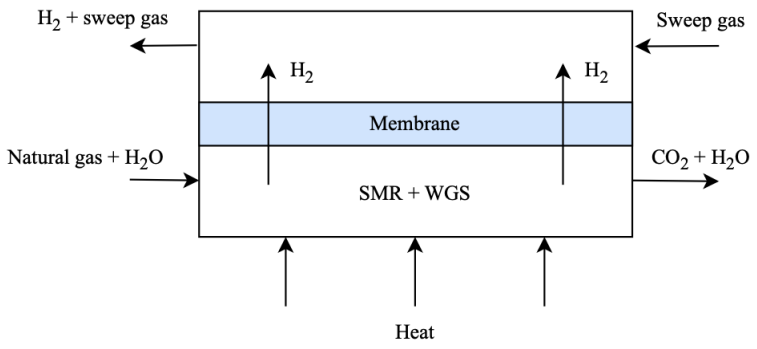

Figure 2.8: Illustration of the principle of an SMR-MR. Reproduced from [16].

Water-Gas Shift Membrane Reactors

In a water-gas shift membrane reactor (WGS-MR), the water-gas shift reaction (2.4) is combined with hydrogen purification. As mentioned, the water-gas shift reaction is mildly exothermic, and conversion is therefore favoured at low temperatures. By using a WGS-MR, the hydrogen is continuously removed, and the equilibrium is shifted. Therefore, the use of a WGS-MR allows for higher conversion at higher temperatures than a conventional WGS reactor. As for the SMR-MR, a sweep gas would also increase the conversion rate [16]. Figure 2.9 illustrates the principle of a WGS-MR.

2.3.3 Chemical Looping Hydrogen Production

Hydrogen production using chemical looping is based on the concept of chemical looping combustion (CLC). In CLC, an oxygen carrier, typically a metal oxide, provides the oxygen required

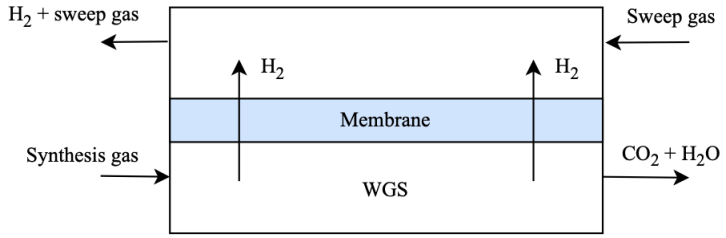

Figure 2.9: Illustration of the principle of a WGS-MR. Reproduced from [16].

for fuel oxidation in a fuel reactor. The oxygen carrier constantly circulates between the fuel reactor and air reactor [16, 20]. Further in this section, a chemical looping process for hydrogen production is described in detail.

Synthesis Gas Chemical Looping Process

A system with three reactors is proposed in the synthesis gas chemical looping process; fuel, steam and air, as illustrated in Figure 2.10. In the fuel reactor, the oxygen carrier is reduced by syngas, producing a flue gas consisting of mainly CO_2 and H_2O, as shown in equation (2.11). The fuel reactor is typically operated at 750-900°C.

$$Fe_2O_3 + CO + H_2 \rightarrow Fe/FeO + CO_2 + H_2O \tag{2.11}$$

Then, the reduced oxygen carrier is to the steam reactor where steam is reduced to hydrogen and the oxygen carrier is partially oxidised, as given in equation (2.12). The steam reactor operates typically at 500-750°C.

$$Fe/FeO + H_2O \rightarrow Fe_3O_4 + H_2 \tag{2.12}$$

Lastly, the oxygen carrier is sent to the air reactor where it is fully oxidised, and the cycle continues, as given in equation (2.13). The air reactor generates heat, which is partially transported to the fuel reactor through the oxygen carriers, while the rest of the heat is in the exhaust air, which can be utilised in the process.

$$Fe_3O_4 + O_2 \rightarrow Fe_2O_3 \tag{2.13}$$

This technology can theoretically produce both high-purity hydrogen and CO_2 at transportation quality. Chemical looping processes require the development of chemically and physically stable oxygen carriers throughout many cycles with oxidation and reduction [16].

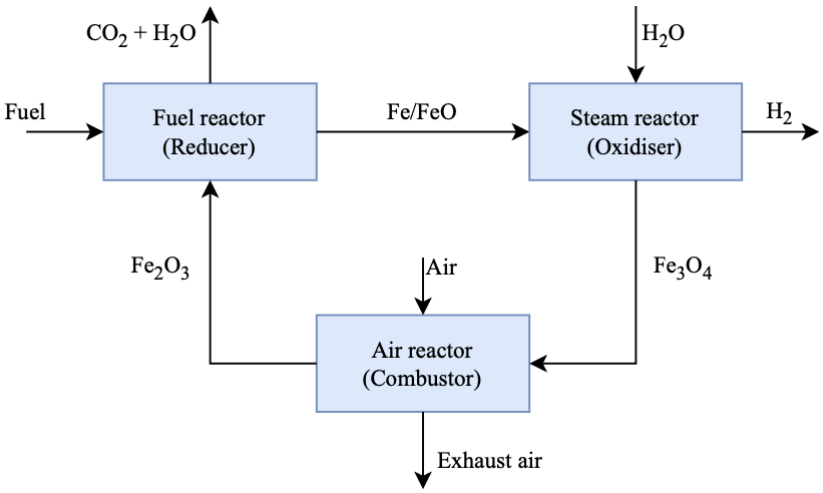

Figure 2.10: Illustration of the synthesis gas chemical looping process principle. Adapted from [16].

2.4 Carbon Capture Technologies

Carbon capture and storage (CCS) can be implemented to capture the CO_2 produced in the process. The main goal of blue hydrogen production is to minimise the carbon emissions by capturing most of the produced CO_2. The criteria of blue hydrogen in industry is still uncertain, but commonly associated with a capture rate above 90-95% [21]. Several technologies can be applied to capture the CO_2, like absorption, adsorption, membrane separation and cryogenic separation. The following section gives a detailed description of the leading carbon capture technologies.

2.4.1 Adsorption

Adsorption is a technology based on selective adsorption of one or more components from a gas or liquid stream. Then, the desired component is separated, concentrated and collected. For CO_2 capture, adsorbents with a high affinity for CO_2 can be used to separate the CO_2 from the gas stream [16, 22].

It is possible to use chemical adsorbents, physical adsorbents or a hybrid of these in the adsorption process to adsorb CO_2. The adsorption phenomenon has strong chemical adsorption with chemical bonds and weak physical adsorption by van der Waals force. In CO_2 capture by physical adsorbents, the CO_2 is adsorbed selectively on the surface of the adsorbent. Then, the adsorbent can easily be regenerated by pressure reduction (PSA) or thermally (TSA) to separate and recover the CO_2. When the component is adsorbed chemically, desorption is generally not

possible. [22, 23]

Temperature swing adsorption (TSA) utilises the thermodynamic properties of the adsorbents. CO_2 is adsorbed at low temperatures, then desorbed at higher temperatures. For CO_2 capture, PSA is most relevant because the shifted synthesis gas is at elevated pressure, which allows for a pressure swing with a limited energy requirement [16]. The principle is similar to the hydrogen purification process by pressure swing adsorption, as illustrated in Figure 2.13.

2.4.2 Chemical Absorption

One of the most common technologies for carbon capture from a gas stream is absorption in a liquid phase, either a chemical, physical or a hybrid solvent [8, 23]. The absorption with physical solvents is further described in section 2.4.3.

In chemical absorption, the solvents react with CO_2 and require considerable heat to regenerate the solvent. Two typical chemical solvents are aqueous solutions of amines, such as MEA, DEA and MDEA, and aqueous solutions of potassium carbonate. Chemical solvents are best suited for absorption when the partial pressure of CO_2 are relatively low due to a relatively high absorption capacity at low partial pressures of CO_2 for chemical solvents. The chemical solvents have an increased absorption capacity with an increased partial pressure of CO_2 until the solution becomes saturated [16]. Figure 2.11 shows a typical flow sheet for an absorption process of CO_2 from a synthesis gas stream using chemical solvents. Further in this section, the chemical absorption processes using aqueous amines and potassium carbonate are described in more detail.

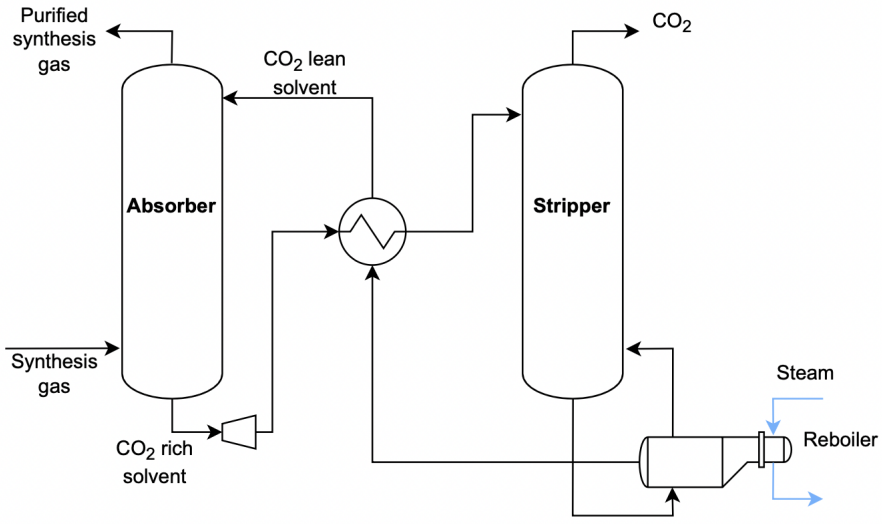

Figure 2.11: Simplified flow sheet of a chemical absorption process. Adapted from [16, 24].

Amine

Amine scrubbing is a chemical absorption process utilising an aqueous amine solution to separate the CO_2 from a synthesis gas stream [23]. Amines, which are organic compounds derived from ammonia (NH_3) by replacing one or more of the hydrogen atoms with a hydrocarbon group or substituents, are categorised as either primary, secondary or tertiary according to the number of substituents present [23, 25]. Of the components in the synthesis gas, only CO_2 can react with the amine/amines in the solution. Aqueous amines are attractive for absorption of CO_2 due to their high absorption capacity and absorption rate [26].

The amine absorption of CO_2 is a cyclic process driven by a temperature swing. In the absorption column, a relatively cold amine solution with a high affinity for CO_2 absorbs the CO_2. Then, to reduce the affinity for CO_2, the solution is heated, and CO_2 is separated [26]. The general overall reaction for both primary and secondary amines is given as,

$$CO_2 + 2\,RNH_2 \rightleftharpoons RNHCO_2^- + RNH_3^+ \tag{2.14}$$

where two molecules of amine are required per molecule of CO_2 absorbed. Therefore, the maximum CO_2 loading in primary and secondary amine solvents is 0.5. The primary and secondary amines have a relatively fast reaction rate and high heat of absorption. The overall reaction of CO_2 absorption using tertiary amines is given as,

$$CO_2 + R_1R_2R_3N + H_2O \rightleftharpoons HCO_3^- + R_1R_2R_3NH^+ \tag{2.15}$$

where only one mole of amine is needed per mole of CO_2 absorbed. Therefore, the CO_2 maximum loading in tertiary amine solvents is 1, which is twice the loading of the primary and secondary amines. In contrast to the primary and secondary amines, the tertiary amines have a slow reaction rate and low heat of absorption [27].

In the stripper, these reactions are reversed to regenerate the amine solvent and separate the captured CO_2. The regeneration of the amine solvent is an energy-intensive process. Due to the high heat of absorption of the primary and secondary amines, the energy requirement for regenerating the solvent is higher than for the tertiary amines. Hence, the reboiler duty is dependent on the solvent [23].

Hot Potassium Carbonate

The hot potassium carbonate process, the Benfield process, is a chemical absorption process utilising an aqueous potassium carbonate solution to capture the CO_2. The CO_2 is absorbed as given in the following equation;

$$K_2CO_3 + CO_2 + H_2O \rightarrow 2KHCO_3. \tag{2.16}$$

The hot potassium carbonate process is well-suited for capturing CO_2 from synthesis gas streams with a relatively high partial pressure of CO_2. The process operates at high temperatures, 110-115 °C, to increase the potassium carbonate solubility [23].

The CO_2 capture process with hot potassium carbonate requires a low regeneration energy, compared to the amine scrubbing, due to a relatively weak bonding between the carbon dioxide and the carbonate [8, 25]. The main disadvantage of this process is its relatively slow reaction rate, causing low mass transfer rates; therefore, the process requires a large contact surface. This drawback can be improved by using an amine activator, such as DEA (Diethanolamine) [23, 28]. As a result, both the capital and operating cost will decrease, and the purity of the treated gas will increase [28].

Carbonate absorbents are particularly attractive since they have a low solvent cost and a high chemical solubility of CO_2 [23, 26]. As illustrated in Figure 2.11, the synthesis gas enters the bottom of the absorber and flows counter-currently to the carbonate solution. The purified synthesis gas exits the top of the absorber, and the CO_2 rich carbonate solution exits the bottom of the absorber. The carbonate solution is normally regenerated in a stripper, where the absorbed CO_2 is separated.

2.4.3 Physical Absorption

Physical absorption is an absorption technology utilising a physical solvent where the solvent does not react chemically with the acid gas. The driving force in the physical absorption process is the high solubility of acid gases in the solvents. Therefore, physical solvents are attractive in absorption when the concentration of carbon dioxide is high. The absorption capacity of physical solvents is lower at a low partial pressure of CO_2 compared to chemical solvents. According to Henry's law, the absorption capacity increases linearly with CO_2 partial pressure [16, 23].

The physical solvents are normally regenerated by pressure reduction and/or by heating. The heat requirements for physical solvents are usually much less than for chemical solvents since the heat of desorption for carbon dioxide for the physical solvent is only a fraction of that for chemical solvents. For physical solvents to be economically viable, they must fulfil specific criteria, such as high selectivity for carbon dioxide, low vapour pressure, low viscosity, heat stability and noncorrosive to metals [23].

Figure 2.12 illustrate a typical flow sheet for a physical absorption process for CO_2 capture with flashing to regenerate the solvent. Several physical absorption processes are commercialised, like Selexol, Rectisol, Sulfinol and Purisol. Further in this section, the Selexol process is described in more detail.

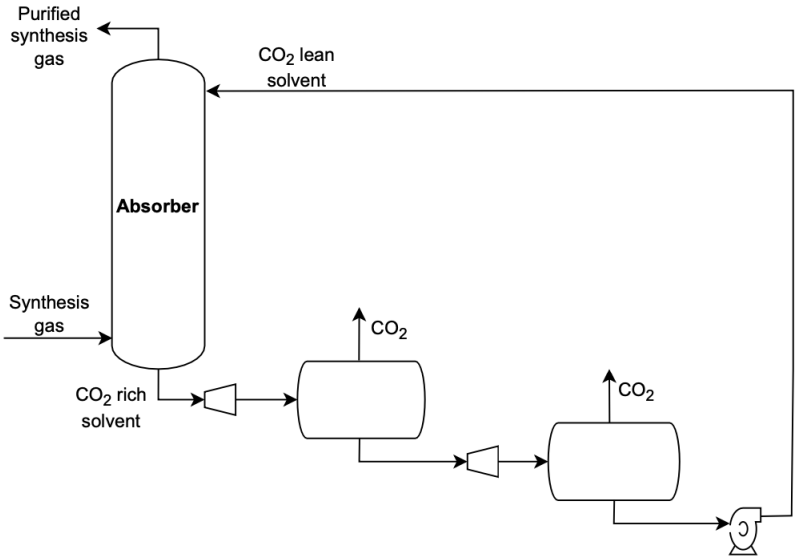

Figure 2.12: Simplified flow sheet of a physical absorption process with flashing to regenerate the solvent. Reproduced from [24]

Selexol Process

The physical absorption process, the Selexol process, uses a solvent made of dimethyl ethers of polyethylene glycol (DEPG) to remove CO_2 from a synthesis gas stream [23]. The Selexol solution has been shown to be a chemically stable, non-toxic and biodegradable material [29]. The Selexol process is suited for gas streams with a high concentration of CO_2 and a low concentration of heavier hydrocarbons since the heavy hydrocarbons have a higher solubility in Selexol than CO_2 [29, 30]. The operating temperature of the Selexol solvent can be reduced to increase the acid gas solubility. The Selexol solvent is suited for operation at temperatures up to 175°C, but due to stability, the minimum operating temperature is -17°C [23, 29].

In the Selexol process, the synthesis gas enters the bottom of the absorber and contacts with regenerated lean DEPG solvent from the top of the absorber counter-currently, as illustrated in Figure 2.12. The synthesis gas leaves the top as purified synthesis gas, while the DEPG solvent leaves the bottom as a CO_2-rich solvent. The desorption process of the rich DEPG can be accomplished either thermally, by flashing, or by stripping gas [23]. The regenerated solvent is then pumped back to the top of the absorber. The purified gas obtained from the top of the absorber contains only a tiny amount of CO_2. The rich CO_2 stream is collected for further processing [31].

2.4.4 Membrane Separation

A membrane is a selective barrier which allows separation based on the molecular properties, such as molecular size [8]. The flow that passes through the membrane and not passes through the membrane are called the permeate and retentate, respectively. The transport of molecules through the membrane occurs due to differences in partial pressure over the membrane [16, 32].

The shifted synthesis gas is at elevated pressure, which provides a sufficient driving force for membrane separation. For hydrogen production, the membranes used can either be hydrogen or carbon dioxide selective. The hydrogen-selective membranes produce a high-purity hydrogen stream at low pressure and a retentate stream at relatively high pressure, and are described further in section 2.5. The CO_2 selective membrane typically produces a CO_2 enriched permeate stream at low pressure and a CO_2 reduced retentate stream at high pressure.

Due to the small molecular size of hydrogen, it is challenging to separate CO_2 selectively from the synthesis gas. Several types of CO_2 selective membranes exist; polymeric membranes, mixed matrix membranes and porous inorganic membranes [16]. One drawback in carbon capture by membrane separation is the low concentration of CO_2 in the permeate stream, which means that CO_2 at transportation quality still needs to be achieved [16].

In general, membrane separation has major advantages, like less maintenance, lower capital and operating costs and require lower energy [23]. The main drawbacks of membrane separation are a short lifetime of the membranes, membrane fouling, concentration polarisation and a linear up-scaling factor [32].

2.4.5 Cryogenic Separation

Cryogenic separation involves cooling the synthesis gas to a very low temperature so the CO_2 can be liquefied and separated. Cryogenic separation is suitable for separation and liquefaction of CO_2 from a relatively pure gas stream with a concentration of at least 90% CO_2. One drawback of cryogenic separation is the substantial energy demand to provide sufficient refrigeration [23].

2.5 Hydrogen Purification

The hydrogen production aims to produce hydrogen with a desired purity of 99.9999%. This purity can be achieved by pressure swing adsorption or membrane purification, as described further in this section.

2.5.1 Pressure Swing Adsorption

The state-of-the-art technology for hydrogen purification is pressure swing adsorption (PSA) [33]. The PSA technology can produce hydrogen with a purity of up to 99.9999 mol%. The

hydrogen recovery ranges between 60-95%, depending on the feed gas composition and desired purity [16, 34].

The synthesis gas is sent through an adsorbent where impurities are adsorbed while hydrogen passes through the column. The adsorption process happens at high pressure, while the regeneration happens at low pressure. Typically, several adsorption units are placed in parallel in industry, operating simultaneously with adsorption, desorption, purge, and pressurisation shifted in time, as illustrated in Figure 2.13. The hydrogen product exits the PSA at a slightly lower pressure, usually a pressure drop of 1 bar, and the PSA off-gas at low pressure[16]. Typically, the PSA off-gas is used as fuel in the process plant.

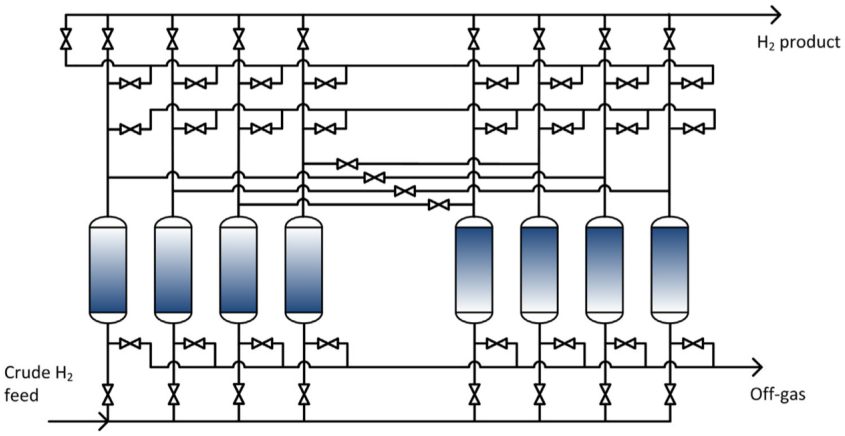

Figure 2.13: Flow sheet of a multiple column pressure swing adsorption (PSA) process by [16].

2.5.2 Membrane Purification

One membrane successfully developed for hydrogen separation is the palladium membrane, developed by the Norwegian companies SINTEF and Hydrogen Mem-Tech. This palladium membrane can achieve a hydrogen purity of up to 99.999% and a recovery rate of up to 99% [35]. Membranes with a thin palladium alloy film applied onto a porous support have a very high flux and selectivity of hydrogen. This membrane can be used in hydrogen production at temperatures in the range of 350-600°C [35, 36]. A major challenge with the palladium membrane is the chemical stability of the material due to sensitivity towards poisoning by components such as CO and H_2S [16]. Additionally, a drawback of membrane purification is the relatively low pressure (up to 7 bar) of the hydrogen product stream [35].

2.6 Process Integration

Process integration is a systematic and general method for designing integrated production systems. Process integration intends to utilise the energy available in the process in order to minimise the use of external heating and cooling utilities. A heat exchanger network must be designed to evaluate possible external utility savings for the overall process. The most widely applied heat exchanger network design method is the Pinch technology [37, 38].

The Pinch technology is a method to achieve maximum heat recovery in the process, which means finding the minimum external and cooling duties required. To perform the analysis, it is required to decide a minimum temperature difference between the hot and cold streams, ΔT_{min}. The range of 5°C to 20°C is typical, but any temperature greater than 0°C will yield a viable heat-exchanger network [39].

The enthalpy of all the hot and cold streams as a function of temperature can be presented graphically, called composite curves. The Composite curves provide valuable information about the maximum heat recovery, $Q_{Recovery}$, minimum external heating, Q_{Hmin}, minimum external cooling, Q_{Cmin} and the heat recovery pinch, as illustrated in Figure 2.14 [40]. Usually, the minimum temperature difference, ΔT_{min}, is observed at only one point between the hot and cold composite curves, referred to as the heat recovery pinch. The pinch point divides the process into two thermodynamic regions. The region above the pinch is in heat balance with the minimum hot utility, Q_{Hmin}, and is considered a heat sink. The region below pinch is in heat balance with the minimum cold utility, Q_{Cmin}, and is considered a heat source [41].

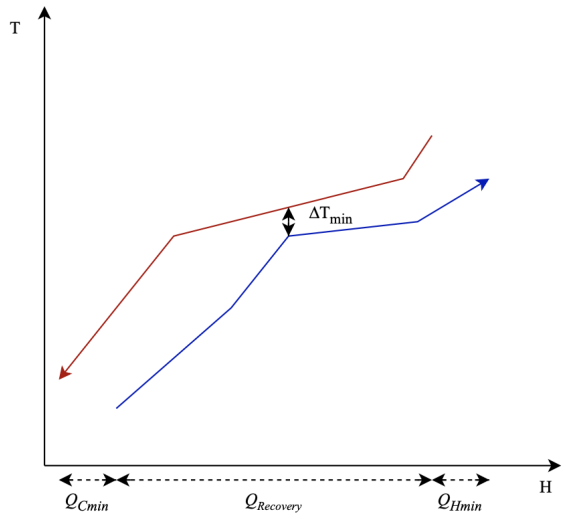

Figure 2.14: General illustration of hot and cold composite curves.

The Problem Table Algorithm is a numerical method for determining the pinch temperatures and the minimum utility requirements without using graphical illustrations [37]. The method follows the steps [37, 41]:

1. The actual stream temperatures, T_{act}, is converted to shifted temperatures, T^*, by adding $\Delta T_{min}/2$ to the cold streams and subtracting $\Delta T_{min}/2$ from the hot streams.
2. Arrange the interval temperatures in the order of magnitude.
3. Calculate the energy balance for each temperature interval from:

$$\Delta H_i = [\Sigma CP_C - \Sigma CP_H]\Delta T_i$$

   where ΔH_i is the heat required in interval i, ΣCP_C and ΣCP_H is the sum of heat capacities of all the cold and hot streams in the interval, respectively. ΔT_i is the temperature difference in interval i.
4. Cascade the heat surplus from one interval to the next down the column of interval temperatures. Cascading the heat from one interval to the next interval implies that the heat available from the hot streams in the interval is hot enough to supply a deficit in the cold streams in the next interval.
5. Introduce the required amount of external heat to the top of the cascade to eliminate negative values.

The heat recovery pinch occurs where the heat flow in the cascade is zero [37, 41]. The pinch divides the system into two thermodynamic regions, where the region above the pinch is a heat sink with a deficit of heat. In contrast, the region below the pinch has a surplus of heat, as illustrated in Figure 2.15. The grand composite curve is obtained by plotting the problem table cascade, which shows the heat flow through the process against temperature. The open parts at the top and bottom represent the minimum heating and cooling requirements, respectively. The heat pockets represent process-to-process heat transfer [41].

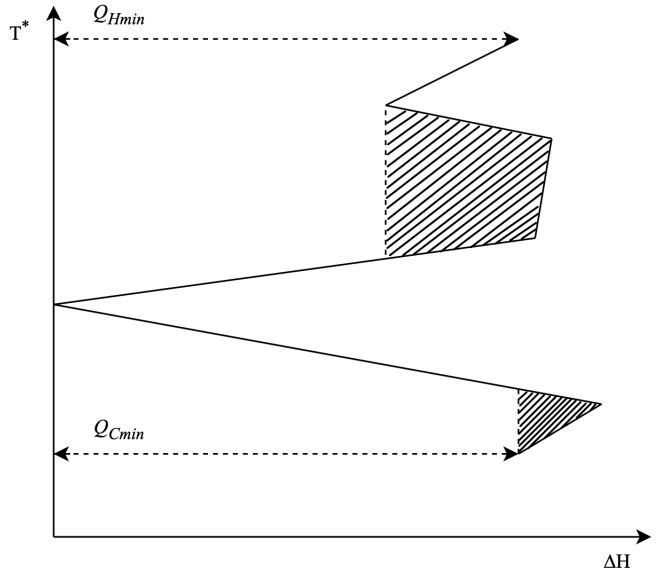

Figure 2.15: General illustration of a grand composite curve.

To ensure a sufficient driving force and that the minimum temperature difference is maintained, the pinch exchangers must fulfil the given heat capacity criteria:

Above Pinch:	Below Pinch:
$CP_C \geq CP_H$	$CP_H \geq CP_C$

where CP_H and CP_C are the heat capacities for the hot and cold streams, respectively. The pinch exchangers are the heat exchangers situated immediately above or below the Pinch [40, 41].

Chapter 3

Process Concepts and Analyses

The main purpose of this thesis is to evaluate and compare the profitability and efficiency of two process designs of blue hydrogen production. This chapter describes the methodology applied to this thesis. Firstly, a process description of the two chosen hydrogen production concepts is introduced. Then, the HYSYS model for both processes will be explained with the given input parameters. In addition, a detailed description of the modelling of the different units will be given.

The simulations of both process designs were performed by using Aspen HYSYS V12. In this thesis, steam production was included in the simulations. This thesis did not include further processing of the produced hydrogen and the captured CO_2. Furthermore, the storage options for the hydrogen product and the captured CO_2 were not evaluated either. Additionally, the air separation unit (ASU) was not included in the simulations.

The simulations were used as a basis for equipment sizing and cost estimation enabling a comparison of the technologies. Capital expenditures (CAPEX), operating expenditures (OPEX) and the levelised cost of hydrogen (LCOH) were calculated for both cases. Lastly, profitability and sensitivity analyses were performed on both process configurations.

3.1 Process Description

In a conventional hydrogen plant, a steam methane reformer (SMR) is used as the primary reformer to convert natural gas to synthesis gas through steam reforming (2.8). As mentioned, the combustion process in the SMR produces a flue gas with a low concentration of CO_2 at atmospheric pressure. As a result, implementation of carbon capture technologies inevitably leads to a high capital cost estimate [42].

Blue hydrogen production involves the production of two product streams, pure hydrogen and CO_2[16, 42]. Steam methane reforming and advanced gas reforming are the two leading tech-

nologies in the production of blue hydrogen. The advanced gas reforming consists either of an autothermal reformer (ATR) or an ATR coupled with a gas heated reformer (GHR). Due to more suitable streams for carbon capture in the advanced gas reforming, this technology is acknowledged to be more appropriate for the production of blue hydrogen [43]. Therefore, this thesis studied two concepts of advanced gas reforming. Further in this section, a detailed description of the two process configurations, referred to as case 1 and case 2, are given.

A carbon capture plant was implemented to separate most of the produced CO_2 at high purity. The advanced technologies for hydrogen production, as described in section 2.3, are novel technologies currently on lab and pilot scale. In addition, limited research has been published on the advanced technologies compared to the carbon capture processes described in section 2.4. Therefore, up-scaling of these technologies may be challenging. Based on the given theory about chemical absorption, described in section 2.4.2, they are relatively energy-intensive processes compared to physical absorption processes. In addition, amine scrubbing is suited for carbon capture from syngas streams with a low concentration of CO_2. Conversely, physical absorption is especially suited for carbon capture from syngas with a high partial pressure of CO_2. Lastly, membrane separation achieves pure hydrogen at low pressure and requires considerable energy for compression. Considering these factors, the physical absorption process, the Selexol process, was chosen as the carbon capture technology in this thesis.

The final production stage is pressure swing adsorption (PSA), which enables further purification of the hydrogen product to 99.999%. In addition, the produced hydrogen is at relatively high pressure. This thesis set the blue hydrogen criteria to capture at least 95% of the produced CO_2.

3.1.1 Case 1 - GHR and ATR

The first process configuration in this thesis is based on a commercialised technology by Johnson Matthey, combining a GHR and an ATR [43]. The process flow diagram (PFD) of the process is given in Figure 3.1.

As illustrated in the PFD (Figure 3.1), the natural gas is pre-heated and mixed with steam before entering the pre-reformer, where the heavy hydrocarbons are converted to methane. Then, the process gas is further heated, and more steam is added before the methane is partially converted in the GHR. In the secondary reformer, ATR, the methane is further converted to synthesis gas. The hot process gas exiting the ATR is used to heat exchange in the GHR, as described in section 2.2.5. The synthesis gas is further cooled before entering the water-gas shift reactor. The produced water is separated before the shifted synthesis gas enters the carbon capture plant. As mentioned, this project chose the Selexol process as the carbon capture technology. A general process flow diagram of the Selexol process is given in Figure 3.2.

After the carbon capture process, the purified synthesis gas is further purified by PSA. Finally, the PSA off-gas is combusted.

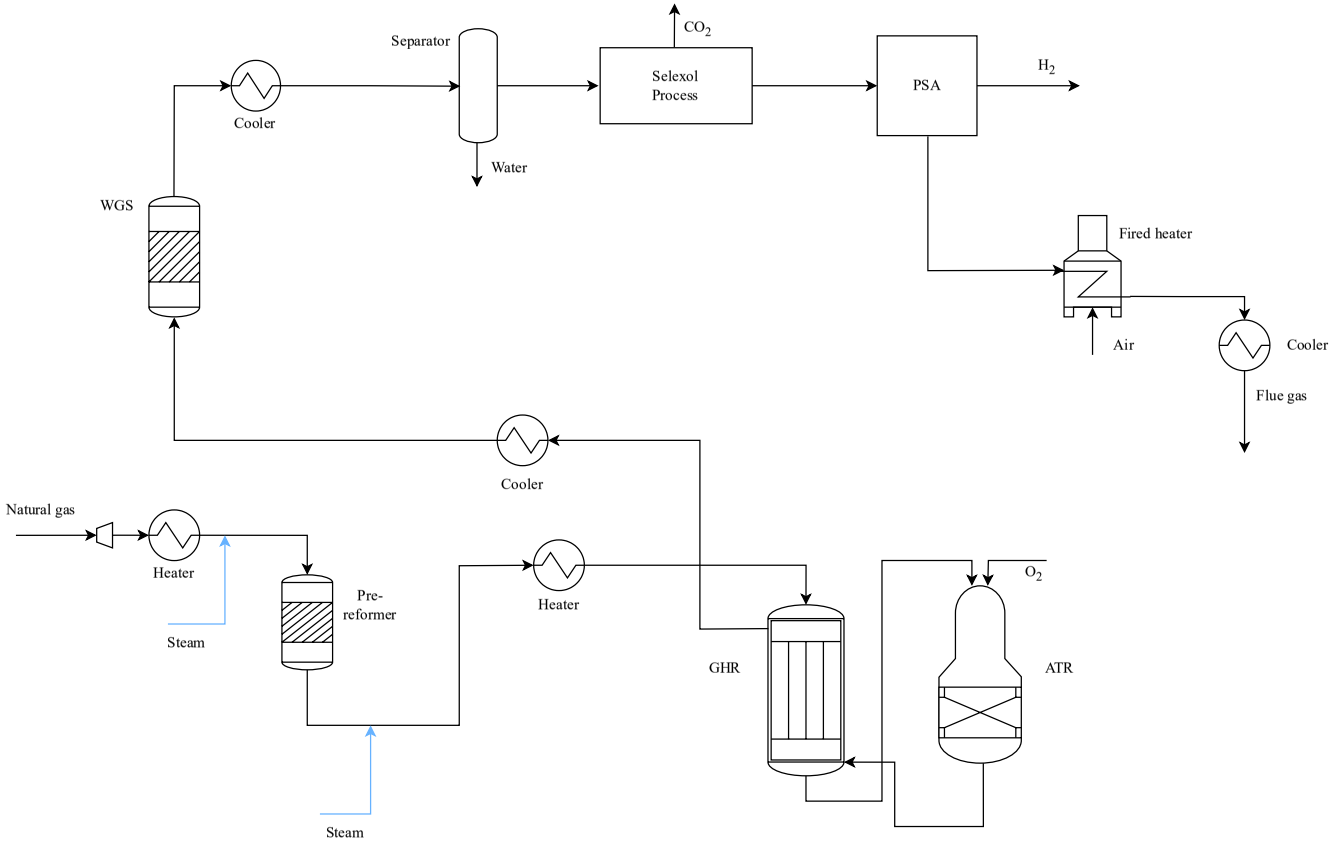

Figure 3.1: Process flow diagram of case 1 with a gas heated reformer (GHR) and an autothermal reformer (ATR). The light blue lines indicate water/steam flows.

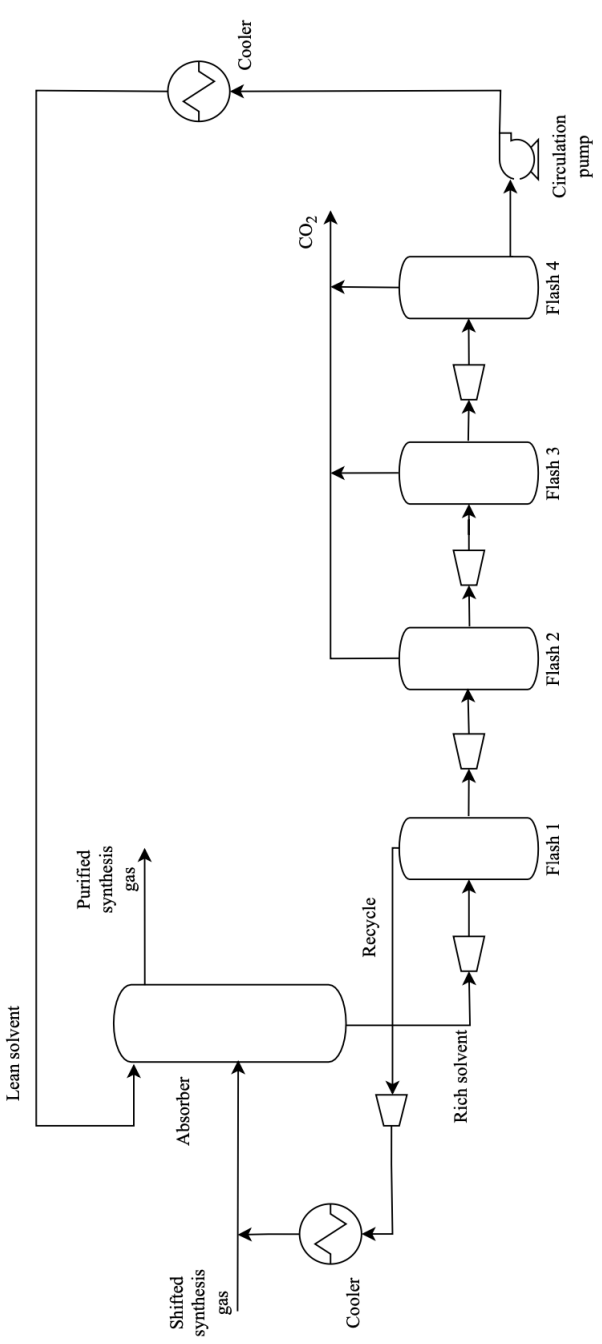

Figure 3.2: Process flow diagram of the Selexol process.

3.1.2 Case 2 - ATR

The second process configuration is based on a commercial technology by Topsoe consisting of an ATR as the primary reformer [11]. Figure 3.3 gives the process flow diagram.

As illustrated in Figure 3.3, the natural gas is pre-heated and mixed with steam before entering the pre-reformer. Then, the process gas is further heated before entering the ATR, where the methane is converted to synthesis gas, as described in section 2.2.3. The synthesis gas is further cooled before entering the shift reactor to shift the carbon monoxide and steam to produce more hydrogen and CO_2. Before entering the carbon capture plant, the produced water is separated out. Like the first process configuration, the Selexol process was chosen as the carbon capture process. Afterwards, the purified synthesis gas was further purified in a PSA, which is only shown as a block in the PFD. The PSA off-gas is combusted in a fired heater.

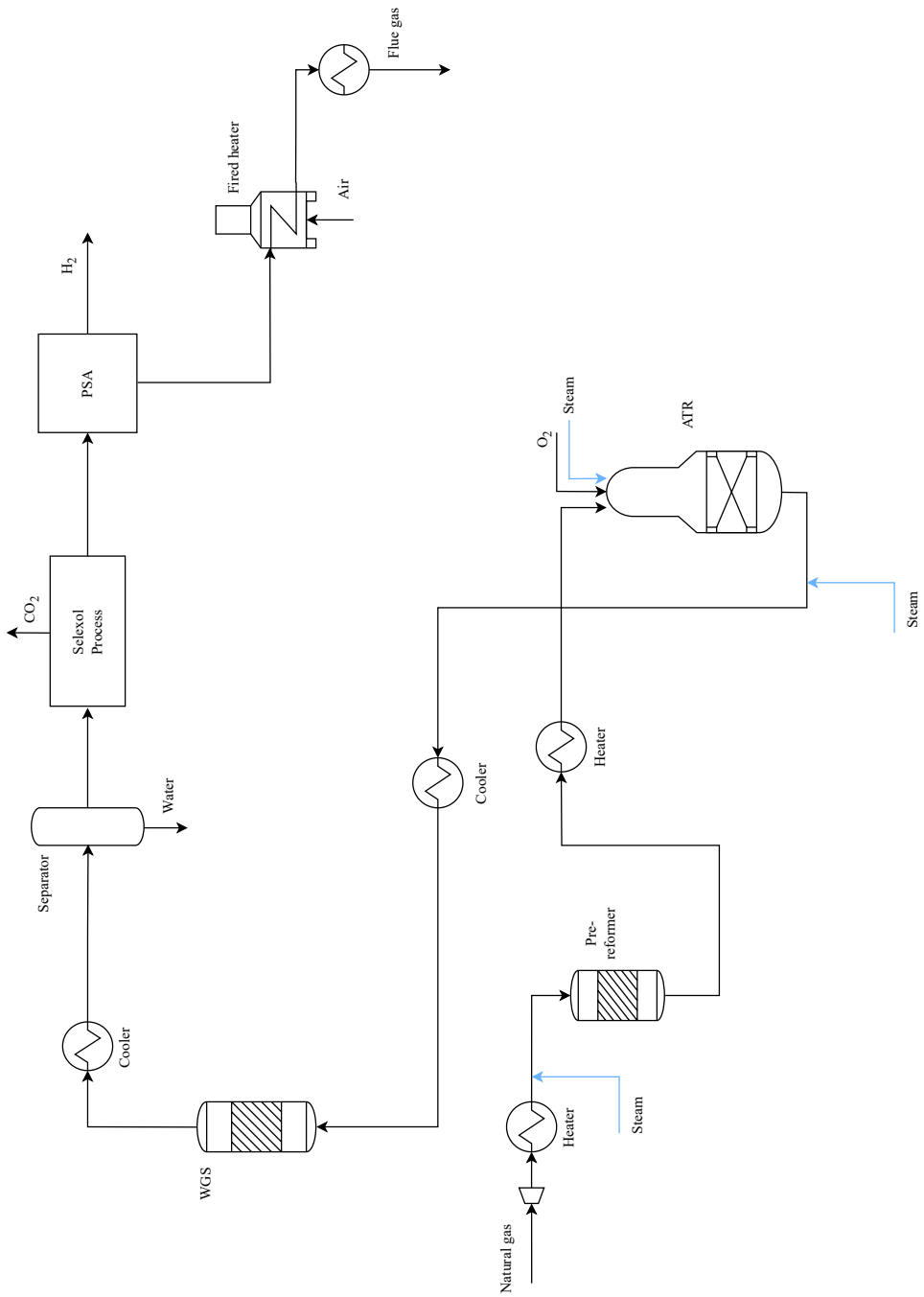

Figure 3.3: Process flow diagram of case 2 with an autothermal reformer (ATR). The light blue lines indicate water/steam flows.

3.2 Process Simulations

In this thesis, a production capacity of 500 tonnes of hydrogen per day was used as a basis for the simulations. In both cases, natural gas was used as feedstock, with the composition given in Table 3.1. Table 3.2 gives the input parameters used in both simulations. As mentioned, the synthesis gas was assumed to be sulphur free; thus, no sulphur removal unit was included in the simulations. Appendix A gives the HYSYS simulation flow sheets of both processes. In the simulations, the main process units, heaters and coolers were assumed to have a pressure drop of 0.5 bar. In both simulations, the steam requirement was fulfilled by pumping water at 1 bar to 36 bar and heated to 245.1°C.

Both process configurations were simulated in Aspen HYSYS V12. The Peng-Robinson equation of state was used to calculate the thermodynamic properties in the synthesis gas production part of the process. The carbon capture part of the processes used the property package, Acid Gas - Physical Solvents, based on the Perturbed-Chain Statistical Associating Fluid Theory (PC-SAFT) equation of state. This property package allowed to model the dimethyl ether of polyethylene glycol (DEPG) and represent the thermodynamic and transport properties of the Selexol solvent properly [39, 44].

Table 3.1: Composition of the natural gas used as feedstock in the simulations [45].

Component	Composition [mol%]
Methane	88.7
Ethane	5.7
Propane	2.0
Butane	0.9
Pentane	0.3
Hexane	0.3
Oxygen	0
Carbon dioxide	1.5
Water	0
Nitrogen	0.5-0.6

3.2.1 Case 1 - GHR and ATR

The natural gas was expanded from 50 to 36.5 bar, heated to 400°C, and mixed with steam at 245.1°C and recycled PSA off-gas, before entering the pre-reformer. A case study, given in Appendix G, was performed in the specialisation project to find the minimal steam-to-carbon (S/C) ratio required to convert the heaviest hydrocarbons to methane. The S/C ratio was set to 0.3 in the pre-reformer to ensure a sufficient conversion of the heavy hydrocarbons and avoid coke formation later in the process [46]. The pre-reformer was modelled as a Gibbs reactor in HYSYS.

Table 3.2: Inputs for the simulation of both process designs, case 1 (GHR and ATR) and case 2 (ATR).

Parameter	Case 1	Case 2
Natural gas feed temperature [°C]	70	70
Natural gas feed pressure [bar]	50	50
Pre-reformer inlet temperature [°C]	400	400
S/C ratio pre-reformer inlet [-]	0.3	0.3
GHR inlet temperature [°C]	600	-
S/C ratio GHR inlet [-]	2.5	-
S/C ratio ATR inlet [-]	-	0.6
ATR inlet temperature [°C]	750	600
WGS inlet temperature [°C]	300	300
S/C ratio WGS inlet [-]	-	2
Separator inlet temperature [°C]	40	40

The outlet stream of the pre-reformer was mixed with steam and further heated to 600°C before entering the GHR. A case study was performed in the specialisation project to study the effect of the S/C ratio in the GHR feed on the hydrogen production. The case study is given in Appendix G. In order to achieve maximal production of hydrogen, the S/C ratio was set to 2.5 in the gas entering the GHR [46]. The GHR was modelled as a Gibbs reactor at 750°C and 34.5 bar.

Further, the process gas entered the ATR and was mixed with oxygen to achieve an outlet temperature of 1,200°C. This outlet temperature results from a case study performed in the autumn project and can be found in Appendix G.

Before entering the water-gas shift reactor, the process gas was cooled to 300°C. The WGS was modelled as an equilibrium reactor operating isothermally at 300°C and 33 bar. Following the WGS, the gas was cooled to 40°C, and the condensate was separated. Then, the shifted synthesis gas entered the carbon capture plant. As mentioned, the Selexol process (described in section 2.4.3) was chosen for both process designs and the simulations are described further in section 3.2.3.

3.2.2 Case 2 - ATR

Like the previous case, the natural feed gas was expanded to 36.5 bar and heated 400°C. Then it was mixed with steam at 245.1°C and recycled PSA off-gas before entering the pre-reformer. The S/C ratio in the pre-reformer feed was 0.3. The pre-reformer was modelled as a Gibbs reactor.

Then, the process gas was mixed with steam and further heated to 600°C before it entered the ATR. As described in section 2.2.3, the ATR operates commercially at a S/C ratio of 0.6 and was

therefore set to 0.6 in this simulation. The amount of oxygen needed to maximise the hydrogen production was studied. The ATR optimum oxygen-to-carbon (O/C) ratio was studied in the specialisation project and was found to be approximately 0.6, as shown in Appendix G. The ATR was modelled as a Gibbs reactor.

A case study was performed to study the amount of steam needed before the WGS to achieve a high conversion of CO. As shown in Figure 3.4, the hydrogen production increased radically up to a steam-to-carbon ratio of 2. Then, the conversion of hydrogen slightly increased at higher steam-to-carbon ratios. In this simulation, the operating S/C ratio in the WGS feed was therefore set to 2.

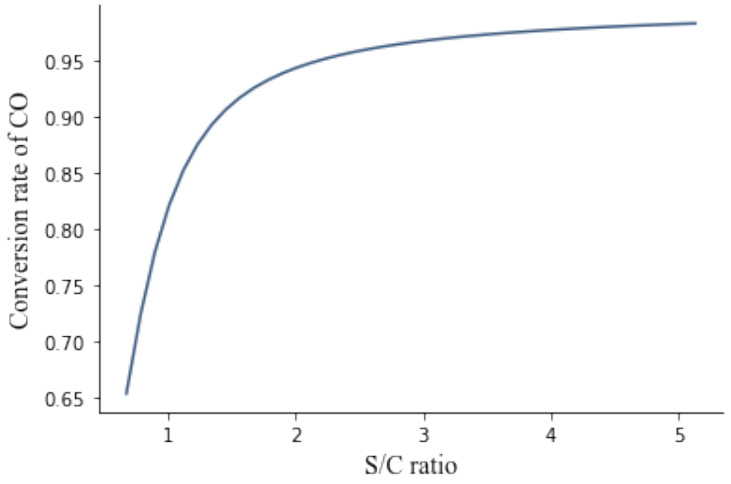

Figure 3.4: Conversion rate of CO in the water-gas shift reactor as a function of the steam-to-carbon ratio.

3.2.3 Carbon Capture Plant - Selexol Process

In order to remove the produced CO_2, a carbon capture plant was implemented. The overall carbon capture rate of the process was set to at least 95%. Since the processes emit CO_2 from both the flue gas from the fired heater and the condensate, the captured CO_2 needs to compensate in order to achieve an overall capture rate of 95%. A Selexol process was simulated in HYSYS for both processes. As shown in Figure 3.2, the Selexol process consists of an absorber, four flash tanks, two heat exchangers and a recycle pump.

The absorber was simulated with 15 stages. The study of the absorber performance is given in Appendix G. The pressure in the absorber was 32 bar. The inlet synthesis gas temperature was 40°C. The Selexol solvent had an inlet temperature of 7.22°C and a pressure of 32 bar. Exiting the absorber, the pressure of the rich Selexol solvent was reduced and heated to 75°C. Then, the flash gas consisting mainly of hydrogen and CO_2 was recycled back to the absorber. Further, to

regenerate the Selexol solvent, the pressure was reduced in three flash tanks; 10 bar, 6.895 bar and 1.013, respectively. Then, the CO_2 gas flow from the top of the flash tanks was mixed.

The carbon capture rate was examined as a function of the L/G ratio, as shown in Figure 3.5. As illustrated, the CO_2 recovery is approximately constant above the L/G ratio of 15. For the L/G ratios lower than 15, the capture rate increases with increasing L/G ratio. The capture rate is about constant at the L/G ratios above 17. At the optimum L/G ratio, there is a sufficient amount of Selexol solvent to dissolve at least 95% of the CO_2. Therefore, the optimal L/G ratio was found to be at least 15 in this simulation, depending on the amount of CO_2 in the flue gas.

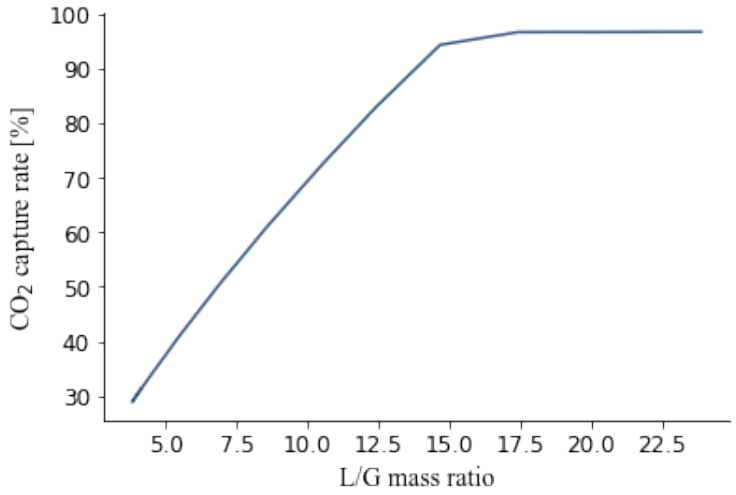

Figure 3.5: The effect of the liquid-to-gas mass ratio on the CO_2 capture rate.

3.2.4 Pressure Swing Adsorption

The purified synthesis gas exiting the Selexol process was further purified in a PSA to obtain a hydrogen purity of 99.9999%. The PSA was set to recover 90% of the hydrogen and was modelled as a component splitter in HYSYS. The pressure drop in the produced hydrogen was set to 1 bar in both cases. The pressure of the PSA off-gas was set to 2.5 bar in both cases. The PSA off-gas was split into two streams in both processes, where one part was used as fuel in a fired heater, and the other part was recycled back into the process. The optimal split fraction was 0.4 for combustion and 0.6 for recycling in both cases to capture at least 95% of the CO_2 due to the effect of the emitted CO_2 in the flue gas.

3.2.5 Fired Heater

The amount of air fed to the fired heater was decided in order to achieve total conversion of methane and CO in the PSA off-gas to CO_2 due to the higher impact on the environment.

3.3 Heat Integration

A heat integration network was designed for both processes with the aim to minimise external heating and cooling. The heat integration was based on the theory given in section 2.6. The chosen hot and cold streams for both cases are summarised:

Hot streams:

- Cooling of feed to the WGS reactor
- Cooling of feed to the separator
- Cooling of lean Selexol solvent
- Cooling of flue gas

Cold streams:

- Pre-heating of feed to the Pre-reformer
- Pre-heating of feed to the primary reformer: GHR in case 1 and ATR in case 2
- Water to steam production
- Heating of rich Selexol solvent

3.4 Steam Production

As mentioned in section 3.3, the water needed to produce the required steam in both processes was included in the heat integration. In addition, the condensate from the separator was reused in the steam production. Furthermore, the external cooling needed in the process was utilised in the steam production in both cases.

3.5 Cooling Cycle

Cooling of the Selexol solvent to 7.2°C and the recycle gas to the absorber to 20.09°C was not feasible with only the cooling water available at 15°C. Therefore, a cooling cycle with ammonia as the refrigerant was simulated. The cooling cycle consists of a compressor, an expansion valve, an evaporator and a condenser, as illustrated in Figure 3.6. The cooling was provided by cold ammonia in the evaporators, where the ammonia vaporised and produced the cooling effect. Then, the ammonia vapour exited the evaporator and was compressed. The ammonia vapour entered the condenser and was cooled and condensed to liquid ammonia. Finally, the ammonia was expanded to a lower pressure, and the cycle continued [41].

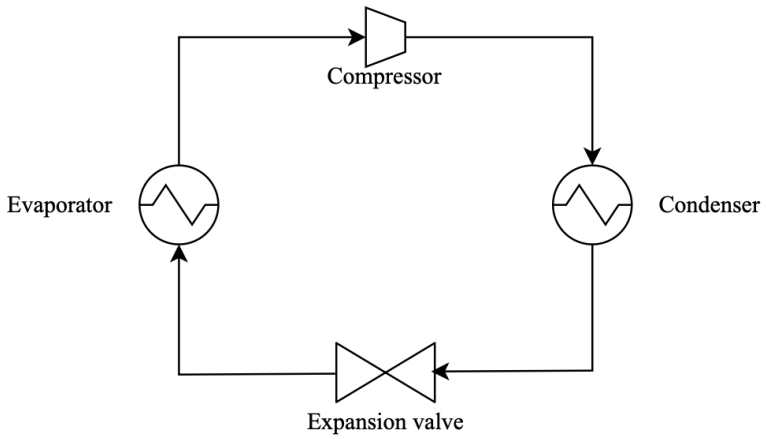

Figure 3.6: Flow sheet of the compression refrigeration cycle.

3.6 Cost Estimations

An essential basis for comparison of industrial plants is the cost estimation of their implementation and operation. The capital expenditures (CAPEX) estimates were based on data from the simulations in HYSYS, by using general sizing protocols based on the textbooks *Analysis, synthesis and design of chemical processes* by Turton et al. and *Chemical engineering design* by Sinnot and Towler, which are described in detail in Appendix E [37, 39]. In addition, historical values were used for specific unit operations and scaled based on the capacity of the equipment. The operating expenditures (OPEX) estimates were based on literature and HYSYS simulation values. In this thesis, the lifetime of the plant was assumed to be 20 years, with an annual operation of 8000 hours.

3.6.1 CAPEX

To obtain an estimate of the capital cost of a plant, the cost associated with the major process equipment was found. The capital cost is related to the capacity of the equipment by the equation,

$$C_2 = C_1\left(\frac{S_2}{S_1}\right)^n \tag{3.1}$$

where C_1 is the ISBL cost of a unit with capacity S_1, S_2 is the capacity of the new unit and n is the scaling-factor [37].

For preliminary estimates of the capital cost, the purchased equipment cost, C_e, can be calculated by the use of the following equation,

$$C_e = a + bS^n \tag{3.2}$$

where a and b are constants, n is the scaling-factor for the given equipment type and S is the sizing parameter. Then, the installed equipment cost was estimated by the factorial method given in equation (3.3) [37].

$$C = \sum_{i=1}^{i=M} C_{e,i,CS}[(1 + f_p)f_m + (f_{er} + f_{el} + f_i + f_c + f_s + f_l)] \tag{3.3}$$

where $C_{e,i,CS}$ is the purchased cost of equipment in carbon steel. Table 3.3 gives a description and the values for the different f-factors used in this thesis.

Table 3.3: Typical installation factors [37].

Parameter	Description	Value
f_p	Piping	0.8
f_m	Material, 304 stainless steel	1.3
f_{er}	Equipment erection	0.3
f_{el}	Electrical work	0.2
f_i	Instrumentation and process control	0.3
f_c	Civil engineering work	0.3
f_s	Structures and buildings	0.2
f_l	Lagging, insulation and paint	0.1

Finally, the cost was adjusted by taking inflation into account by the following equation,

$$C_2 = C_1\left(\frac{I_2}{I_1}\right) \tag{3.4}$$

where C_1 and C_2 are the cost in two different years, with their respective index I. This thesis used the Chemical Engineering Plant Cost Index (CEPCI) to scale the equipment cost to a 2022 basis.

Total Investment

The total investment cost required is the sum of the total fixed capital investment and the working capital. The inside battery limit (ISBL) cost was assumed to be the total installed equipment cost and the cost of the catalyst and adsorbent. The catalyst in the reformers and WGS reactor, as well as the adsorbent in the PSA, were assumed to be replaced every fifth year. Therefore,

considering the time value of money, the investment of the catalyst and adsorbent was determined based on the present value of the future investment. Then, the investment of the catalyst and adsorbent can be described by the following equation,

$$I_{cat} = I_1 + \frac{I_1}{(1+p)^5} + \frac{I_1}{(1+p)^{10}} + \frac{I_1}{(1+p)^{15}} \tag{3.5}$$

where I_1 is the total cost of the initial fill of catalyst and adsorbent, and p is the discount rate. The cost of the catalyst was calculated based on the estimated amount of catalyst and adsorbent in Table E.8 and the price of the catalyst and PSA adsorbent in Table 3.4.

The fixed capital investment, C_{FC}, was estimated through equation (3.6).

$$C_{FC} = C(1+OS)(1+D\&E+X) \tag{3.6}$$

where C is the ISBL cost, OS is the outside battery limit(OSBL)/offsite cost, $D\&E$ is the design and engineering cost, and X is the contingency charges. The OSBL cost was set to 0.3, $D\&E$ was set to 0.1, and X was set to 0.1. The working capital is the additional money needed to start and run the plant before it earns income. In this project, the working capital was set to 10% of the fixed investment cost in addition to the cost of the Selexol solvent and ammonia solution [37].

3.6.2 OPEX

The operating expenditures (OPEX) include variable and fixed operating costs. The variable operating costs are proportional to the production rate of the plant, and the fixed operating costs are incurred regardless of the production rate of the plant [37].

The variable operating cost was the cost of the natural gas, oxygen, water, Selexol solvent and carbon taxes, summarised in Table 3.4.

A description of the fixed operating costs is given in Table 3.5. Both process plants were assumed to operate with five shifts with an estimated number of operators per shift by equation (3.7) [53].

$$N_{\text{operators}} = (6.29 + 0.23N_{\text{units}})^{0.5} \tag{3.7}$$

where N_{units} is the number of major process equipment. The average salary for the process operators was based on 702,000 NOK (73,003.3 USD) [54].

Table 3.4: Values of raw material, catalysts, adsorbent material, solvents and carbon tax prices.

Variable	Value	Source
Natural gas	6.5 USD/MMBtu	[47]
Oxygen	0.17 USD/Nm^3 [1]	[48]
Cooling water	0.5 USD/tonne	[37]
Carbon tax	764 kr/tonne CO_2	[49]
Selexol	10.04 USD/L [1]	[50]
Ammonia	1,300 USD/tonne	[51]
Pre-reformer catalyst	44,143.4 USD/m^3 [1]	[52]
Reformer catalyst	15,891.6 USD/m^3 [1]	[52]
WGS catalyst	16950.8 USD/m^3 [1]	[52]
PSA Adsorbent	5297.2 USD/m^3 [1]	[52]

[1] Cost in 2018.

Table 3.5: Fixed operating costs.

	Description
Operating labour	73,003.3 USD · number of operators
Supervision	25% of operating labour
Direct salary	50% of operating labour + supervision
Maintenance	4% of ISBL
Property tax	2% of ISBL
Rent of land	2% of ISBL + OSBL
General plant overhead	65% of total labour + supervision

3.7 Profitability Analysis

As mentioned, the economic lifetime of the plant was set to 20 years. In this thesis, the tax was set to 22%, the declining-balance depreciation fraction was set to 0.2, and the discount rate was set to 6%. The profitability analysis was based on a hydrogen selling price of 2.2 USD/kg H_2. All calculations in the profitability analyses were done in Excel.

In the declining-balance depreciation method, the annual depreciation charge is a fixed fraction of the book value, F_d. The following equations give the depreciation, D_m, and book value,B_m, in year m.

$$D_m = C(1-F_d)^{m-1}F_d \tag{3.8}$$

$$B_m = C(1-F_d)^m \tag{3.9}$$

Where C is the depreciable value of the asset (the fixed capital investment), and B_m is the book value after m years of depreciation.

The net cash flow, CF, was calculated through the following equation,

$$CF = P \cdot (1-t_r) + D \cdot t_r \tag{3.10}$$

where P is the gross profit, D is the depreciation and t_r is the tax rate. The gross profit is the difference between annual revenues and annual operating costs.

To assess the economic viability of both process designs, the net present value (NPV) was calculated. The NPV of a project is a measure of economic performance, where a positive NPV indicate a profitable project. The NPV of a project is the sum of the present values of the future cash flows and was calculated by equation (3.11).

$$\text{NPV} = \sum_{i=0}^{n} \frac{CF_i}{(1+p)^i} \tag{3.11}$$

where CF_n is the cash flow in year i, n is the economic lifetime of the project and p is the discount rate. The internal rate of return (IRR) is defined as the rate that makes the NPV equal to zero [37].

A simplified method to calculate the pay-back time is to assume that all the investment is made in year 0 and the revenues begin immediately. In addition, it neglects taxes and depreciation [37]. The simple pay-back time was calculated as follows,

$$\text{Simple pay-back time} = \frac{\text{total investment}}{\text{average annual cash flow}} \tag{3.12}$$

Sensitivity analyses were performed for both cases to explore the impact of a change in feedstock prices, solvent prices, carbon tax and ISBL investment on the levelised cost of hydrogen (LCOH). These sensitivity analyses were carried out by increasing and decreasing the cost.

3.7.1 Levelised Cost of Hydrogen

The levelised cost of hydrogen (LCOH) is the discounted lifetime cost of building and operating a hydrogen production plant, expressed as cost per kg produced hydrogen. The main purpose of the LCOH is to provide a simple comparison of hydrogen production technologies [55]. The levelised cost of hydrogen (LCOH) was calculated based on the annuity method presented by

Kost et al. [56]. By assuming constant annual hydrogen production and constant annual operating costs over the lifetime of the plant, the LCOH was calculated by the following equation;

$$\mathrm{LCOH} = \frac{(I_0 \cdot ANF) + A}{M} \tag{3.13}$$

where A are the annual operating costs, M are the amount of hydrogen produced annually, and the ANF are the annuity factor given by equation (3.14).

$$ANF = \frac{p(1+p)^n}{(1+p)^n - 1} \tag{3.14}$$

where n is the economic lifetime of the process plant and p is the discount rate [56]. The discount rate was assumed to be 6% in both cases.

Chapter 4

Results and Discussion

In this chapter, the simulation results, the cost estimations and profitability analyses are presented and discussed. First, the results from the process simulations are given. Then, the result from the sizing and cost estimations of both cases are presented. Subsequently, the results from the profitability analyses and sensitivity analyses are given. Finally, a comparison of the two process configurations is given.

4.1 Case 1 - GHR and ATR

In the first process configuration, case 1, a GHR was coupled with an ATR. The process flow diagram (PFD) of the process is given in Figure 4.1, and a picture of the simulation model is given in Figure A.3. An overview of the compositions and operating conditions of the streams in the PFD is given in Table 4.2.

The carbon capture plant is an essential part of the production of blue hydrogen. The carbon capture performance of the Selexol solvent was studied as a function of the L/G ratio, as shown in Figure 3.5. As illustrated, a 100% capture rate of the CO_2 present in the synthesis gas was not achievable. Therefore, to accomplish an overall capture rate of 95%, the amount of CO_2 in the flue gas needed to be reduced to an absolute minimum. As a result, parts of the PSA off-gas were recycled back into the process. The off-gas consists of reactants in the reforming reactions and the water-gas shift reaction, CO, CO_2, hydrogen, water, and methane. In addition, the PSA off-gas contains a small part of nitrogen, which is inert. Therefore, by recycling, the natural gas efficiency increased. Figure 4.2 gives the PFD of the Selexol process in case 1. The values and results from the carbon capture process are summarised in Table 4.4, and the composition and operating conditions of the main streams in the carbon capture process are given in Table 4.3.

Since the simulation was performed in Aspen HYSYS, the conservation of mass and energy was controlled to conclude whether the simulation was reasonable. The overall mass and energy

balance of the process was found to be 0.011% and 0.089%, respectively. This imbalance was assumed to be acceptable, and the calculations are given in Appendix B.

The feed streams in the process are natural gas, steam, oxygen and air. Based on the given production rate of 500 tonnes of hydrogen per day, 3,319 kmol/h of natural gas, 10,287 kmol/h of steam, 1,779 kmol/h of oxygen and 2,690 kmol/h of air was needed, as summarised in Table 4.1.

Table 4.1: Overview of the total amount, temperature and pressure of the feed streams in case 1, with a GHR and an ATR.

Feed	Amount [kmol/h]	Temperature [°C]	Pressure [bar]
Natural gas	3,319	70	50
Steam	10,287	245.1	36
Oxygen	1,779	250	34
Air	2,690	20	1.013

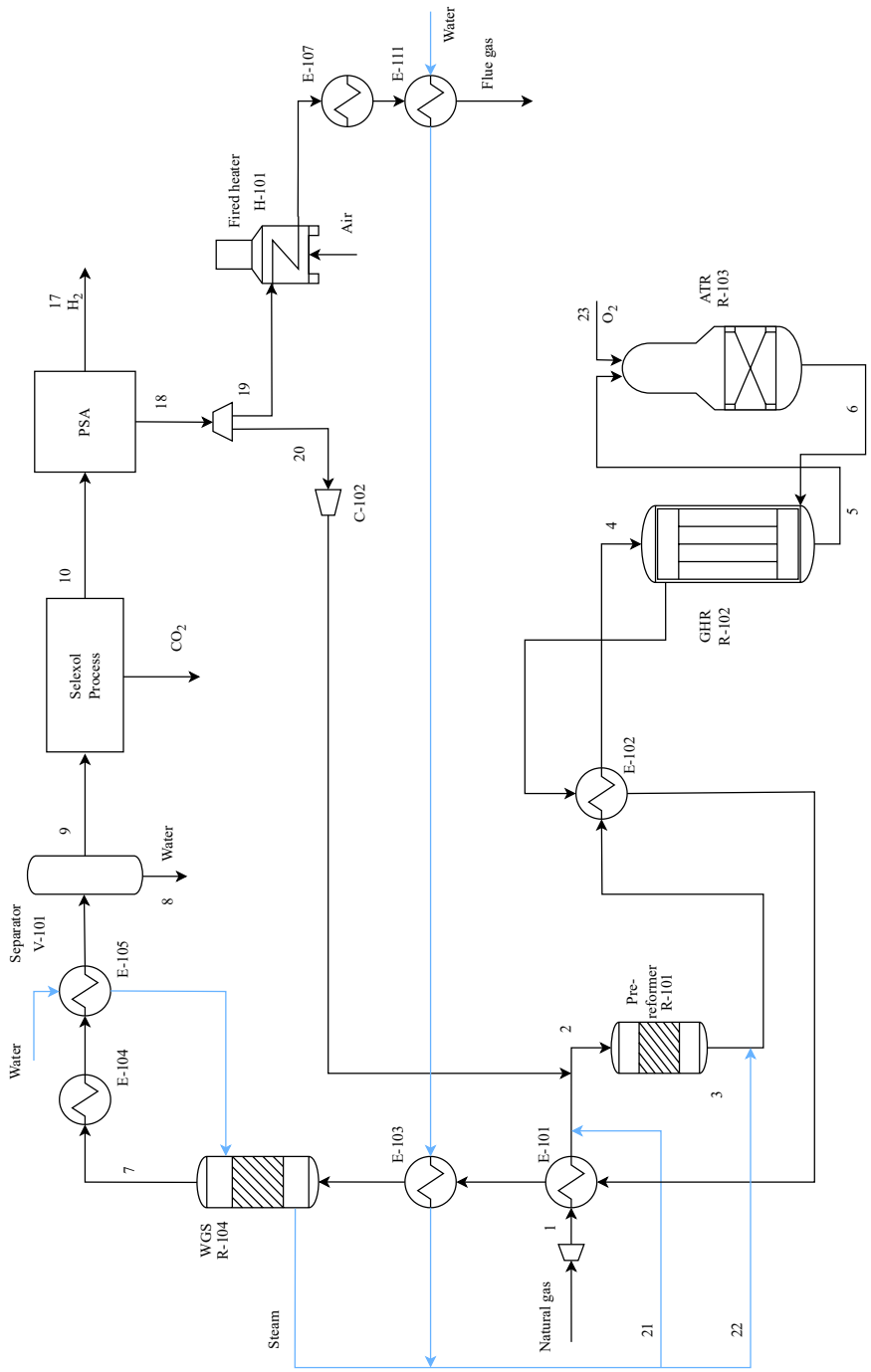

Figure 4.1: Process flow diagram of case 1 with a gas heated reformer (GHR) and an autothermal reformer (ATR). The light blue lines indicate water/steam flows. The heat integration is integrated in this PFD.

Table 4.2: Overview of temperature, pressure, molar flow, mass flow and composition of the main streams in the process flow diagram of case 1 with a GHR and an ATR.

Stream Number	Natural gas	1	2	3	4	5	6	7	8	9
Temperature [°C]	70	400	375.8	491.3	347.3	750	1,200	300	40	40
Pressure [bar]	50	36	36	35.5	35.5	34.5	33.5	33	32	32
Molar flow [kmol/h]	3,319	3,319	5,430	5,463	14,610	17,916	22,078	22,078	6,385	15,693
Mass flow [tonnes/h]	61.89	61.89	94.15	94.15	258.9	258.9	315.9	315.9	115.4	200.4
Vapour fraction	1	1	1	1	1	1	1	1	0	1
Mole fraction [-]										
Hydrogen	0	0	0.1269	0.0617	0.0231	0.3436	0.4009	0.5237	0	0.7368
Methane	0.8874	0.8874	0.5428	0.6838	0.2557	0.1163	0.0002	0.0002	0	0.0002
Ethane	0.057	0.057	0.0349	0.0001	0.0001	0	0	0	0	0
Propane	0.02	0.02	0.0122	0	0	0	0	0	0	0
Butane	0.009	0.009	0.0055	0	0	0	0	0	0	0
Pentane	0.003	0.003	0.0018	0	0	0	0	0	0	0
Hexane	0.003	0.003	0.0018	0	0	0	0	0	0	0
Oxygen	0	0	0	0	0	0	0	0	0	0
Nitrogen	0.0055	0.0055	0.0082	0.0082	0.0031	0.0025	0.002	0.002	0	0.0028
Water	0	0	0.21	0.1876	0.6962	0.4246	0.4133	0.2905	0.9974	0.0029
Carbon monoxide	0	0	0.0183	0.0032	0.0012	0.0424	0.1305	0.0077	0	0.0108
Carbon dioxide	0.015	0.015	0.0375	0.0553	0.0207	0.0677	0.0531	0.1759	0.0025	0.2465
Stream Number	10	11	16	17	19	20	21	22	23	CO2
Temperature [°C]	7.543	17.71	7.22	7	4.942	4.942	245.1	245.1	250	66.89
Pressure [bar]	32	32	32	31	2.5	2.5	36	36	34	1.013
Molar flow [kmol/h]	11,953	16,140.2	12,300	10,334.58	647.3	971	1,140	9,147	1,779	3,742
Mass flow [tonnes/h]	40.38	3223.9	3060.87	20.83	7.82	11.73	20.54	164.8	56.94	160.1
Vapour fraction	1	0	0	1	1	1	1	1	1	1
Mole fraction [-]										
Hydrogen	0.9607	0.007	0	1	0.7096	0.7096	0	0	0	0.0212
Methane	0.0003	0	0	0	0.002	0.002	0	0	0	0.0001
Ethane	0	0	0	0	0	0	0	0	0	0
Propane	0	0	0	0	0	0	0	0	0	0
Butane	0	0	0	0	0	0	0	0	0	0
Pentane	0	0	0	0	0	0	0	0	0	0
Hexane	0	0	0	0	0	0	0	0	0	0
Oxygen	0	0	0	0	0	0	0	0	1	0
Nitrogen	0.0037	0.0001	0	0	0.0272	0.0272	0	0	0	0.0002
Water	0.0001	0.0822	0.1042	0	0.0004	0.0004	1	1	0	0.0124
Carbon monoxide	0.0215	0.0003	0	0	0.1022	0.1022	0	0	0	0.001
Carbon dioxide	0.0138	0.2403	0.0163	0	0.1586	0.1586	0	0	0	0.9652
DEPG	0	0.6702	0.8795	0	0	0	0	0	0	0

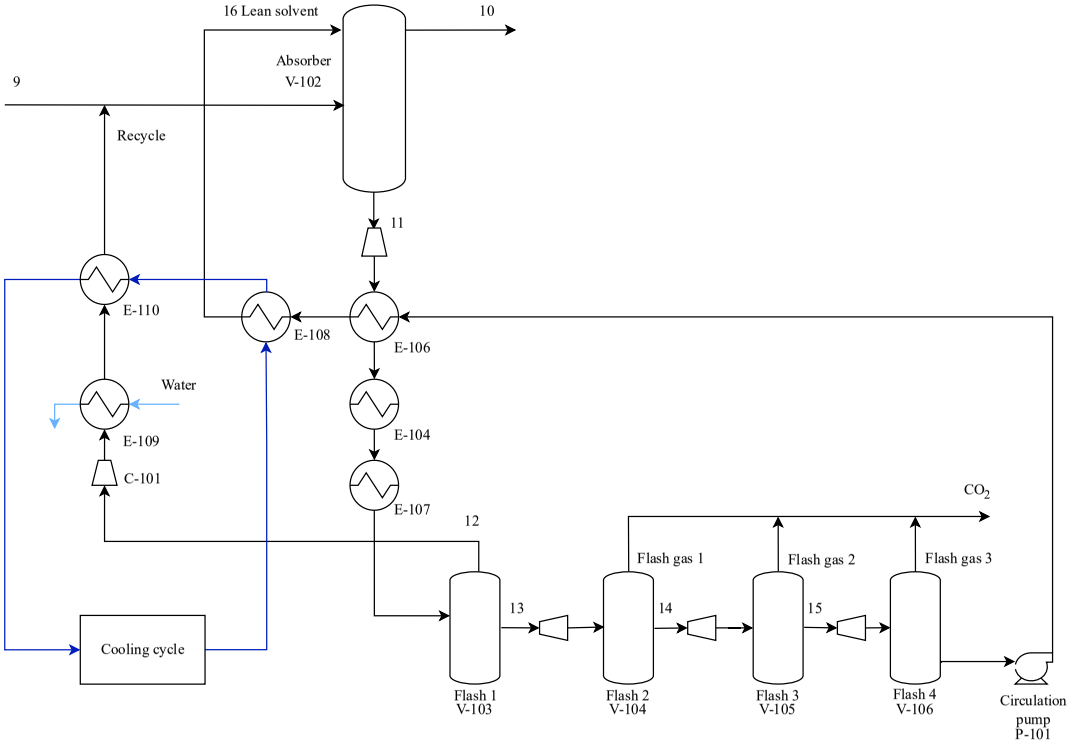

Figure 4.2: Process flow diagram of the Selexol process in case 1 (GHR and ATR). The light blue lines indicate water/steam flows, and the dark blue lines indicate ammonia. The heat integration is integrated in this PFD.

Table 4.3: Operating condition and composition of the streams in the regeneration process of the Selexol solvent in case 1, with a GHR and an ATR.

Stream Number	12	13	Flash gas 1	14	Flash gas 2	15	Flash gas 3
Temperature [°C]	75	75	72.76	72.76	71.98	71.98	70.06
Pressure [bar]	29.19	29.19	10	10	6.895	6.895	1.013
Molar flow [kmol/h]	100	15,971	1,960	14,011	560	13,451	1,221
Mass flow [tonnes/h]	2.997	3,219	82.79	3,136	24.5	3,111	52.85
Vapour fraction	1	0	1	0	1	0	1
Mole fraction [-]							
Hydrogen	0.3298	0.005	0.039	0.0002	0.0047	0	0.0002
Methane	0.0002	0	0.0001	0	0	0	0
Ethane	0	0	0	0	0	0	0
Propane	0	0	0	0	0	0	0
Butane	0	0	0	0	0	0	0
Pentane	0	0	0	0	0	0	0
Hexane	0	0	0	0	0	0	0
Oxygen	0	0	0	0	0	0	0
Nitrogen	0.0017	0	0.003	0	0.0001	0	0
Water	0.0015	0.079	0.0036	0.0896	0.0049	0.0931	0.0291
Carbon monoxide	0.0075	0.0002	0.0018	0	0.0004	0	0
Carbon dioxide	0.6592	0.2386	0.9552	0.1384	0.9898	0.1029	0.9706
DEPG	0	0.6771	0	0.7718	0	0.804	0.0001

Table 4.4: An Overview of the specifications of the absorption and desorption in the carbon capture process in case 1, with a GHR and an ATR.

Absorption	
Absorbent	Selexol (DEPG)
Pressure	32 bar
Inlet absorbent flow	3,059 tonnes/h
Inlet gas flow	200.4 tonnes/h
Stages	15
L/G ratio	15.26
Desorption	
Flash 1	29.19 bar
Flash 2	10 bar
Flash 3	6.895 bar
Flash 4	1.013 bar

4.1.1 Energy Efficiency

In this thesis, the natural gas efficiency was defined as the lower heating value (LHV) of the hydrogen product divided by the lower heating value of the natural gas feed, as illustrated in equation (4.1). In case 1, the natural gas efficiency was calculated to be 85.5%.

$$\text{Natural Gas Efficiency} = \frac{\text{LHV}_{\text{Hydrogen}}}{\text{LHV}_{\text{Natural gas}}} \tag{4.1}$$

The energy efficiency was defined as the lower heating value of the products divided by the lower heating value of the natural gas feed and the external duty needed for the compressors and pumps in the process, as shown in equation (4.2). In case 1, 82.68% of the energy ended up in the hydrogen product, 3.35% was used in excess steam production, and 13.97% was lost in the process, as illustrated in Figure 4.3. The values used in the calculations are given in Appendix C.

$$\text{Energy Efficiency} = \frac{\text{LHV}_{\text{Hydrogen}}}{\text{LHV}_{\text{Natural gas}} + W_c} \tag{4.2}$$

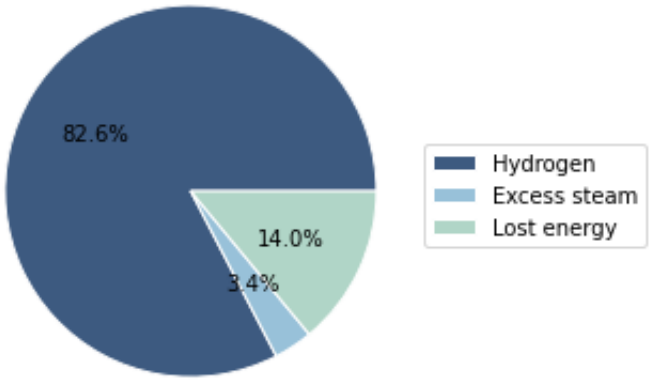

Figure 4.3: Overview of the energy in case 1, with a GHR and an ATR.

4.1.2 Heat Integration

A heat exchanger network was designed for case 1, as shown in Figure 4.4. An overview of the streams included, the supply and target temperatures, and the heat flows are given in Table 4.5. The heat capacities for the streams were assumed to be constant in the given temperature interval. The steam required in the process was included in the heat integration.

As illustrated in Table 4.6, the process did not need external heating when heat integration (HI) was included. In addition, the external cooling demand in the process was reduced by 448.36 MW. As shown in Figure 4.5, the external duty in E-111 and E-103 was used in steam production. The external cooling of stream 16, E-108, was performed by a cooling cycle, as described in section 4.1.4.

The heat recovery pinch was found to be the highest available temperature, 1,251°C, by using the problem table algorithm. The calculations and the grand composite curve are given in Appendix D.

Table 4.5: Overview of the heat demand and the heat available in case 1, with a GHR and an ATR.

Heat available			
Stream nr.	Supply temp. [°C]	Target temp. [°C]	Heat Load [MW]
Flue gas	1,251	100	34.29
6	1,200	300	204
7	300	40	129.1
16	70.17	7.22	118.53
WGS	-	-	29.1
Heat demand			
Stream nr.	Supply temp. [°C]	Target temp. [°C]	Heat Load [MW]
1	51.2	400	16.96
4	347.3	600	46.5
11	17.62	75	116.9
Water	26.25	245.1	143.2
GHR	-	-	124.8
Total excess heat			66.66 MW

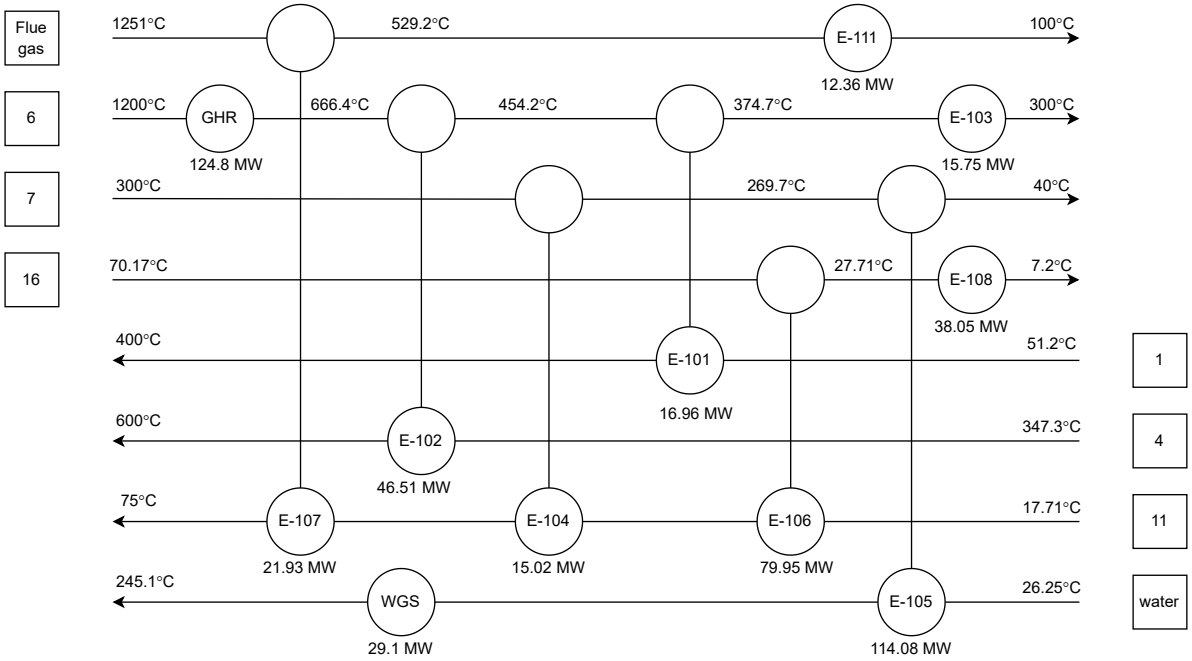

Figure 4.4: Proposed heat exchanger network for case 1 with a GHR and an ATR.

Table 4.6: Overview of the total external heating and cooling demand in case 1 (GHR and ATR) with and without heat integration.

	Without HI	With HI
Cooling demand [MW]	515.02	66.66
Heating demand [MW]	448.36	0

4.1.3 Steam Production

In the process, 115 tonnes/h of water was separated prior to the carbon capture plant. As illustrated in Figure 4.5, this water was reused in the process. The total steam demand in the process was 185.34 tonnes/h, which means that the total amount of water needed to produce the required steam was reduced by approximately 60%.

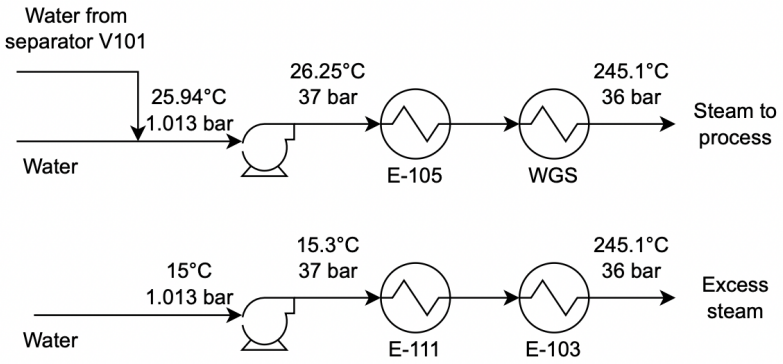

Figure 4.5: Overview of the steam production in the first process configuration with a GHR and an ATR (case 1).

4.1.4 Cooling Cycle

The recycle stream in the Selexol process was cooled to 20.09°C before it was recycled to the absorber column. Due to both low duty and low temperatures, this stream was not included in the heat integration. The recycle stream was cooled first with cooling water (E-109) and then with ammonia (E-110) in the cooling cycle. The Selexol solvent was cooled from 70.17 to 7.2°C before it was fed to the absorber column. As shown in Figure 4.4, the stream was heat integrated, so external cooling was needed from 27.71 to 7.2°C with a duty of 38.58 MW (E-108). This thesis used a cooling cycle with ammonia, as illustrated in Figure 4.6. The cooling cycle was assumed to be a closed system where the heat from the Selexol solvent evaporates the ammonia solution. Then, ammonia vapour was compressed into a liquid, cooled and expanded. The amount of ammonia needed in the cooling cycle was found in HYSYS to be 131.1 tonnes/h.

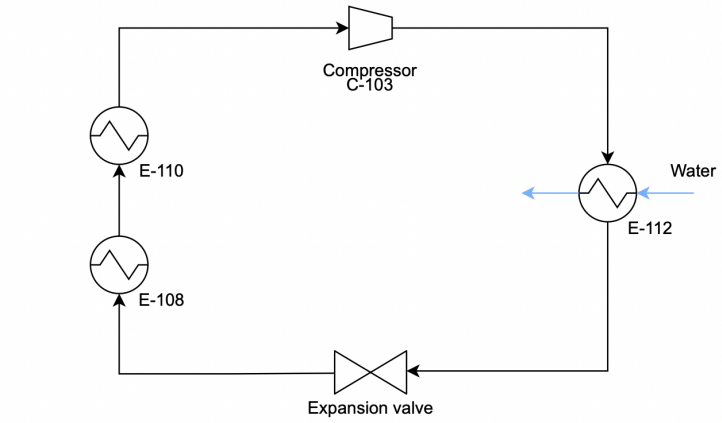

Figure 4.6: Flow sheet of the cooling cycle in both process configurations with ammonia to cool the Selexol solvent to 7.22°C and the recycle gas to 20.09°C.

4.2 Case 2 - ATR

The process flow diagram of the process is given in Figure 4.7, and a picture of the HYSYS simulation model is given in Figure A.6. Table 4.8 gives an overview of the compositions and operating conditions of the main streams in the PFD. The PFD of the Selexol process in case 2 is given in Figure 4.8. The values and results from the carbon capture process are summarised in Table 4.10. The composition and operating conditions of the main streams in the carbon capture process are given in Table 4.9.

Like the previous case, the overall mass and energy balance was controlled. In this case, the mass and energy balance was found to be -0.0096% and -0.0093%, respectively. The imbalance was assumed to be acceptable, and the calculations are given in Appendix B.

The feed streams in the process are natural gas, steam, oxygen and air. Based on a production of 500 tonnes/day of hydrogen, 3,673 kmol/h of natural gas, 8,612 kmol/h of steam, 2,479 kmol/h of oxygen and 2,446 kmol/h of air was needed, as presented in Table 4.7.

Table 4.7: Overview of the total amount, temperature and pressure of the feed streams in case 2 with an ATR.

Feed	Amount [kmol/h]	Temperature [°C]	Pressure [bar]
Natural gas	3,673	70	50
Steam	8,612	245.1	36
Oxygen	2,497	250	34
Air	2,446	20	1.013

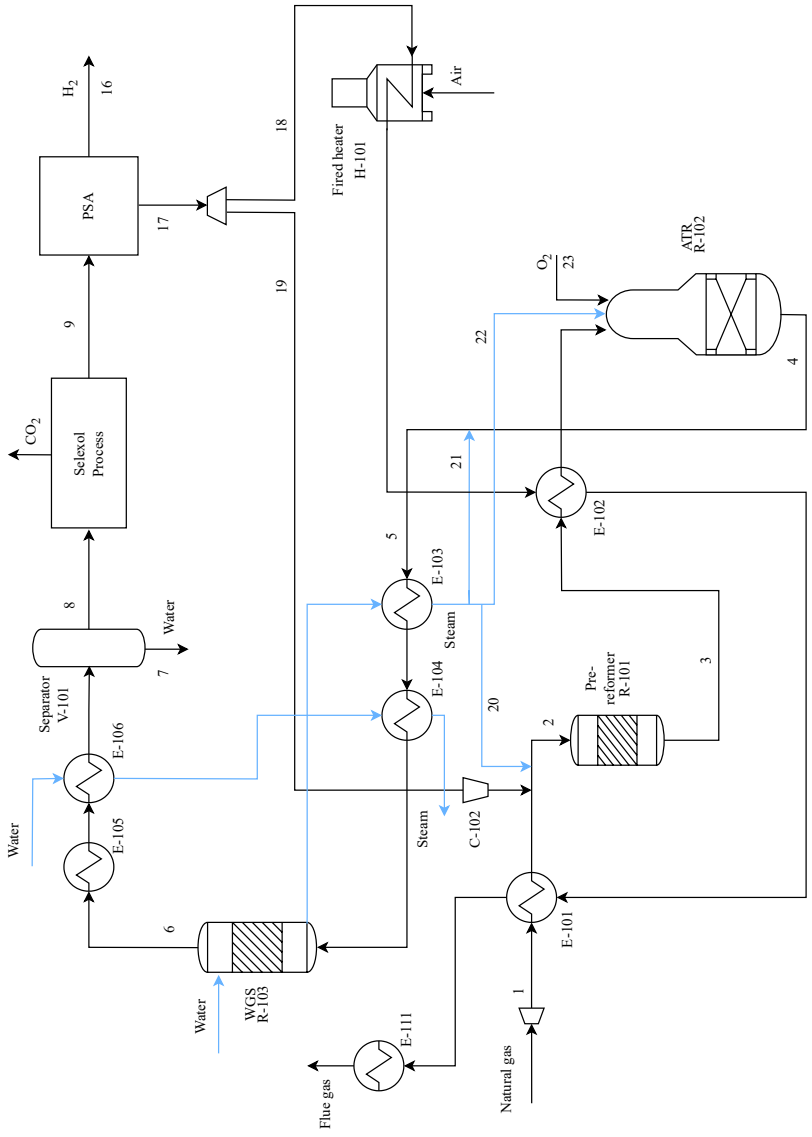

Figure 4.7: Process flow diagram of case 2 with an autothermal reformer (ATR). The light blue lines indicate water/steam flows. The heat integration is integrated in this PFD.

Table 4.8: Overview of temperature, pressure, molar flow, mass flow and composition of the main streams in the process flow diagram of case 2, with an ATR.

Stream Number	Natural gas	1	2	3	4	5	6	7	8	9
Temperature [°C]	70	51.2	373.7	484.7	1112	846.8	300	39.95	39.95	7.339
Pressure [bar]	50	36.5	36	35.5	33.5	33.5	32.5	31.5	31.5	32
Molar flow [kmol/h]	3673	3673	6029	6089	15594.6	21538.63	21538.63	5414	16125.1	12008.93
Mass flow [tonnes/h]	68.5	68.5	104.6	104.6	208.2	315.3	315.3	97.89	217.4	40.34
Vapour fraction	1	1	1	1	1	1	1	0	1	1
Mole fraction [-]										
Hydrogen	0	0	0.1143	0.0599	0.5131	0.3715	0.5362	0	0.7161	0.9562
Methane	0.8874	0.8874	0.5471	0.6832	0.0043	0.0031	0.0031	0	0.0042	0.0053
Ethane	0.057	0.057	0.0347	0.0001	0	0	0	0	0	0
Propane	0.02	0.02	0.0122	0	0	0	0	0	0	0
Butane	0.009	0.009	0.0055	0	0	0	0	0	0	0
Pentane	0.003	0.003	0.0018	0	0	0	0	0	0	0
Hexane	0.003	0.003	0.0018	0	0	0	0	0	0	0
Oxygen	0	0	0	0	0	0	0	0	0	0
Nitrogen	0.0055	0.0055	0.0082	0.0081	0.0032	0.0023	0.0023	0	0.0031	0.0041
Water	0	0	0.224	0.1939	0.1955	0.4175	0.2529	0.9973	0.0029	0
Carbon monoxide	0	0	0.021	0.0027	0.2412	0.1747	0.01	0	0.0133	0.0175
Carbon dioxide	0.015	0.15	0.0294	0.052	0.0427	0.0309	0.1956	0.0026	0.2604	0.0168
Stream Number	10	15	16	18	19	20	21	22	23	CO2
Temperature [°C]	18.11	7.22	7	4.565	4.565	245.1	245.1	245.1	250	67.37
Pressure [bar]	32	32	31	2.5	2.5	36	35.5	34	34	1.013
Molar flow [kmol/h]	17229.1	12912.96	10334.6	669.7	1005	1350	1318	5944	2497	4116
Mass flow [tonnes/h]	3430	3246	20.83	7.804	11.71	24.32	23.74	107.1	79.89	177.1
Vapour fraction	0	0	1	1	1	1	1	1	1	1
Mole fraction [-]										
Hydrogen	0.0068	0	1	0.6858	0.6858	0	0	0	0	0.0158
Methane	0.0003	0	0	0.0382	0.0382	0	0	0	0	0.0003
Ethane	0	0	0	0	0	0	0	0	0	0
Propane	0	0	0	0	0	0	0	0	0	0
Butane	0	0	0	0	0	0	0	0	0	0
Pentane	0	0	0	0	0	0	0	0	0	0
Hexane	0	0	0	0	0	0	0	0	0	0
Oxygen	0	0	0	0	0	0	0	0	1	0
Nitrogen	0.0001	0	0	0.0292	0.0292	0	0	0	0	0.0002
Water	0.0735	0.0944	0	0.0003	0.0003	1	1	1	0	0.0111
Carbon monoxide	0.0003	0	0	0.1258	0.1258	0	0	0	0	0.001
Carbon dioxide	0.2526	0.2526	0	0.1207	0.1207	0	0	0	0	0.971
DEPG	0.6664	0.8891	0	0	0	0	0	0	0	0

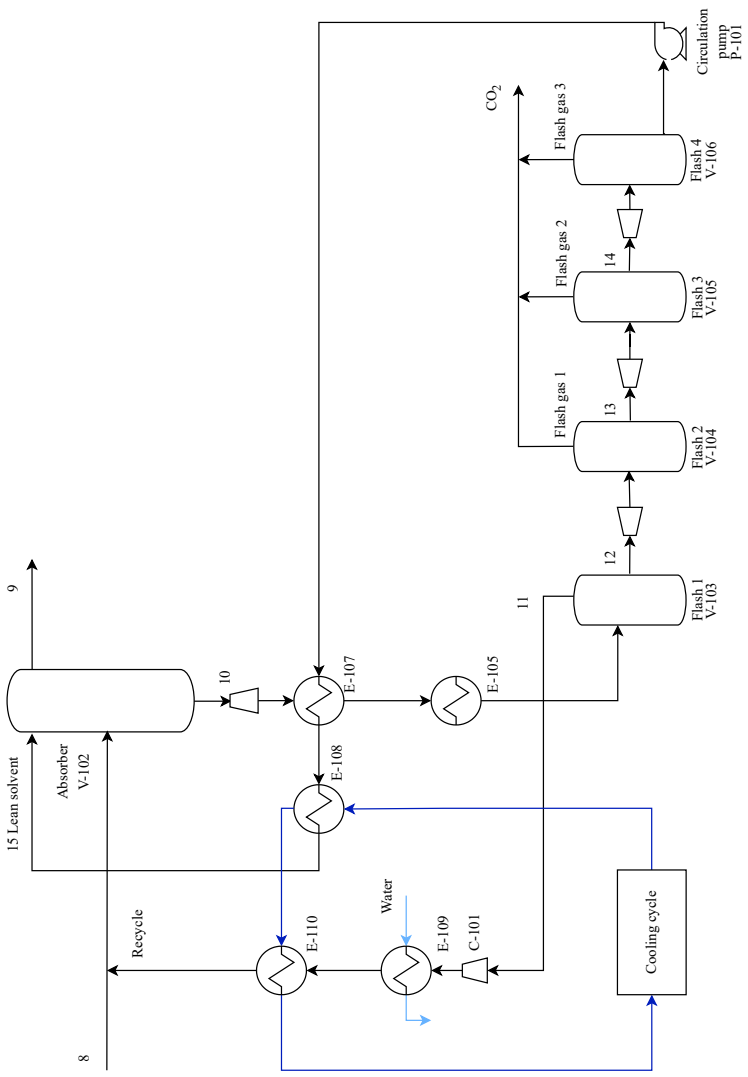

Figure 4.8: Process flow diagram of the Selexol process in case 2 with an ATR. The light blue lines indicate water/steam flows and the dark blue lines indicate ammonia. The heat integration is integrated in this PFD.

Table 4.9: Operating condition and composition of the streams in the regeneration process of the Selexol solvent in case 2, with an ATR.

Stream Number	11	12	Flash gas 1	13	Flash gas 2	14	Flash gas 3
Temperature [°C]	75	75	72.52	72.52	71.71	71.71	69.79
Pressure [bar]	27.55	27.55	10	10	6.895	6.895	1.013
Molar flow [kmol/h]	200	17,029	2,198	14,831	616	14,215	1,301
Mass flow [tonnes/h]	6.512	3,423	93.77	3,329	26.94	3,302	56.37
Vapor fraction	1	0	1	0	1	0	1
Mole fraction [-]							
Hydrogen	0.2649	0.0038	0.0285	0.0001	0.0033	0	0.0001
Methane	0.0044	0.0002	0.0015	0	0.0005	0	0.0001
Ethane	0	0	0	0	0	0	0
Propane	0	0	0	0	0	0	0
Butane	0	0	0	0	0	0	0
Pentane	0	0	0	0	0	0	0
Hexane	0	0	0	0	0	0	0
Oxygen	0	0	0	0	0	0	0
Nitrogen	0.0016	0	0.0003	0	0.0001	0	0
Water	0.0015	0.0743	0.0034	0.0848	0.0046	0.0883	0.0273
Carbon monoxide	0.0085	0.0002	0.0018	0	0.0004	0	0
Carbon dioxide	0.719	0.2472	0.9646	0.1408	0.9911	0.104	0.9723
DEPG	0	0.6742	0	0.7742	0	0.8077	0.0001

Table 4.10: Overview of the specification of the absorption and desorption process in the carbon capture process in case 2, with an ATR.

Absorption	
Absorbent	Selexol (DEPG)
Pressure	32 bar
Inlet absorbent flow	3,246 tonnes/h
Inlet gas flow	217.4 tonnes/h
Stages	15
L/G ratio	14.93
Desorption	
Flash 1	27.55 bar
Flash 2	10 bar
Flash 3	6.895 bar
Flash 4	1.013 bar

4.2.1 Energy Efficiency

In the second case, the natural gas efficiency was calculated to be 77.3%. In the process, 74.7% of the total energy ended up in the hydrogen product, 12.1% was used for excess steam production, and 13.2% was lost, as illustrated in Figure 4.9. The values used in the energy efficiency calculations are given in Appendix C.

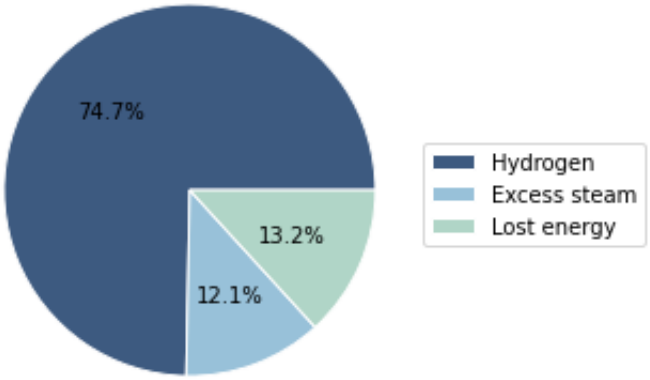

Figure 4.9: Overview of the energy in case 2 with an ATR.

4.2.2 Heat Integration

A heat exchanger network was designed for case 2, as shown in Figure 4.10. An overview of the streams included, the supply and target temperatures, and the heat flows are given in Table 4.11. Like the previous case, the heat capacities were assumed to be constant in the given temperature interval. The steam required in the process was included in the heat integration, where water was pumped to 36 bar and heated to 245.1°C.

As illustrated in Table 4.12, the process did not need external heating when heat integration (HI) was included. In addition, the external cooling demand in the process was reduced by 272 MW. The external duty in E-104 and E-106 was used in steam production, as shown in Figure 4.11. The external cooling of stream 15, E-108, was performed by a cooling cycle with ammonia, as described in section 4.1.4.

The heat recovery pinch was found to be 1,542°C by using the problem table algorithm. The calculations and the grand composite curve are given in Appendix D.

Table 4.11: Overview of the heat demand and the heat available in case 2 with an ATR.

Heat available			
Stream nr.	Supply temp. [°C]	Target temp. [°C]	Heat Load [MW]
Flue gas	1542	100	41.43
5	848.1	300	116.9
6	300	40	116.5
15	69.94	7.22	125.1
WGS	-	-	38.11
Heat demand			
Stream nr.	Supply temp. [°C]	Target temp. [°C]	Heat Load [MW]
1	51.2	400	18.79
3	484.5	600	11.08
10	17.9	75	123.6
Water	30.68	245.1	119
Total excess heat			165.57 MW

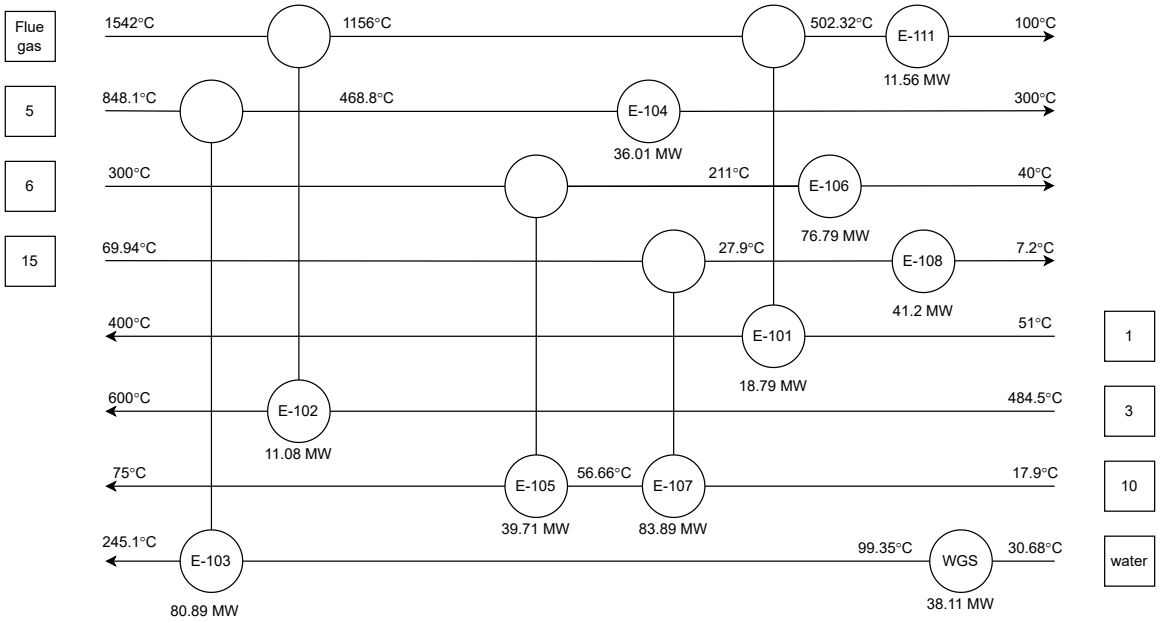

Figure 4.10: Proposed heat exchanger network for case 2 with an ATR.

Table 4.12: Overview of the total external heating and cooling demand in case 2 (ATR), with and without heat integration.

	Without HI	With HI
Cooling demand [MW]	438.04	165.57
Heating demand [MW]	272.47	0

4.2.3 Steam Production

Like the previous case, water was separated prior to the carbon capture process and reused in steam production. In the process, 97.27 tonnes/h of water was separated and reused to produce the required steam for the process, as shown in Figure 4.11. The total steam demand in case 2 was 155.16 tonnes/h, which means that the water needed in the required steam production was reduced by approximately 60%. In addition, in order to exploit the excess heat in the process, excess steam was produced.

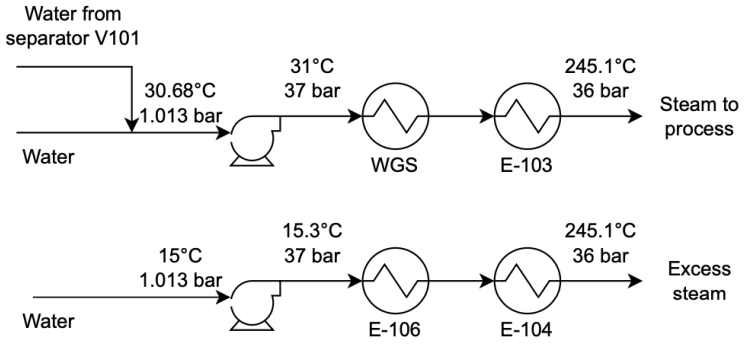

Figure 4.11: Overview of the steam production in case 2 with an ATR.

4.2.4 Cooling Cycle

The cooling cycle in Case 2 is identical to the cooling cycle in case 1, as described in section 4.1.4 and shown in Figure 4.6. In this case, 132.8 tonnes/h of ammonia was needed in the cooling cycle.

4.3 Equipment Sizing

The size of the different process equipment was calculated and is summarised in Table 4.13. A detailed calculation of the sizing of the different equipment is given in Appendix E. In this thesis, all equipment was assumed to be made of 304 stainless steel, with a density of 8000

kg/m^3 [37]. The sizing parameters for the main equipment in both cases are summarised in Table 4.13. The sizing parameters for the GHR are given in Table 4.14.

Table 4.13: Overview of the sizing of the different equipment in case 1 (GHR and ATR) and case 2 (ATR).

Equipment	Tag nr.	Case 1	Case 2	Unit
Pre-reformer	R-101	103.57	115.06	tonnes/h
ATR	R-103/2	347.49	229.24	tonnes/h
WGS reactor	R-104/3	8339.76	8329.2	tonne/day
Separator	V-101	20.34	20.08	tonne
Absorber	V-102	74.09	78.55	tonne
Flash tank 1	V-103	275.72	277.02	tonne
Flash tank 2	V-104	90.25	95.94	tonne
Flash tank 3	V-105	61.49	65.23	tonne
Flash tank 4	V-106	8.77	9.59	tonne
PSA	-	22913	22913	kg H_2/h
Fired heater	H-101	135.74	164.06	GJ/h
Compressor 1	C-101	10.5	34.3	kW
Compressor 2	C-102	3841.2	3989.7	kW
Compressor 3	C-103	23397	26356	kW
Circulation pump	P-101	850	902	L/s
Heat exchanger 1	E-101	250.03	70.7	m^2
Heat exchanger 2	E-102	1251.25	30.8	m^2
Heat exchanger 3	E-103	603	297.7	m^2
Heat exchanger 4	E-104	118.22	699.6	m^2
Heat exchanger 5	E-105	5837.94	371.64	m^2
Heat exchanger 6	E-106	23952.8	8146.3	m^2
Heat exchanger 7	E-107	49.65	24184.4	m^2
Heat exchanger 8	E-108	1056	1560	m^2
Heat exchanger 9	E-109	8.2	17.4	m^2
Heat exchanger 10	E-110	0.13	0.5	m^2
Heat exchanger 11	E-111	255	172.7	m^2
Heat exchanger 12	E-112	1087	1017.2	m^2

Table 4.14: Sizing of the gas heated reformer (GHR).

Duty [MW]	137.28
Length [m]	12
Shell mass [tonne]	166.18

4.4 Cost Estimations

This section includes the capital expenditures (CAPEX) and operating expenditures (OPEX) estimates for both process configurations.

4.4.1 CAPEX

The purchased and installed equipment cost for the main equipment in both cases is given in Table 4.15. The equations and correlations used in the equipment cost estimation are given in section 3.6. As mentioned, all the process equipment was assumed to be made of stainless steel. However, the cost correlations used are given for carbon steel equipment. Consequently, the purchased equipment cost is given for carbon steel equipment, while the installed equipment cost is given for equipment made of stainless steel.

Table 4.15: Purchased and installed cost of the main equipment in case 1 (GHR and ATR) and case 2 (ATR). (All values in MUSD).

	Case 1		Case 2	
Equipment	Purchased	Installed	Purchased	Installed
Pre-reformer	-	2.08	-	2.21
GHR	-	43.6	-	-
ATR	-	8.42	-	6.56
WGS reactor	-	14.07	-	14.06
Separator	0.52	1.95	0.52	1.93
Flash tanks	7.34	25.64	7.53	28.14
Absorber	3.1	11.59	3.27	12.21
PSA	-	26.29	-	26.29
Fired heater	-	6.36	-	7.12
Heat exchangers	7.81	29.23	8.42	31.48
Pumps	0.25	0.94	0.27	1.02
Compressors	17.45	65.28	18.49	69.14
Catalyst and adsorbent	-	32.95	-	27.92
Total ISBL investment		268.39		228.08

Since the GHR is a relatively novel technology, obtaining an accurate cost estimate of the reformer is difficult. Still, it is possible to provide an estimate based on available data. In this thesis, the GHR was cost estimated based on a conventional steam methane reformer (SMR) and by subtracting the cost of a box furnace and adding the cost of a pressure vessel, which resulted in an installed cost of 43.6 MUSD. This estimate has a high degree of uncertainty; however, it is assumed to be adequate as a preliminary cost estimate.

The total investment is the sum of the fixed capital investment and the working capital investment. As summarised in Table 4.16, the total investment in case 1 and 2 was 530.6 and 456.95 MUSD, respectively.

Table 4.16: Total investment in both cases. (All values in MUSD).

Cost	Case 1	Case 2
Total ISBL investment	268.39	228.08
OSBL	80.52	68.42
Design and engineering	80.52	68.42
Contingency	26.84	22.81
Fixed capital investment	456.27	387.74
Working capital	74.33	69.22
Total investment	530.6	456.95

The contribution to the ISBL investment in case 1 and case 2 is illustrated in Figure 4.12. The equipment included in the synthesis gas production is the reformers, the WGS reactor and the separator. The carbon capture process includes the flash tanks and the absorber. The heat exchanger part includes all the heat exchangers in the processes. In case 1 and 2, the synthesis gas production count for 26.1% and 10.9% of the total ISBL investment, respectively. The contribution of the synthesis gas production to the ISBL investment in case 2 is nearly halved compared to case 1, a result likely due to the GHR accounting for 16.2% of the total ISBL investment in case 1.

4.4.2 OPEX

The operating costs include both variable and fixed operating costs. As stated, the plant was assumed to operate 8000 hours annually. The variable and fixed operating costs for both process configurations are summarised in Table 4.17. The variable cost estimation was based on literature values for the cost of raw materials and taxes from the Norwegian government listed in Table 3.4 in Chapter 3. The estimated total annual variable operating costs were 207.28 MUSD in case 1 and 246.03 MUSD in case 2. The most notable result is the difference in the natural gas and oxygen requirements in the two process designs, leading to notably higher annual operating costs in case 2 compared to case 1.

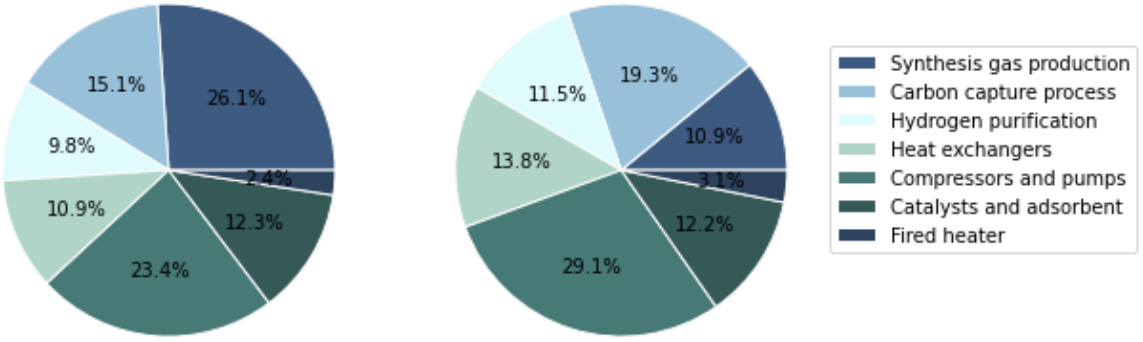

(a) ISBL breakdown in case 1 **(b)** ISBL breakdown in case 2

Figure 4.12: Illustration of the contribution from different parts of the process to the ISBL investment in case 1 (GHR and ATR) and case 2 (ATR).

The fixed costs were based on the description given in Table 3.5 in Chapter 3. The total number of operators was calculated to be 20 distributed on five shifts with four operators per shift. Then, the total operating labour was found from the average salary of a process operator in Norway of 702,000 NOK/year [54]. As a result, the total fixed operating costs were 34.576 MUSD in case 1 and 30.062 MUSD in case 2. Then, the total operating costs were estimated to be 241.856 and 276.092 in case 1 and case 2, respectively.

Table 4.17: Variable and fixed operating costs in case 1 (GHR and ATR) and case 2 (ATR). (All values in MUSD/year).

Variable costs	Case 1	Case 2
Natural gas	143.99	159.52
Oxygen	54.47	76.44
Cooling water	0.43	0.82
Selexol	3.64	3.89
Carbon tax	4.76	5.37
Total variable costs	207.28	246.03
Fixed costs		
Operating labour	1.46	1.46
Supervision	0.365	0.365
Direct salary	0.913	0.913
Maintenance	10.735	9.123
Property tax	5.368	4.562
Rent of land	6.978	5.93
General plant overhead	8.758	7.71
Total fixed costs	34.576	30.062
Total operating costs	241.856	276.092

4.5 Profitability Analysis

The NPV of case 1 and 2 was 675.47 MUSD and 430.44 MUSD, respectively. The internal rate of return was found to be 20% and 17% in case 1 and 2, respectively.

The levelised cost of hydrogen (LCOH) was 1.729 and 1.896 USD/kg H_2 in case 1 and 2, respectively. These values are within the global average LCOH from natural gas with integrated CCS reported by IEA at 1.2-2.1 USD/kg H_2 in 2019 [57], indicating that the calculated LCOH in both cases is reasonable.

4.6 Sensitivity Analysis

Sensitivity analyses were conducted to account for uncertainties in major variables and the impacts on the financial results of hydrogen production. In this thesis, the natural gas, oxygen, cooling water, Selexol and the carbon tax are the key financial factors influencing the profitability of the process designs. In addition, the ISBL investments used in this thesis have high uncertainties due to the preliminary sizing and costing of the process equipment. In the sensit-

ivity analyses, only one variable was changed, and the others were kept constant.

The natural gas price is one of the key parameters that significantly impact the economic performance of both process designs. The natural gas price used in this thesis was the average price in 2022 of 6.5 USD/MMBtu. In the analysis, the natural gas price varied from 1-12 USD/MMBtu, as shown in Figure 4.13a. As illustrated, the increased natural gas price had a more significant influence on the LCOH in case 2, which is reasonable due to the higher consumption of natural gas as feed.

As mentioned, the carbon tax is expected to increase to 2000 NOK/tonne CO_2, which equals approximately 200 USD/tonne CO_2 [49]. Therefore, the impact of the carbon tax on the LCOH was examined. The scenario of no carbon tax to the future scenario of 200 USD/tonne was studied, as illustrated in Figure 4.13b. As seen, the increased carbon tax impacts the LCOH in both cases. The overall increase in LCOH was 4.2% and 4.4% in case 1 and case 2, respectively. The relatively low effect of the carbon tax is reasonable since both process designs are blue hydrogen technologies, which are low on carbon emissions compared to conventional hydrogen production with zero carbon capture.

The impact of the oxygen price on the levelised cost of hydrogen is shown in Figure 4.13c. As previously discussed, the second process design (case 2), with an ATR, had a notably higher oxygen consumption than case 1. Consequently, the increase in the oxygen price had a greater effect on the LCOH in case 2.

Hydrogen production has a large steam consumption. In both process designs, the required steam is produced from water by utilising the surplus heat in the process. In addition, both process designs also have an additional production of steam. As illustrated in Figure 4.13d, the effect of reduction and increase in the cooling water price on the LCOH was minimal in both cases. The cooling water cost is relatively low compared to the other operating costs in both cases and has a relatively low impact on the LCOH in both cases.

As mentioned, both cases have an annual loss of Selexol, which impacts the annual operating costs. Therefore, the LCOH sensitivity to the cost of the Selexol solvent was studied, as shown in Figure 4.13e. As expected, an increase in the Selexol price gave a higher LCOH in both cases.

As a consequence of the uncertainties in the calculations of the ISBL investment, the LCOH sensitivity to the ISBL investment was studied. Figure 4.13f illustrated the effect of reducing and enlarging the ISBL investment by 50% on the LCOH. As expected, the LCOH in both cases decreased with a decreased ISBL investment and increased with an increased ISBL investment.

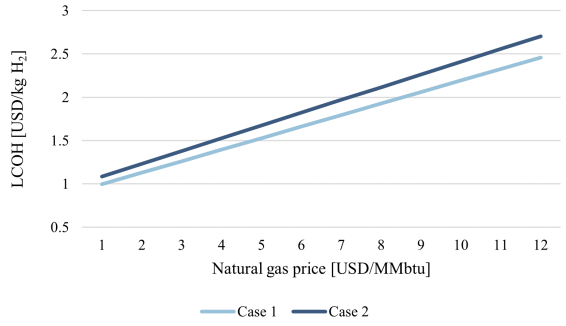

(a) LCOH sensitivity to the natural gas price.

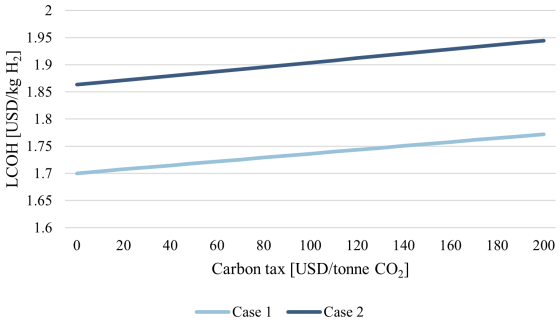

(b) LCOH sensitivity to the carbon tax.

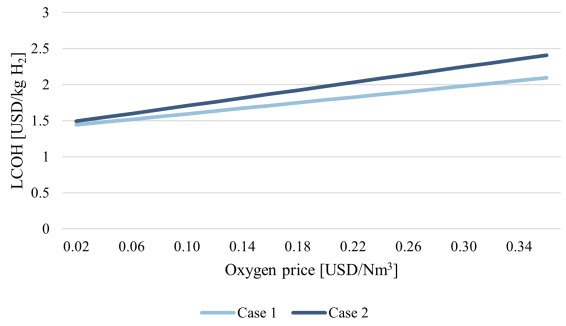

(c) LCOH sensitivity to the oxygen price.

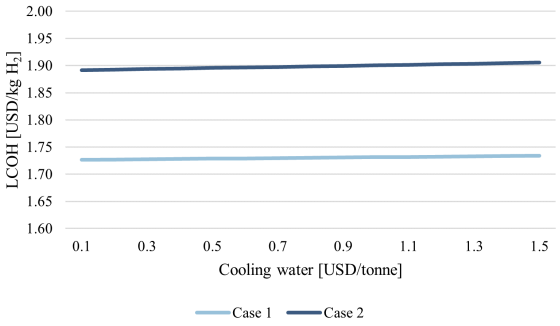

(d) LCOH sensitivity to the cooling water price.

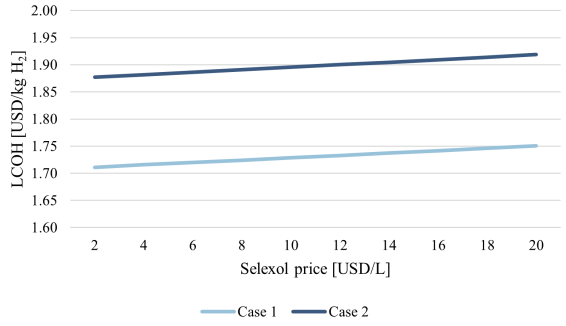

(e) LCOH sensitivity to the Selexol price.

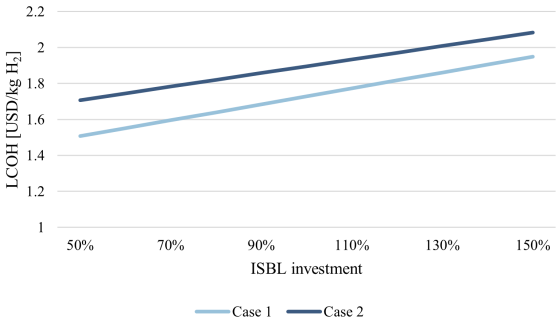

(f) LCOH sensitivity to the ISBL investment.

Figure 4.13: Sensitivity analyses of case 1 (GHR and ATR) and case 2 (ATR). The LCOH sensitivity to the natural gas price, carbon tax, oxygen price, cooling water price, Selexol price and the ISBL investment.

4.7 Comparison of the Technologies

The main results from the simulations and the profitability analyses are summarised in Table 4.18 and will be further discussed in this section.

Table 4.18: Comparison of the two process configurations, case 1 (GHR and ATR) and case 2 (ATR).

Parameter	Case 1	Case 2	Units
Natural Gas Feed	61.89	68.5	tonnes/h
Natural Gas Energy	811.5	898.05	MW
Hydrogen Production	500	500	tonnes/day
Hydrogen Energy	694.14	694.14	MW
Steam Demand	185.34	155.16	tonnes/h
Oxygen Consumption	1,779	2,497	kmol/h
Natural Gas Efficiency	85.5	77.3	%
Power Demand	28.02	31.11	MW
Steam Export	35.76	143.6	tonnes/h
CO_2 Captured	158.96	175.87	tonnes/h
CO_2 Captured	95.12	95.11	%
CO_2 Emitted	7.44	8.49	tonnes/h
Total Investment	530.59	456.95	MUSD
Net Present Value [1]	675.47	430.44	MUSD
Internal Rate of Return [1]	20	17	%
Pay-back Time [1]	5.15	6.04	years
LCOH	1.729	1.896	USD/kgH_2

[1] Based on a hydrogen selling price of 2.2 USD/kg H_2 and a discount rate of 6%.

As shown in Table 4.18, both processes produce 500 tonnes/day of hydrogen; however, the natural gas consumption had a noticeable difference. The second process design (case 2) had a 10% higher natural gas consumption, which significantly impacted the energy efficiency. The natural gas efficiency in case 1 and case 2 were 85.5% and 77.3%, respectively. In addition, case 2 had a 40% higher oxygen consumption, which, together with the natural gas consumption, greatly impacted the operating costs.

The first process design (case 1) had a steam consumption of approximately 20% more than the second process design (case 2). As mentioned, a commercialised S/C ratio by Topsoe of 0.6 was used in the simulations of the ATR in case 2. The additional steam needed to maximise

the hydrogen production in case 2 was added prior to the WGS reactor. This resulted in a significantly lower total steam consumption in case 2 than in case 1. The second process design had a significant production of surplus steam compared to the first process design. However, in this thesis, the excess steam was not further utilised for power production. Consequently, both cases require an external power supply. It should be noted that utilisation of the excess steam by power production may impact the energy efficiency in case 2.

Additionally, both processes achieved a minimum capture rate of 95% of the CO_2 in the shifted synthesis gas and are qualified as blue hydrogen processes. However, the second process design emitted 14% more CO_2 with 8.49 tonnes/h compared to the first process, which emitted 7.44 tonnes/h. By reducing the overall carbon emissions by at least 95%, both processes significantly reduced the carbon emissions compared to the conventional hydrogen production.

The economic performances of the two process configurations are essential results in this thesis. As shown, the total investment in case 1 was significantly higher than in case 2. On the other hand, the annual operating costs in case 2 were considerably higher than in case 1. Based on a hydrogen selling price of 2.2 USD/kg H_2 and a discount rate of 6%, the NPV of case 1 was 675.47 MUSD and the NPV in case 2 was 430.44 MUSD. Furthermore, the internal rate of return (IRR) in case 1 and 2 was 20% and 17%, respectively. In addition, case 1 had a shorter pay-back time of approximately one year compared to case 2. These findings underscore the importance and influence of the annual operating costs of a production plant. In addition, it should be noted that the value and possible revenue of the excess high-pressure steam produced in both cases is not included in the evaluation of the economic performance of both cases.

Chapter 5

Conclusion and Further Work

5.1 Conclusion

In this thesis, two blue hydrogen production process designs were studied and compared. Both processes were successfully simulated in Aspen HYSYS V12. From the CAPEX and OPEX estimates for both cases, profitability analyses were performed.

Based on the simulations, it was found that the process design with a coupled GHR and ATR (case 1) had both a greater energy efficiency and natural gas efficiency than the process design with an ATR (case 2). In addition, case 1 had a lower natural gas consumption, oxygen consumption and CO_2 emissions than case 2. Both process designs utilised excess heat to produce the required steam. The levelised cost of hydrogen (LCOH) was estimated to be 1.729 and 1.896 USD/kg H_2 in case 1 and 2, respectively.

Based on a hydrogen selling price of 2.2 USD/kg H_2 and a discount rate of 6%, the first process design (case 1) had a greater net present value, internal rate of return and a shorter pay-back time. Therefore, based on the simulation and profitability results, the first process design (case 1) had the most favourable design.

5.2 Further Work

During the work with this master thesis, several topics for further work were identified. As mentioned, metal dusting is a severe problem in synthesis gas production. Thus, further research on materials in the GHR and the heat exchanger after the ATR, which is resistant to metal dusting corrosion, is essential.

As mentioned, the further processing of the captured CO_2 was out of the scope of this thesis. Therefore further processing, transportation and utilisation of the captured CO_2 needs further study.

Furthermore, the impact of different carbon capture processes should be evaluated. In this thesis, the Selexol process was used; however, studying other carbon capture technologies and their influence on energy efficiency, capture rate, investment cost and operating costs would be interesting.

The profitability analysis of both processes could be improved by obtaining more accurate and reliable cost values to reduce the uncertainties associated with the ISBL investment.

In this thesis, oxygen was assumed to be purchased from an outside source. However, an on-site air separation unit (ASU) may be preferable since the oxygen consumption is relatively high in both process configurations. Therefore, further study on the effect of incorporating the ASU on the investment cost, energy consumption and operating costs would be interesting.

If the hydrogen end-use is in an ammonia plant, it would be interesting to study the effect of an air-blown ATR on both the investment and the operating costs. Finally, the possibility of using the excess steam for power production should also be investigated.

Bibliography

[1] *The paris agreement*, https://www.un.org/en/climatechange/paris-agreement, (Accessed: 30.05.2023).

[2] *Net zero by 2050*, https://www.iea.org/reports/net-zero-by-2050, (Accessed: 21.05.2023).

[3] *Hydrogen*, https://www.iea.org/reports/hydrogen, (Accessed: 21.05.2023).

[4] O. Massarweh, M. Al-khuzaei, M. Al-Shafi, Y. Bicer and A. S. Abushaikha, 'Blue hydrogen production from natural gas reservoirs: A review of application and feasibility,' *Journal of CO2 Utilization*, vol. 70, p. 102 438, 2023.

[5] K. T. Møller, T. R. Jensen, E. Akiba and H.-w. Li, 'Hydrogen-a sustainable energy carrier,' *Progress in Natural Science: Materials International*, vol. 27, no. 1, pp. 34–40, 2017.

[6] H. Idriss, M. Scott and V. Subramani, '1 - introduction to hydrogen and its properties,' in *Compendium of Hydrogen Energy*, Woodhead Publishing, 2015, pp. 3–19.

[7] J. O. Abe, A. P. Popoola, E. Ajenifuja and O. M. Popoola, 'Hydrogen energy, economy and storage: Review and recommendation,' *International Journal of Hydrogen Energy*, vol. 44, pp. 15 072–15 086, 2019.

[8] J. A. Moulijn, M. Makkee and A. E. Van Diepen, *Chemical Process Technology*, 2. Wiley, 2013.

[9] T. S. Christensen, 'Adiabatic prereforming of hydrocarbons—an important step in syngas production,' *Applied Catalysis A: General*, vol. 138, no. 2, pp. 285–309, 1996.

[10] M. H. Wesenberg, 'Gas heated steam reformer modelling,' PhD thesis, NTNU, 2006.

[11] *Syncor - autothermal reformer (atr)*, https://www.topsoe.com/our-resources/knowledge/our-products/equipment/syncortm-autothermal-reformer-atr, (Accessed: 24.11.2022).

[12] *Hydrogen, syngas and carbon monoxide*, https://www.thyssenkrupp-uhde.com/en/products-and-technologies/hydrogen-and-gas-technologies/hydrogen-syngas-and-carbon-monoxide, (Accessed: 12.12.2022).

[13] J. Hwang, 'Initial stages of metal dusting corrosion,' M.S. thesis, NTNU, 2015.

[14] M. Holland and H. De Bruyn, 'Metal dusting failures in methane reforming plant,' *International Journal of Pressure Vessels and Piping*, vol. 66, pp. 125–133, 1996.

[15] K. Dalane, 'Once-through gas-to-liquid process concept for offshore applications,' M.S. thesis, NTNU, 2015.

[16] M. Voldsund, K. Jordal and R. Anantharaman, 'Hydrogen production with co2 capture,' *International Journal of Hydrogen Energy*, vol. 41, pp. 4969–4992, 2016.

[17] *Water gas shift*, `https://globalsyngas.org/syngas-technology/syngas-conditioning-purification/water-gas-shift/`, (Accessed: 22.05.2023).

[18] Linde Engineering, *Co shift conversion*, `https://www.linde-engineering.com/en/process-plants/hydrogen_and_synthesis_gas_plants/gas_generation/co_shift_conversion/index.html`, (Accessed: 11.11.2022).

[19] T. Y. Amiri, K. Ghasemzageh and A. Iulianelli, 'Membrane reactors for sustainable hydrogen production through steam reforming of hydrocarbons: A review,' *Chemical Engineering and Processing-Process Intensification*, vol. 157, p. 108 148, 2020.

[20] M. Luo, Y. Yi, S. Wang, Z. Wang, M. Du, J. Pan and Q. Wang, 'Review of hydrogen production using chemical-looping technology,' *Renewable and Sustainable Energy Reviews*, vol. 81, pp. 3186–3214, 2018.

[21] Y. Ghiyati, N. Bansal and M. Ilyas, *The best of blue hydrogen*, brochure, (Accessed: 12.09.2022).

[22] S.-i. Nakao, K. Yogo, K. Goto, T. Kai and H. Yamada, 'Co2 capture with adsorbents,' in *Advanced CO2 Capture Technologies: Absorption, Adsorption, and Membrane Separation Methods*. Springer International Publishing, 2019, pp. 45–63.

[23] S. Mokhatab and W. A. Poe, 'Natural gas sweetening,' *Hydrocarbon Engineering*, vol. 8, pp. 253–290, 2012.

[24] M. I. Stewart, 'Chapter nine - gas sweetening,' in *Surface Production Operations*, Third Edition, vol. 2, Gulf Professional Publishing, 2014, pp. 433–539.

[25] S. A. Rackley, *Carbon capture and storage*. Butterworth-Heinemann, 2017.

[26] G. Puxty and M. Maeder, 'The fundamentals of post-combustion capture,' *Absorption-Based Post-Combustion Capture of Carbon Dioxide*, pp. 13–33, 2016.

[27] I. M. Bernhardsen and H. K. Knuutila, 'A review of potential amine solvents for co2 absorption process: Absorption capacity, cyclic capacity and pka,' *International Journal of Greenhouse Gas Control*, vol. 61, pp. 27–48, 2017.

[28] A. L. Kohl and R. B. Nielsen, 'Chapter 5 - alkaline salt solutions for acid gas removal,' in *Gas Purification*, Fifth Edition, Gulf Professional Publishing, 1997, pp. 330–414.

[29] A. L. Kohl and R. B. Nielsen, 'Chapter 14 - physical solvents for acid gas removal,' in *Gas Purification*, Fifth Edition, Gulf Professional Publishing, 1997, pp. 1187–1237.

[30] S. A. Rackley, '6 - absorption capture systems,' in *Carbon Capture and Storage*, Second Edition, Butterworth-Heinemann, 2017, pp. 115–149.

[31] A. Padurean, C.-C. Cormos and P.-S. Agachi, 'Pre-combustion carbon dioxide capture by gas–liquid absorption for integrated gasification combined cycle power plants,' *International Journal of Greenhouse Gas Control*, vol. 7, pp. 1–11, 2012.

[32] M. Mulder, *Basic Principles of Membrane Technology*, 2. The Netherlands, Kluwer Academic Publishers, 1996.

[33] Sintef, *Hydrogen pufication by adsorption processes*, https://www.sintef.no/en/expertise/sintef-industry/process-technology/hydrogen-purification-by-adsorption-processes/, (Accessed: 01.03.2023).

[34] J. A. Ritter and A. D. Ebner, 'State-of-the-art adsorption and membrane separation processes for hydrogen production in the chemical and petrochemical industries,' *Separation Science and Technology*, vol. 42, pp. 1123–1193, 2007.

[35] Hydrogen Mem-Tech, *Product information*, https://hydrogen-mem-tech.com/policies/, (Accessed: 04.04.2023).

[36] SINTEF, *Co2 capture with membranes*, https://www.sintef.no/en/expertise/sintef-industry/sustainable-energy/co2-capture-with-membranes/, (Accessed: 11.10.2022).

[37] G. Towler and R. Sinnot, *Chemical Engineering Design*, 1. Butterworth-Heinemann, 2008.

[38] T. Gundersen and L. Naess, 'The synthesis of cost optimal heat exchanger networks: An industrial review of the state of the art,' *Computers & chemical engineering*, vol. 12, pp. 503–530, 1988.

[39] R. Turton, J. A. Shaeiwitz, D. Bhattacharyya and W. B. Whiting, *Analysis, synthesis and design of chemical processes*, 5. Pearson Education, 2018.

[40] T. Gundersen, *A process integration primer*, https://iea-industry.org/app/uploads/a-process-integration-primer-iea-t-gundersen_2002.pdf, 2002.

[41] R. Smith, *Chemical Process Design and Integration*, 2. United Kingdom, Wiley, 2016.

[42] Bill Cotton, *Lch process for the production of blue hydrogen*, https://matthey.com/documents/161599/440415/Reprint+-+Hydrogen+from+Natural+Gas+Through+Cost+Effective+CO2+Capture+%28c2021%29.pdf/a4e2aead-46c9-1a45-7fcf-cf6987262944?t=1653488219254, (Accessed: 12.09.2022).

[43] Johnson Matthey, *Lch process for the production of blue hydrogen*, https://matthey.com/documents/161599/474986/26367+JM+LCH+Process++Production+of+Low+Carbon+Hydrogen+TP+%28screen%29+13.pdf/71bb11a0-47ce-e609-412b-0678b1b4e5da?t=1654695668629, (Accessed: 12.09.2022).

[44] *Aspentech blog*, https://www.aspentech.com/en/resources/blog/questions-on-acid-gas-removal-weve-got-the-answers, (Accessed: 07.12.2022).

[45] Equinor, *Composition of natural gas*, 2021.

[46] A. Torset, 'Large scale production of blue hydrogen,' NTNU, 2022.

[47] U.S. Energy Information Administration, *Natural gas*, https://www.eia.gov/dnav/ng/hist/rngc1A.htm, (Accessed: 05.05.2023).

[48] Intratec, *Oxygen price*, https://www.intratec.us/chemical-markets/oxygen-price, (Accessed: 08.05.2023).

[49] Regjeringen.no, *Statsbudsjettet 2022: Endringer i klimaavgiftene*, https://www.regjeringen.no/no/statsbudsjett/2022/statsbudsjettet-2022-skatter-og-avgifter/statsbudsjettet-2022-endringer-i-klimaavgiftene/id2873756/, (Accessed: 04.05.2023).

[50] E. Robert, D. Kearins, M. Turner, M. Woods, N. Kuehn and A. Zoelle, 'Cost and performance baseline for fossil energy plants volume 1: Bituminous coal and natural gas to electricity,' National Energy Technology Laboratory (NETL), Tech. Rep., 2019.

[51] Ammpower, *Why are ammonia prices so high in 2022*, https://www.iamm.green/ammonia-prices/, (Accessed: 05.05.2023).

[52] R. Stevens, E. Lewis and S. McNaul, 'Comparison of commercial, state-of-the-art, fossil-based hydrogen production technologies,' National Energy Technology Laboratory (NETL), Tech. Rep., 2021.

[53] *Cost of operating labour*, https://pressbooks.bccampus.ca/chbe220/chapter/cost-of-operating-labour/.

[54] Utdanning.no, *Fagoperatør i kjemisk prosessindustri (prosesstekniker)*, https://utdanning.no/yrker/beskrivelse/fagoperator_i_kjemisk_prosessindustri_prosesstekniker, (Accessed: 08.05.2023).

[55] U. K. Government, 'Hydrogen production costs 2021,' Department for Business, Energy and Industrial Strategy, Tech. Rep., 2021.

[56] C. Kost, S. Shammugam, V. Jülch, H. Nguyen and T. Schlegl, 'Levelized cost of electricity renewable energy technologies,' Fraunhofer Institute for Solar Energy Systems ISE, Tech. Rep., 2018.

[57] IEA, *Global average levelised cost of hydrogen production by energy source and technology, 2019 and 2050*, https://www.iea.org/data-and-statistics/charts/global-average-levelised-cost-of-hydrogen-production-by-energy-source-and-technology-2019-and-2050, (Accessed: 19.05.2023).

[58] S.Skogestad, *Prosessteknikk*, Norwegian, 3. Norway, Tapir akademiske forlag, 2009.

[59] B. Guo, X. Liu and X. Tan, 'Chapter 10 - separation systems,' in *Petroleum Production Engineering*, Second Edition, Gulf Professional Publishing, 2017, pp. 243–274.

[60] R. Y. Purcell and G. S. Shareef, 'Handbook of control technologies for hazardous air pollutants,' 1988.

[61] The University of Manchester, *Chemical engineering plant cost index*, https://personalpages.manchester.ac.uk/staff/tom.rodgers/Interactive_graphs/CEPCI.html?reactors/CEPCI/index.html, (Accessed: 21.04.2023).

[62] Y. Jiang, *Techno-economic studies of coal-biomass to liquids (CBTL) plants with CO 2 capture and storage (CCS)*. West Virginia University, 2017.

Appendix A

Process Simulation

This appendix includes pictures of the HYSYS simulation flow sheet of both process designs. The HYSYS flow sheet for case 1 is given in Figure A.3. The HYSYS simulation of the cooling cycle with ammonia and the steam production in case 1 is shown in Figure A.1 and A.2, respectively.

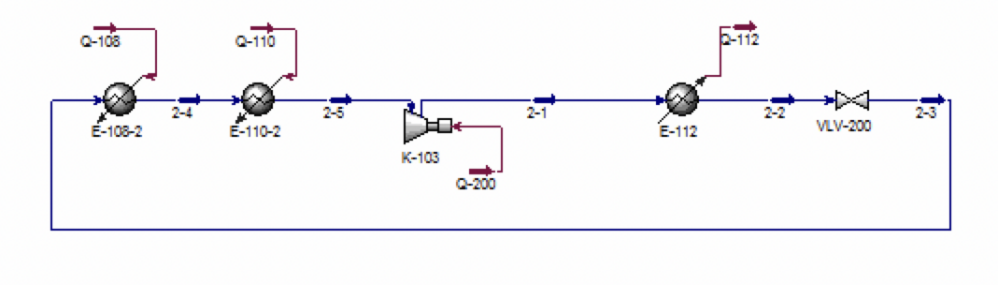

Figure A.1: HYSYS flow sheet for the simulation of the cooling cycle in case 1 (with a coupled GHR and ATR).

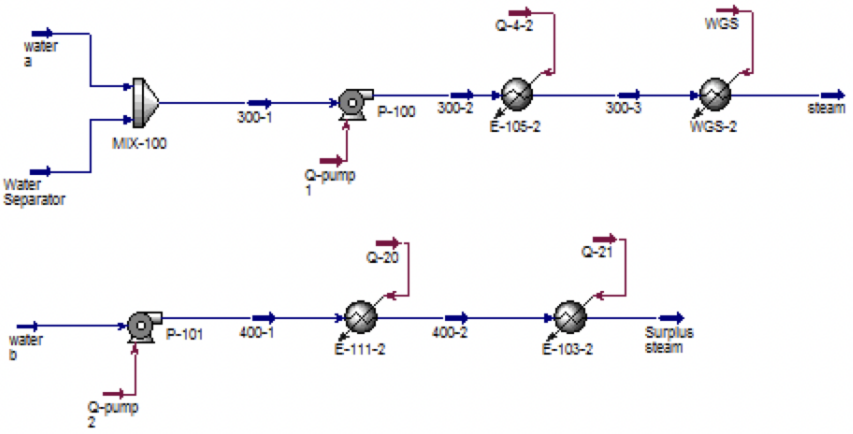

Figure A.2: HYSYS flow sheet for the simulation of the steam production in case 1 (with a coupled GHR and ATR).

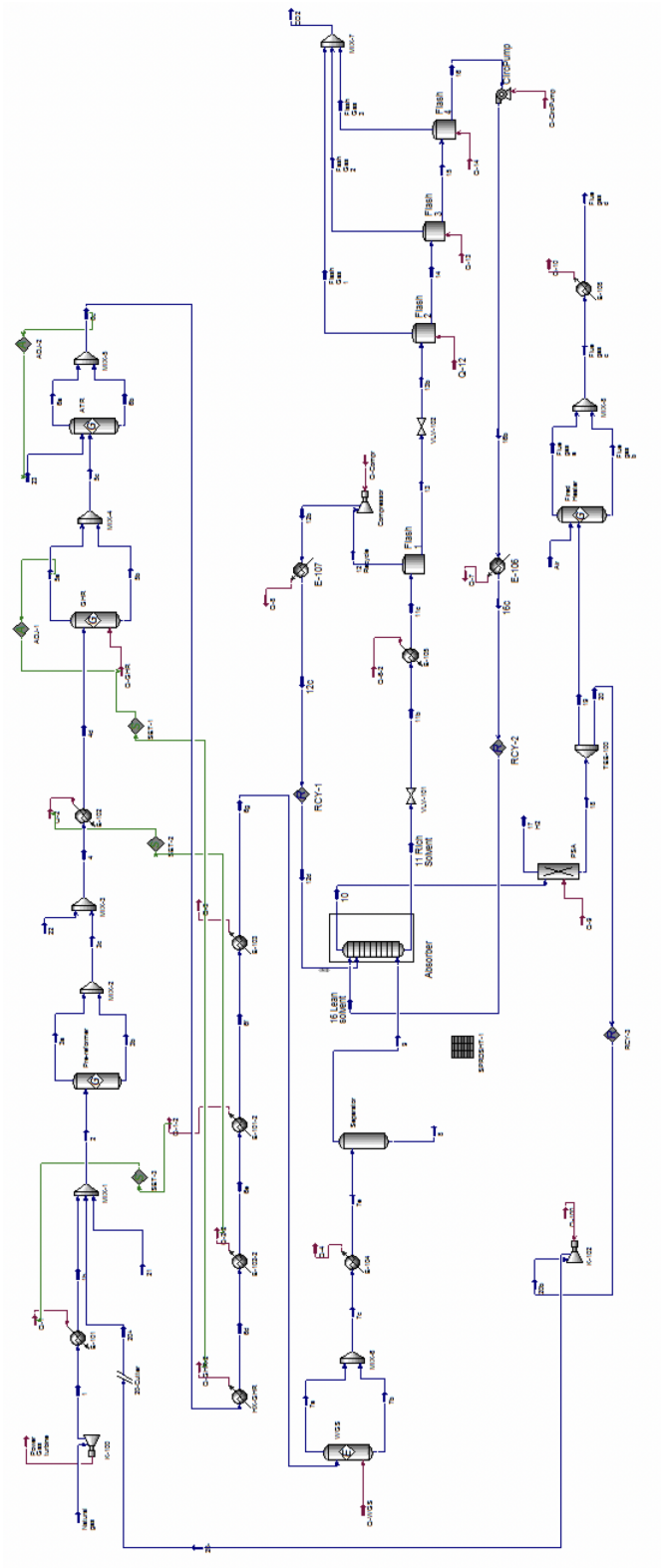

Figure A.3: HYSYS flow sheet of case 1 with a gas heated reformer and an autothermal reformer.

The HYSYS flow sheet for case 1 is given in Figure A.6. The HYSYS simulation of the cooling cycle with ammonia and the steam production in case 2 is shown in Figure A.4 and A.5, respectively.

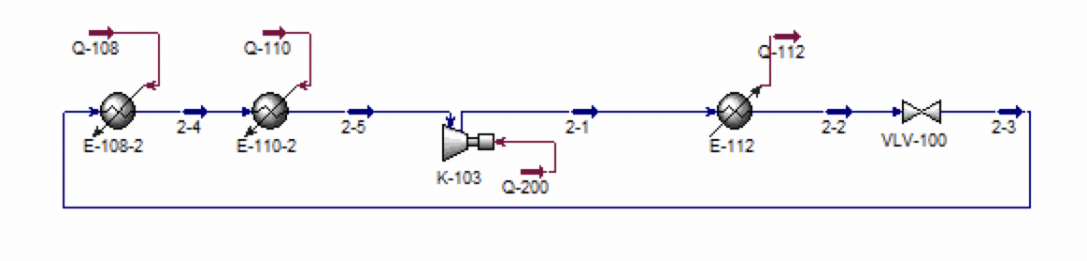

Figure A.4: HYSYS flow sheet for the simulation of the cooling cycle in case 2 (with an ATR).

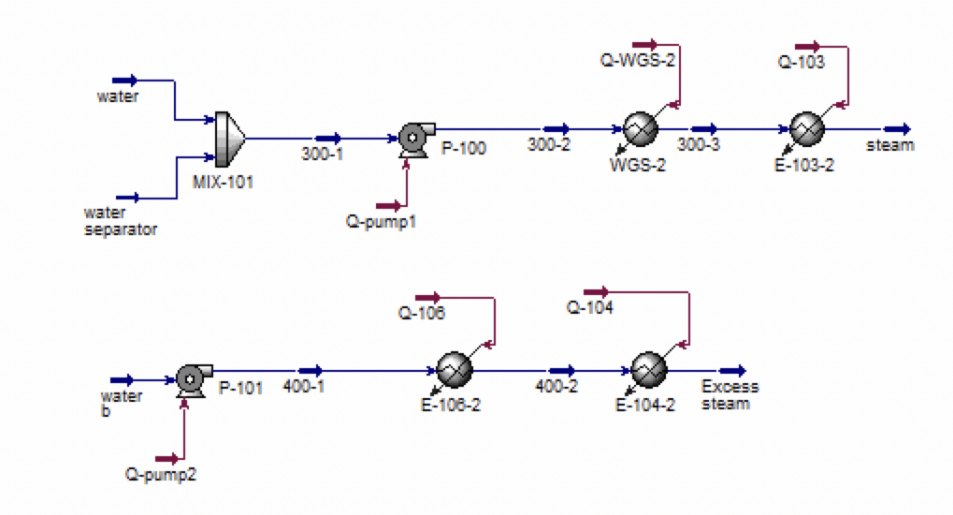

Figure A.5: HYSYS flow sheet for the simulation of the steam production in case 2 (with an ATR).

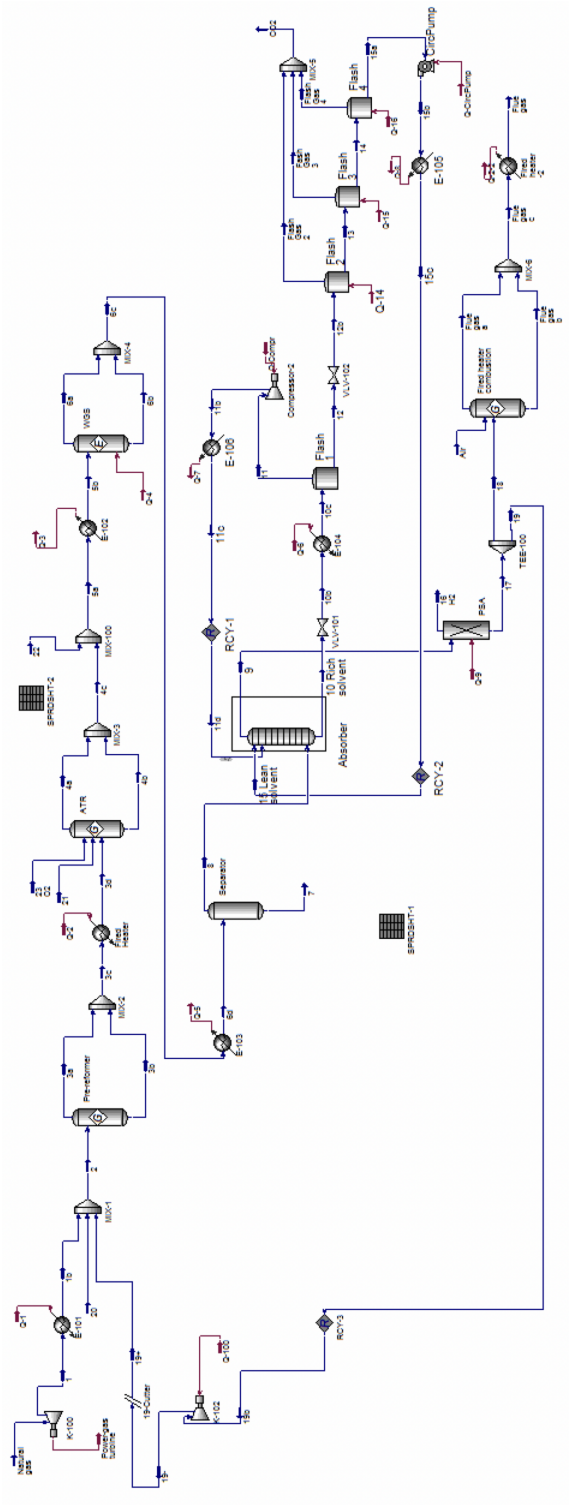

Figure A.6: HYSYS flow sheet of case 2 with an autothermal reformer.

Appendix B

Mass and Energy Balance

This appendix includes the calculation of the overall mass and energy balance of the HYSYS simulation of both processes.

B.1 Mass Balance

The mass balance for a process at steady state is given as,

$$\dot{m}_{in} = \dot{m}_{out}, \tag{B.1}$$

where $\dot{m}_{in}$ and $\dot{m}_{out}$ is the mass flow in and out of the system respectively [37]. All values used in the calculations are taken from the HYSYS simulations and are shown in Table B.1 for both cases.

$$\text{Imbalance} = \frac{\dot{m}_{in} - \dot{m}_{out}}{\dot{m}_{in}} \tag{B.2}$$

The imbalance in the mass balance is calculated by equation (B.2), 0.011% and -0.0096% for the first and second case, respectively.

Table B.1: Mass balance for case 1 and case 2.

Case 1			
Inlet streams	$\dot{m}$ [kg/h]	Outlet streams	$\dot{m}$ [kg/h]
Natural gas	61,891.45	Hydrogen	20,833.66
Water	106,397.18	CO_2	160,053.67
Oxygen	56,926.59	Flue gas	85,374.88
Air	77,607.79	Excess steam	35,796
Condensate	114,720.16	Condensate	115,438.93
Sum	417,543.18	Sum	417,497.148
Case 2			
Inlet streams	$\dot{m}$ [kg/h]	Outlet streams	$\dot{m}$ [kg/h]
Natural gas	68,499.24	Hydrogen	20,829.25
Water	201,426.84	CO_2	177,049.12
Oxygen	79,893.44	Flue gas	78,351.82
Air	70,553.65	Excess steam	143,580.35
Condensate	97,299.56	Condensate	97,911.81
Sum	517,672.72	Sum	517,722.35

B.2 Energy Balance

The energy balance for a process at steady state is given as,

$$\dot{W}_{out} - \dot{Q}_{in} = \dot{W}_{in} - \dot{Q}_{out}, \tag{B.3}$$

where $\dot{W}_{in}$ and $\dot{W}_{out}$ is the work done to the system and the work done by the system respectively, and $\dot{Q}_{in}$ and $\dot{Q}_{out}$ is the heat flow in and out of the system [58]. All values used in the calculations are taken from the HYSYS simulations and are shown in Table B.2 for both cases.

The energy imbalance is 0.0899% and -0.0093% in the first and second case, respectively.

Table B.2: Energy balance for both processes.

Case 1			
Inlet streams	Q [MW]	Outlet streams	Q [MW]
Natural Gas	-74.167	Hydrogen	-1.365
Water	-470.917	Flue gas	-47.583
Oxygen	3.325	CO_2 Captured	-396.11
Air	-0.115	Excess Steam	-130.25
Condensate	-505.278	Condensate	-505.833
Compressors	3.27	Turbines	0.55
Heaters	350.59	Coolers	487.54
GHR	125	WGS	29.07
Pumps	3.81		
Sum	-564.487	Sum	-563.98
Case 2			
Inlet streams	Q [MW]	Outlet streams	Q [MW]
Natural Gas	-82.083	Hydrogen	-1.365
Water	-891.277	Flue gas	-53.22
Oxygen	4.664	CO_2 Captured	-438.33
Air	-0.104	Excess Steam	-522.5
Condensate	-427.77	Condensate	-429.166
Compressors	3.41	Turbines	0.611
Heaters	384.27	Coolers	401.028
Pumps	4.12	WGS	38.08
Sum	-1,004.769	Sum	-1,004.362

Appendix C

Energy Efficiency

This appendix gives the values used in the calculations of the natural gas efficiency and the energy efficiency of both processes. The lower heating values (LHV) for the different compounds are taken from HYSYS and are summarised in Table C.1.

Table C.1: Lower heating values (LHV) for the compounds in the process.

Compound	LHV [kJ/kmol]
Natural gas	880,184.5
Hydrogen	241,820

The natural gas efficiency is defined as the lower heating value of the hydrogen product divided by the lower heating value of the natural gas, as shown in equation (4.1). The energy efficiency is defined as the useful energy out of the system divided by the useful energy put into the system, which is in this thesis the lower heating value of the products divided by the lower heating value of the natural gas feed and the mechanical work for the compressors and pumps, as shown in equation (4.2) [58].

The calculation of the natural gas efficiency and energy efficiency for both cases are summarised in Table C.2.

Table C.2: Overview of the natural gas energy, hydrogen energy, natural gas efficiency and energy efficiency in both cases.

	Case 1	Case 2	Unit
Hydrogen energy	694.14	694.14	MW
Natural gas energy	811.5	898.05	MW
Natural gas efficiency	85.5	77.3	%
Energy efficiency	82.68	74.7	%

Appendix D

Heat Integration

This appendix describes the heat integration in both process configurations in further detail. The streams chosen for the heat integration are given in section 3.3. The supply and target temperatures and heat loads available in case 1 and 2 are presented in section 4.1.2 and 4.2.2, respectively.

D.1 Case 1

The problem table for case 1 is given in Table D.1 with the corresponding grand composite curve in Figure D.1. As illustrated, this process design has a heat surplus of 191.48 MW. When the heat needed in the GHR is subtracted, the heat surplus in the process is 66.6 MW.

Table D.1: The temperature interval heat balances of case 1.

Temperature interval [°C]	ΔT_i	Hot Streams	Cold Streams	ΔH_i [MW]
1,246-1,195	51	FG		-1.52
1,195-605	590	FG + 6		-151.32
605-405	200	FG + 6	4	-14.49
405-352.3	52.7	FG + 6	4 + 1	-1.25
352.3-295	57.3	FG + 6	1	-11.91
295-295	0	WGS		-29.1
295-250.1	44.9	FG + 7	1	-21.45
250.1-95	155.1	FG + 7	1 + w	27.39
95-80	15	7	1 + w	3.1
80-65.17	14.83	7	1 + 11 + w	33.32
65.17-56.2	8.97	7 + 16	1 + 11 + w	3.26
56.2-35	21.2	7 + 16	11 + w	6.68
35-31.25	3.75	16	11 + w	3.04
31.25-22.71	8.54	16	11	1.35
22.71-2.22	20.49	16		-38.58
$\Sigma\Delta H_i$ [MW]				-191.48

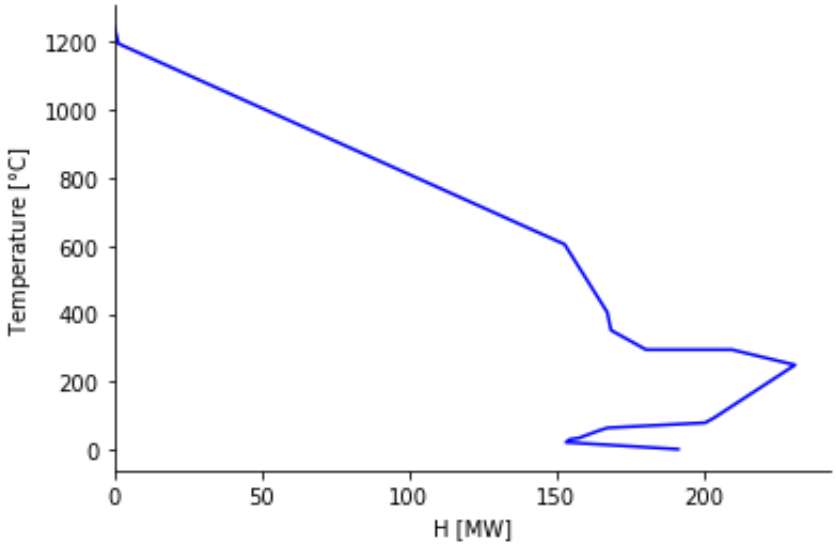

Figure D.1: The grand composite curve for case 1 with a coupled GHR and ATR.

D.2 Case 2

The problem table for case 2 is given in Table D.2 with the corresponding grand composite curve in Figure D.2. As illustrated, this process design has a heat surplus of 165.57 MW.

Table D.2: The temperature interval heat balances of case 2.

Temperature interval [°C]	ΔT_i	Hot Streams	Cold Streams	ΔH_i [MW]
1,537-843.1	693.9	FG		-19.94
843.1-605	238.1	FG + 5		-57.62
605-489.5	115.5	FG + 5	3	-16.87
489.5-405	84.5	FG + 5		-20.45
405-295	110	FG + 5	1	-20.70
295-295	0	WGS		-38.11
295-250.1	44.9	FG + 6	1	-18.99
250.1-95	155.1	FG + 6	1 + w	20.48
95-80	15	6	1 + w	2.41
80-64.94	15.06	6	1 + w + 10	35.02
64.94-56.2	8.74	6 + 15	1 + w + 10	2.89
56.2-35.68	20.52	6 + 15	w + 10	5.68
35.68-35	0.68	6 + 15	10	-0.19
35-22.9	12.1	15	10	2.06
22.9-2.22	20.68	15		-41.25
$\Sigma\Delta H_i$ [MW]				-165.57

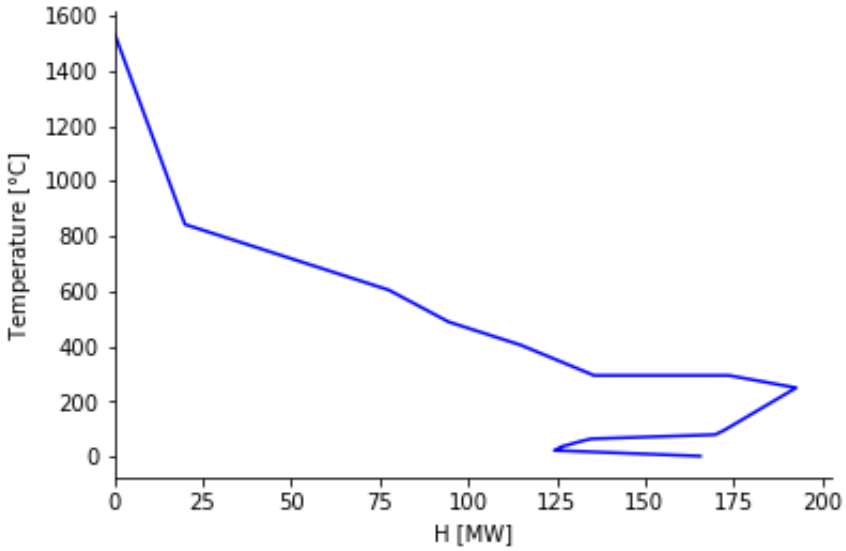

Figure D.2: The grand composite curve for case 2 with an ATR.

Appendix E

Equipment Size Calculations

This appendix gives the calculations used for the sizing of the main equipment. All equipment was assumed to be made of stainless steel. In the size estimations, the design pressure was set to 10% above the operating pressure.

E.1 Pressure Vessels

E.1.1 Vertical Separators

The separator prior to the carbon capture plants was modelled as a vertical pressure vessel. The size was found by using the method for gas-liquid separators by Sinnot and Towler [37]. The settling velocity of the liquid droplets, u_t, was estimated by the following equation,

$$u_s = 0.07[(\rho_l - \rho_v)/\rho_v]^{1/2} \tag{E.1}$$

where ρ_L and ρ_V are the liquid and vapour density, respectively. The minimum allowable diameter, D_v, of the separator is given by,

$$D_v = \sqrt{\left(\frac{4q_v}{\pi u_s}\right)} \tag{E.2}$$

where q_v is the gas or vapour volumetric flow. The height of the liquid in the vessel, h_v, is estimated by equation (E.3). The residence time, τ, was assumed to be 10 minutes.

$$h_v = \frac{q_l \tau}{A_c} = \frac{q_l \tau}{\frac{\pi}{4} D_v^2} \tag{E.3}$$

where q_l is the liquid volumetric flow and A_c is the cross section area of the vessel. Then, the total height of the pressure vessel, h_{tot}, was calculated by the following equation,

$$h_{tot} = h_v + \frac{D_v}{2} + D_v + 0.4 \tag{E.4}$$

In the cost estimations, an adequate wall thickness, t_w, of the pressure vessel must be ensured. To calculate the wall thickness of a pressure vessel the following equation was used [37],

$$t_w = \frac{PD}{2SE - 1.2P} \tag{E.5}$$

where P is the design pressure, D is the diameter of the vessel, S is the maximum allowable stress of the material, and E is the joint efficiency, which was assumed to be 1 in the calculations.

$$\text{Shell mass} = \pi D h_{tot} t_w \rho \tag{E.6}$$

The values used in the sizing of the separators was taken from the HYSYS simulations and are given in Table E.1.

Table E.1: Values used in the sizing calculations and the results from the calculations.

	Case 1	Case 2	Unit
ρ_l	997.8	997.9	kg/m^3
ρ_v	16.01	16.93	kg/m^3
q_l	0.032	0.027	m^3/s
q_v	3.478	3.569	m^3/s
P	35.2	35.2	bar
S	20	20	ksi
u_s	0.548	0.533	m/s
D_v	2.84	2.92	m
h_{tot}	7.7	7.2	m
t_w	0.037	0.038	m
Shell mass	20335.3	20078.85	kg

E.1.2 Horizontal Separators

The flash tanks were modelled as horizontal separators. The most economical length-to-diameter ratio for a horizontal separator operating at 0-20 bar is 3, and operating between 20-35 bar is 4 [37]. The horizontal separators was sized with a residence time of at least 5 minutes [59]. Due

to large amounts of liquid Selexol solvent, it was assumed that the liquid would account for 50% of the cross-section area in the vessel.

From the settling velocity (E.1) and the volumetric vapour flow rate, q_v, the minimum required diameter of the horizontal separator can be estimated based on the given assumptions. From the cross-section area of vapor flow, A_c, the vapour velocity, u_v can be calculated,

$$u_v = \frac{q_v}{A_c} \tag{E.7}$$

Then, the vapour residence time required for the droplets to settle was calculated,

$$\text{Vapour residence time} = \frac{h_v}{u_s} \tag{E.8}$$

where h_v is the height above the liquid level, which was assumed to be $0.5D_v$. The actual residence time is defined as,

$$\text{Actual residence time} = \frac{L_v}{u_v} \tag{E.9}$$

For satisfactory separation, the required vapour residence equals the actual residence time. Then, the diameter of the vessel can be estimated. The liquid holdup volume was calculated by,

$$V_l = A_{c,l} \cdot L_v, \tag{E.10}$$

where $A_{c,l}$ is the liquid cross-section area and L_v is the length of the vessel. Then, the holdup time is calculated by,

$$\tau = \frac{V_l}{q_l} \tag{E.11}$$

where q_l is the liquid volumetric flow rate. While the holdup time is lower than the required residence time, the liquid volume in the vessel needs to be increased, which is done by increasing the vessel diameter. Then, when the residence time is at least 5 minutes, the horizontal pressure vessel is sized sufficiently.

The wall thickness and shell mass were calculated as described in section E.1.1. The values used in the calculations and the results are given in Table E.2 and Table E.3 for case 1 and 2, respectively.

Table E.2: Values used in the sizing calculations and the results from the calculations in case 1.

	Flash tank 1	Flash tank 2	Flash tank 3	Flash tank 4	Unit
q_v	0.0344	1.5	0.637	9.52	m^3/s
q_l	0.907	0.878	0.87	0.87	m^3/s
ρ_v	38.52	15.18	10.76	1.542	kg/m^3
ρ_l	986.4	993.1	995.1	998.4	kg/m^3
P	32.13	11	7.58	1.11	bar
S	15	15	15	15	ksi
D_v	5.575	6.07	6.05	6.006	m
h_{tot}	22.3	18.21	18.15	18.018	m
t_w	0.088	0.032	0.022	0.003	m
Shell mass	275723.6	90252.1	61493.1	8771.6	kg

Table E.3: Values used in the sizing calculations and the results from the calculations in case 2.

	Flash tank 1	Flash tank 2	Flash tank 3	Flash tank 4	Unit
q_v	0.0559	1.683	0.6997	0.955	m^3/s
q_l	0.965	0.93	0.92	0.93	m^3/s
ρ_v	32.38	15.35	10.79	10.79	kg/m^3
ρ_l	985.5	992.9	992.9	995	kg/m^3
P	30.3	11	7.58	1.11	bar
S	15	15	15	15	ksi
D_v	5.695	6.195	6.17	6.187	m
L_v	22.78	18.585	18.51	18.561	m
t_w	0.085	0.033	0.0227	0.0033	m
Shell mass	277023.3	95943.42	65225.26	9588.7	kg

E.1.3 GHR

When sizing the GHR, a SMR with the same capacity was used as a basis. Then a furnace was sized and a pressure vessel. Assuming the height of the GHR is equal to the length of the reformer tubes. The number of tubes placed inside the reformer is assumed to be 500 tubes with a length of 12 m. The diameter of the tubes was estimated from an assumed residence time of 0.2 minutes, to 0.133 m. Assuming the cross-section surface area of the GHR is twice the sum of the cross-section area of the tubes. The diameter of the vessel is then estimated to be 4.6 m. The sizing parameters and results are summarised in Table E.4.

Table E.4: Sizing of the GHR

		Unit
Duty	124.8	MW
P	37.95	bar
S	10.8	ksi
h	12	m
t_w	0.12	m
Shell mass	166176.8	kg

E.1.4 Adsorption Column

The diameter of the adsorption column was found by the method presented in *Chemical Engineering Design* by Sinnot and Towler [37]. A pressure drop of 20 mm H_2O per meter of packing was assumed. The diameter and the cross-sectional area of the absorption column at the given pressure drop was estimated from the generalised pressure-drop correlation given by Sinnot and Towler [37].

The percentage flooding in the column is defined as,

$$\text{Percentage flooding} = \left[\frac{K_4}{K_{4,flooding}}\right]^{1/2} \tag{E.12}$$

where K_4 at design pressure drop and $K_{4,flooding}$ are constants found in Sinnot and Towler [37]. The packing was decided to be Pall Rings (51 mm). Then, the gas mass flow per unit of cross-sectional area, V_w^*, was found by the equation,

$$V_w^* = \left[\frac{K_4 \rho_v (\rho_l - \rho_v)}{13.1 F_p (\frac{\mu_L}{\rho_l})^{0.1}}\right] \tag{E.13}$$

where F_p is the packing factor found in Sinnot and Towler, μ_L is the liquid viscosity, and ρ_l and ρ_v are the liquid and vapor densities, respectively. Then, the required column area is found by the equation,

$$A_c = \frac{q_v}{V_w^*} \tag{E.14}$$

where q_v is the gas flow rate. The diameter of the column, D_c, was then found by the following equation,

$$D_c = \sqrt{\frac{4A_c}{\pi}} \tag{E.15}$$

The packed column height, h_c, was found by the following equation,

$$h_c = N_{OG} \cdot H_{OG} \tag{E.16}$$

where N_{OG} is the number of gas transfer units and H_{OG} is the height of an overall gas transfer unit, which was assumed to be 0.5 m in this thesis. The amount of packing was based on the packing volume, V,

$$V = A_c \cdot h_c \tag{E.17}$$

The total height of the column, accounting for the additional height of liquid distributors and packing support, was found through the following equation [60];

$$h_{tot} = h_c + 2 + (0.25 \cdot D_c) \tag{E.18}$$

The wall thickness of the column was calculated by equation (E.5). Then, the shell mass can be estimated by equation (E.6). The values used in the calculations and the results for both cases are given in Table E.5. The cost was based on the cost of a vertical pressure vessel and the Pall ring packing.

Table E.5: Values used in the sizing calculations and the results from the calculations.

	Case 1	Case 2	Unit
P	35.2	35.2	bar
S	20	20	ksi
K_4	0.18	0.18	m^2/s^3
$K_{4,flooding}$	0.8	0.8	m^2/s^3
ρ_v	15.76	16.67	kg/m^3
ρ_l	1077	1077	kg/m^3
F_p	66	66	1/m
V_w^*	3.315	3.407	kg/m^2s
q_v	55.64	60.38	kg/s
A_c	16.785	17.72	m^2
D_c	4.62	4.75	m
h_c	7.5	7.5	m
h_{tot}	10.655	10.688	m
t_w	0.06	0.062	m
V	125.89	132.9	m^3
Shell mass	74086.9	78553.8	kg

E.2 Heat Exchangers

The following equation gives the size estimation of the heat exchanger,

$$A = \frac{Q}{U\Delta T_{lm}} \tag{E.19}$$

where A is the total heat transfer area, Q is the duty, U is the overall heat transfer coefficient, and ΔT_{lm} is the logarithmic mean temperature difference between the hot and cold side of the heat exchanger [37]. The logarithmic mean temperature difference is given by,

$$\Delta T_{lm} = \frac{\Delta T_1 - \Delta T_2}{ln\frac{\Delta T_1}{\Delta T_2}} \tag{E.20}$$

$$\Delta T_1 = T_{H,in} - T_{C,out} \tag{E.21}$$

$$\Delta T_2 = T_{H,out} - T_{C,in} \tag{E.22}$$

where H and C indicate hot and cold stream, respectively.

The values used for calculating the heat transfer area in case 1 and 2 are summarised in Table E.6 and E.7, respectively. The sizing parameter, heat transfer area, was scaled by 10% to ensure a sufficient cost estimation.

Table E.6: Sizing of the heat exchangers in case 1 (GHR and ATR).

	Tag nr.	ΔT_{lm} [°C]	Q [MW]	U [W/m^2°C]	A [m^2]
Process-Process heat exchangers	E-107	758.93	21.93	570	49.65
	E-102	85.05	46.51	450	1251.25
	E-101	150.74	16.96	450	250.03
	E-104	222.9	15.02	570	118.22
	E-105	34.28	114.08	570	5837.94
	E-106	11.05	79.95	300	23952.8
Coolers	E-111	161.56	12.36	300	255
	E-103	86.97	15.75	300	603
	E-108	48.72	38.05	750	1056
	E-109	26.38	0.0647	750	8.2
	E-110	52.8	0.0053	750	0.13
	E-112	78.7	59.85	700	1087

Table E.7: Sizing of the heat exchangers in case 2 (ATR).

	Tag nr.	ΔT_{lm} [°C]	Q [MW]	U [W/m^2°C]	A [m^2]
Process-Process heat exchangers	E-102	799.13	11.08	450	30.8
	E-101	590.62	18.79	450	70.7
	E-103	476.75	80.89	570	297.7
	E-105	187.46	39.71	570	371.64
	E-107	11.56	83.89	300	24184.4
Coolers	E-111	223.15	11.56	300	172.7
	E-104	171.57	36.01	300	699.6
	E-106	31.42	76.79	300	8146.3
	E-108	35.22	41.2	750	1560
	E-109	28.22	0.147	300	17.4
	E-110	24.96	0.01	750	0.5
	E-112	91.53	65.17	700	1017.2

E.3 Catalyst

The amount of catalyst needed in the pre-reformer, ATR, WGS and PSA was estimated based on the information from Stevens et al. [52]. The amount of catalyst needed in the GHR was estimated from the volume of the tubes in the reformer. Table E.8 summarises the catalyst and adsorbent needed in both cases.

Table E.8: Estimated amount of catalyst and adsorbent.

Equipment	Case 1	Case 2	Unit
Pre-reformer	13.54	15.05	m^3
GHR	91.96	-	m^3
ATR	82.57	54.47	m^3
WGS	215.7	215.4	m^3
PSA	957.9	957.9	m^3

Appendix F

Cost Estimation

This appendix gives the additional information needed in the equipment calculations. This thesis used the CEPCI index to scale the equipment cost to a 2022 basis. The relevant CEPCI indexes are given in Table F.1.

Table F.1: The Chemical Engineering Plant Cost Index (CEPCI) used in cost calculations [39].

Year	CEPCI
January 2007	509.7 [37]
2013	567 [39]
2015	557 [39]
2014	576 [39]
2016	542 [39]
2022	813[61]

The relevant exchange rates used are summarised in Table F.2

Table F.2: Exchange rate.

Year	USD	CAD	NOK	EUR
2014	0.9056	1	-	-
2022	1	-	9.616	-
2018	1	-	-	0.8475

F.1 Equipment Cost

As mentioned, one of the correlations for estimating the equipment cost is given in equation (3.2). The a, b and n used are found in Sinnot and Towler [37], and the relevant values are summarised in Table F.3. The cost calculated from this correlation is given in a January 2007 basis.

Table F.3: The constants used to estimate the purchased equipment cost. The prices are for carbon steel equipment.

Equipment	Size unit	a	b	n
Vertical pressure vessel, 304 ss	shell mass, kg	15,000	68	0.85
Horizontal pressure vessel, 304 ss	shell mass, kg	11,000	63	0.85
Pall rings, 304 ss	m^3	0	7,700	1
Furnace	Duty, MW	37,000	95,000	0.8
Compressor	driver power, kW	490,000	16,800	0.6
Centrifugal pump	flow, L/s	6900	206	0.9

The cost of the pre-reformer, ATR, PSA, WGS reactor, fired heater and SMR are based on historical values and scaled to fit the systems. The relevant cost, capacities, purchased year and exponent are given in Table F.4. The capacity of the equipment was scaled by 10% to ensure a sufficient cost estimation.

Table F.4: Values used in the cost estimation of the pre-reformer, ATR, PSA, SMR, WGS reactor and fired heater.

	C_1 [MUSD]	S_1	S_{max}	Basis	Unit	n	Year
Pre-reformer [52]	2.847	288,000	-	feed	kg/h	0.6	2018
ATR [52]	7.086	429,000	-	output	kg/h	0.6	2018
PSA [52]	21.762	27,500	-	H_2	kg/h	0.6	2018
SMR [52]	43.825	265,000	-	output	kg/h	0.6	2018
WGS reactor [62]	3.16	2556	2600	output	tonne/day	0.65	2015
Fired heater [52]	10.431	510	-	duty	GJ/h	0.6	2018

The GHR was cost estimated from a conventional SMR with the same capacity by subtracting the cost of a furnace and adding the cost of a pressure vessel. The cost of the different parts are summarised in Table F.5

The purchased and installed equipment cost of the main equipment in case 1 with a coupled GHR and ATR, and in case 2 with an ATR is summarised in Table F.6 and F.7, respectively.

Table F.5: Estimation of the purchased equipment cost of a GHR based on the equipment cost of a SMR, furnace and pressure vessel. (All values in MUSD).

	Purchased	Installed
SMR	-	61.687
Furnace	7.83	29.28
Pressure vessel	2.994	11.197
GHR	-	43.6

Table F.6: Purchased and installed equipment cost for case 1 with a coupled GHR and ATR. (All values in MUSD).

Equipment	Purchased	Installed
Pre-reformer	-	2.078
GHR	-	43.6
ATR	-	8.417
WGS reactor	-	14.07
Separator	0.522	1.95
Absorber packing	1.7	6.358
Absorber column	1.4	5.236
Flash Tank 1	4.249	15.89
Flash Tank 2	1.655	4.359
Flash Tank 3	1.1995	4.49
Flash Tank 4	0.24	0.898
PSA	-	26.29
Fired heater	-	6.355
E-107	0.03	0.11
E-102	0.274	1.024
E-101	0.063	0.235
E-104	0.0398	0.149
E-105	1.324	4.95
E-106	5.4496	20.38
E-111	0.0638	0.239
E-103	0.136	0.509
E-108	0.14	0.54
E-109	0.025	0.092
E-110	0.024	0.09
E-112	0.245	0.92
Compressor 1	0.891	3.33
Compressor 2	4.57	17.101
Compressor 3	11.99	44.85
Pump 1	0.25	0.935
Catalyst and adsorbent	-	32.95
Total		268.39

Table F.7: Purchased and installed equipment cost for case 2 with an ATR. (All values in MUSD).

Equipment	Purchased	Installed
Pre-reformer	-	2.21
ATR	-	6.558
WGS reactor	-	14.06
Separator	0.517	1.93
Absorber packing	1.795	6.713
Absorber column	1.47	5.5
Flash Tank 1	4.266	15.95
Flash Tank 2	1.74	6.508
Flash Tank 3	1.26	4.71
Flash Tank 4	0.26	0.97
PSA	-	26.29
Fired heater	-	7.12
E-102	0.027	0.1
E-101	0.0325	0.12
E-103	0.072	0.27
E-105	0.0866	0.32
E-107	5.505	20.59
E-111	0.049	0.18
E-104	0.158	0.59
E-106	1.855	6.94
E-108	0.35	1.32
E-109	0.026	0.096
E-110	0.024	0.09
E-112	0.23	0.86
Compressor 1	1.01	3.76
Compressor 2	4.66	17.43
Compressor 3	12.82	47.95
Pump 1	0.27	1.02
Catalyst and adsorbent	-	27.92
Total		228.08

Appendix G

Case Studies

G.1 Steam-to-Carbon Ratio Pre-reformer

The result from the case study (performed in the specialisation project) to determine the required steam to convert the heavy hydrocarbons to methane in the pre-reformer is illustrated in Figure G.1 [46]. As seen, all the heavier hydrocarbons were converted at a S/C ratio of around 0.2.

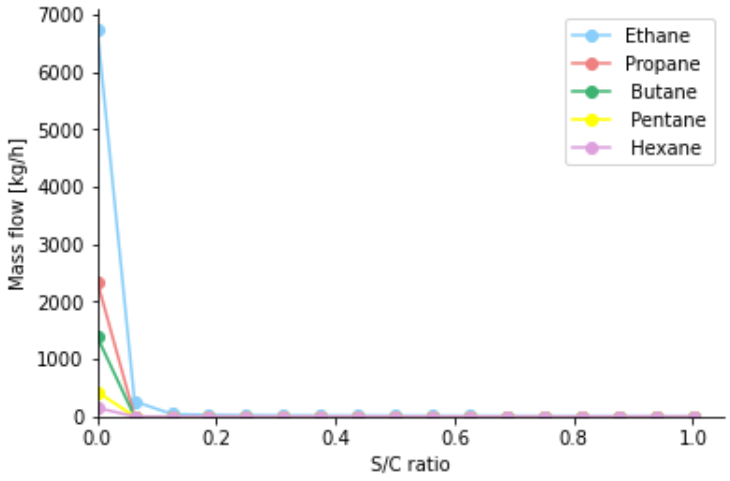

Figure G.1: Mass flow of the heavy hydrocarbons exiting the pre-reformer as a function of S/C ratio prior to the pre-reformer.

G.2 Steam-to-Carbon Ratio GHR

A case study performed in the specialisation project focused on the effect of the S/C ratio in the GHR feed on the hydrogen production [46]. As illustrated in Figure G.2, the optimal S/C ratio

in the GHR is 2.5.

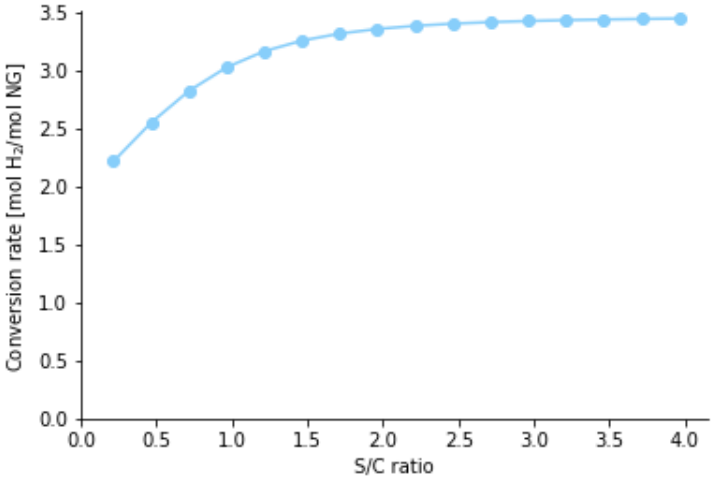

Figure G.2: Hydrogen produced as a function of the S/C ratio prior to the GHR.

G.3 Oxygen Feed to ATR - case 1

A case study performed in the specialisation project studied the outlet temperature of the ATR as a function of the oxygen amount added to the reformer. Since the hot exiting gas from the ATR is supposed to heat exchange in the GHR and provide the required heat for the steam reforming reaction (2.8). Therefore, a sufficient driving force is needed to minimise the reactor size. As seen in Figure G.3, the conversion rate is highest at an outlet temperature of approximately 1000°C. By using 1000°C, the driving force in the GHR was not maintained. Therefore, an outlet temperature of 1200°C was chosen, which gave a driving force of 50°C between the cold stream entering the GHR and the hot stream from the ATR exiting the GHR [46].

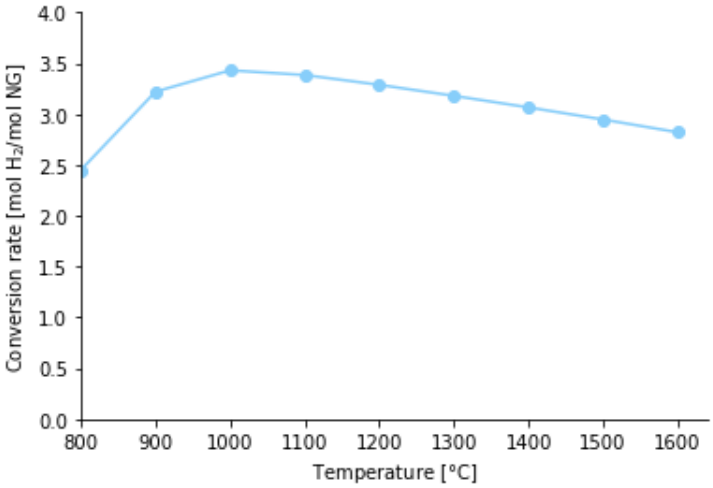

Figure G.3: Hydrogen production as a function of the outlet temperature of the autothermal reformer (ATR).

G.4 Oxygen-to-Carbon ATR - case 2

A case study performed in the specialisation project studied the oxygen-to-carbon (O/C) ratio in the ATR feed stream [46]. As shown in Figure G.4, the hydrogen production was maximised at an O/C ratio of approximately 0.6.

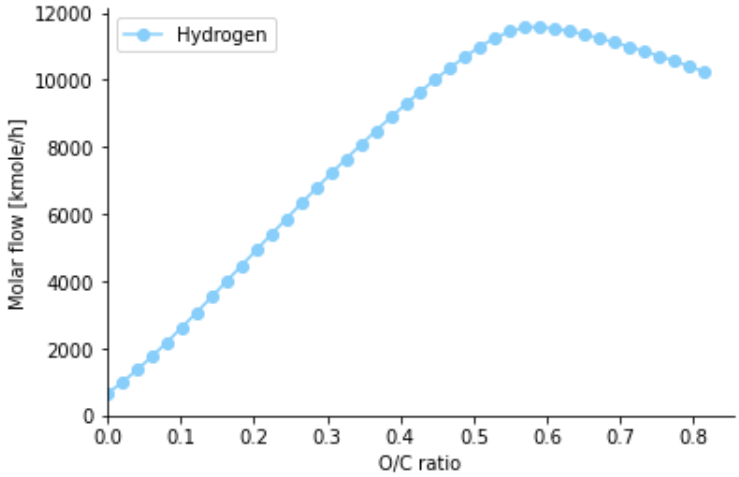

Figure G.4: Hydrogen produced as a function of the oxygen-to-carbon (O/C) ratio at the ATR inlet.

G.5 Number of Stages

The number of stages in the absorber column was determined by studying the performance in the absorber. Figure G.5 illustrates the composition of Selexol (DEPG) and CO_2 through the trays in the absorber. As seen, the amount of CO_2 captured increased up to approximately stage 14 and was constant afterwards. Therefore, the absorber was set to operate at 15 stages in this project.

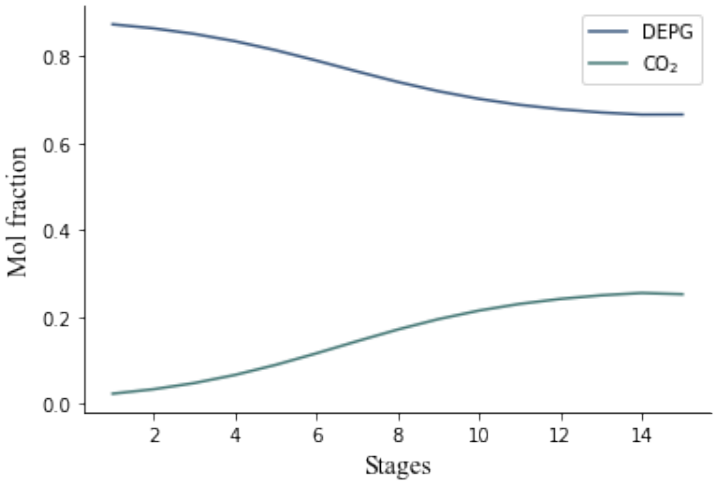

Figure G.5: Composition of the Selexol (DEPG) and captured CO_2 through the column.

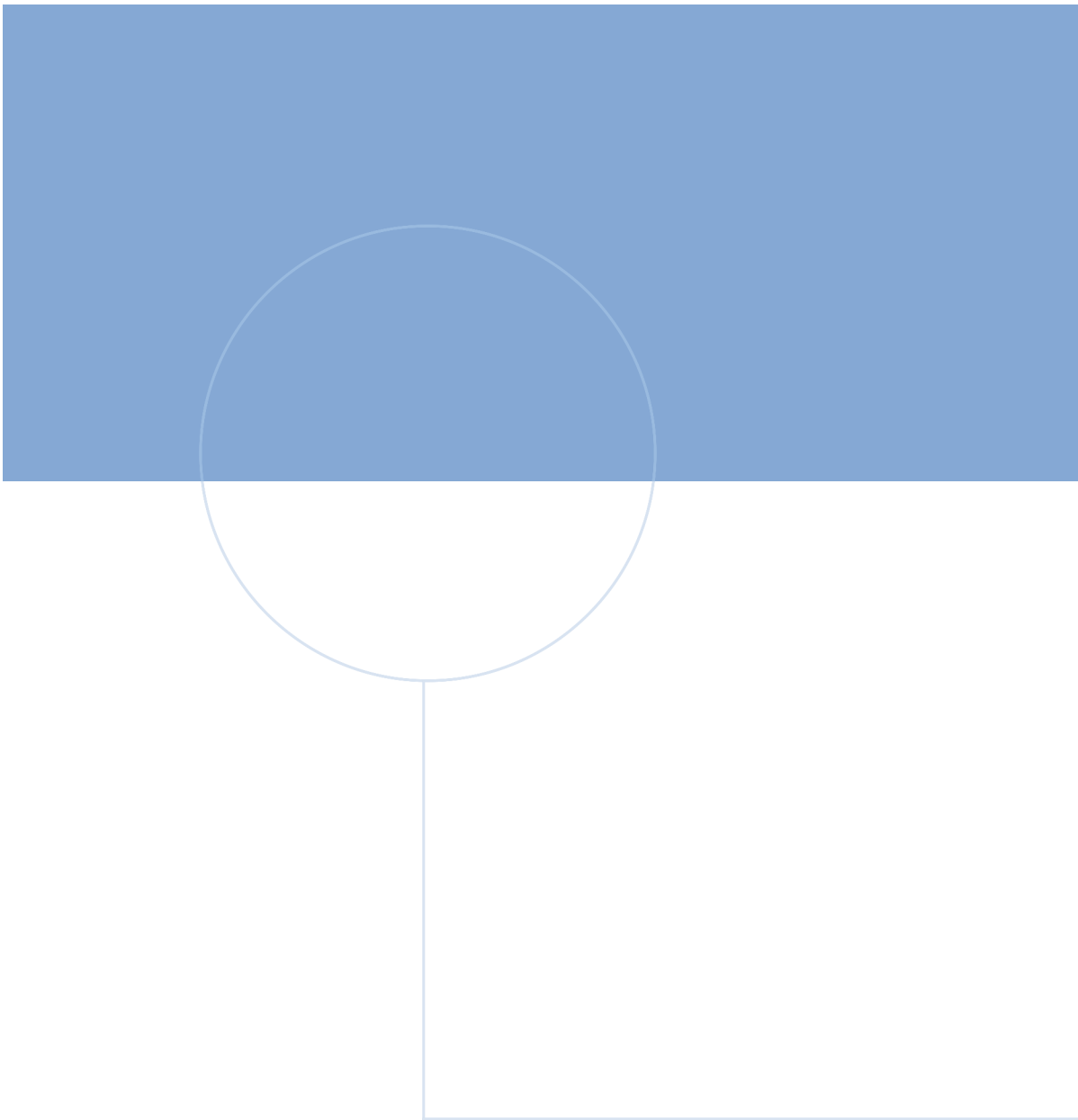

NTNU

Norwegian University of
Science and Technology